

NOAA LISD SEATTLE

NOAA TECHNICAL MEMORANDUM NWS CR-101



NUMERICAL SOLUTIONS TO THE SHALLOW WATER EQUATIONS AS APPLIED TO A LOCAL METEOROLOGICAL FORECAST PROBLEM

Eric R. Thaler
National Weather Service Forecast Office
Denver, Colorado

MARCH 1990

QC
995
.U61
NO.101

**U.S. DEPARTMENT OF
COMMERCE**

National Oceanic and
Atmospheric Administration

National Weather
Service

The National Weather Service Central Region (CR) subseries provides an informal medium for the documentation and quick dissemination of results not appropriate, or not yet ready, for formal publication. The series is used to report on work in progress, to describe technical procedures and practices, or to relate progress to a limited audience. These Technical Memoranda report on investigations devoted primarily to regional and local problems of interest mainly to regional personnel, and hence will not be widely distributed.

Papers 1 through 15 are in the former series, ESSA Technical Memoranda, Central Region Technical Memoranda (CRTM); Papers 16 through 36 are in the former series, ESSA Technical Memoranda, Weather Bureau Technical Memoranda (WBTM). Beginning with Paper 37, the papers are part of the series, NOAA Technical Memoranda NWS.

Papers that have a PB or COM number are available from the National Technical Information Service, U. S. Department of Commerce, 5285 Port Royal Road, Springfield, VA 22151. Order by accession number shown in parenthesis at the end of each entry. Prices vary for all paper copies. Microfiche are \$4.50. All other papers are available from the National Weather Service Central Region, Scientific Services, Room 1836, 601 East 12th Street, Kansas City, MO 64106.

ESSA Technical Memoranda

- CRTM 1 Precipitation Probability Forecast Verification Summary Nov. 1965 - Mar. 1966, SSD Staff, WBCRH, May 1966.
- CRTM 2 A Study of Summer Showers Over the Colorado Mountains. William G. Sullivan, Jr., and James O. Severson, June 1966.
- CRTM 3 Areal Shower Distribution - Mountain Versus Valley Coverage. William G. Sullivan, Jr., and James O. Severson, June 1966.
- CRTM 4 Heavy Rains in Colorado June 16 and 17, 1965. SSD Staff, WBCRH, July 1966.
- CRTM 5 The Plum Fire. William G. Sullivan, Jr., August 1966.
- CRTM 6 Precipitation Probability Forecast Verification Summary Nov. 1965 - July 1966. SSD Staff, WBCRH, September 1966.
- CRTM 7 Effect of Diurnal Weather Variations on Soybean Harvest Efficiency. Leonard F. Hard, October 1966.
- CRTM 8 Climatic Frequency of Precipitation at Central Region Stations. SSD Staff, WBCRH, November 1966.
- CRTM 9 Heavy Snow or Glazing. Harry W. Waldheuser, December 1966.
- CRTM 10 Detection of a Weak Front by WSR-57 Radar. G. W. Polensky, December 1966.
- CRTM 11 Public Probability Forecasts. SSD Staff, WBCRH, January 1967.
- CRTM 12 Heavy Snow Forecasting in the Central United States (an Interim Report). SSD Staff, January 1967.
- CRTM 13 Diurnal Surface Geostrophic Wind Variations Over the Great Plains. Wayne E. Sangster, March 1967.
- CRTM 14 Forecasting Probability of Summertime Precipitation at Denver. Wm. G. Sullivan, Jr., and James O. Severson, March 1967.
- CRTM 15 Improving Precipitation Probability Forecasts Using the Central Region Verification Printout. Lawrence A. Hughes, May 1967.
- WBTM CR 16 Small-Scale Circulations Associated with Radiational Cooling. Jack R. Cooley, June 1967.
- WBTM CR 17 Probability Verification Results (6-month and 18-month). Lawrence A. Hughes, June 1967.
- WBTM CR 18 On the Use and Misuse of the Brier Verification Score. Lawrence A. Hughes, August 1967 (PB 175 771).
- WBTM CR 19 Probability Verification Results (24 months). Lawrence A. Hughes, February 1968.
- WBTM CR 20 Radar Prediction of the Topeka Tornado. Norman E. Prosser, April 1968.
- WBTM CR 21 Wind Waves on the Great Lakes. Lawrence A. Hughes, May 1968.
- WBTM CR 22 Seasonal Aspects of Probability Forecasts: 1. Summer. Lawrence A. Hughes, June 1968 (PB 185 733).
- WBTM CR 23 Seasonal Aspects of Probability Forecasts: 2. Fall. Lawrence A. Hughes, September 1968 (PB 185 734).
- WBTM CR 24 The Importance of Areal Coverage in Precipitation Probability Forecasting. John T. Curran and Lawrence A. Hughes, September 1968.
- WBTM CR 25 Meteorological Conditions as Related to Air Pollution, Chicago, Illinois, April 12-13, 1963. Charles H. Swan, October 1968.
- WBTM CR 26 Seasonal Aspects of Probability Forecasts: 3. Winter. Lawrence A. Hughes, December 1968 (PB 185 735).
- WBTM CR 27 Seasonal Aspects of Probability Forecasts: 4. Spring. Lawrence A. Hughes, February 1969 (PB 185 736).
- WBTM CR 28 Minimum Temperature Forecasting During Possible Frost Periods at Agricultural Weather Stations in Western Michigan. Marshall E. Soderberg, March 1969.
- WBTM CR 29 An Aid for Tornado Warnings. Harry W. Waldheuser and Lawrence A. Hughes, April 1969.
- WBTM CR 30 An Aid in Forecasting Significant Lake Snows. H. J. Rothrock, November 1969.
- WBTM CR 31 A Forecast Aid for Boulder Winds. Wayne E. Sangster, February 1970.
- WBTM CR 32 An Objective Method for Estimating the Probability of Severe Thunderstorms. Clarence L. David, February 1970.
- WBTM CR 33 Kentucky Air-Soil Temperature Climatology. Clyde B. Lee, February 1970.
- WBTM CR 34 Effective Use of Non-Structural Methods in Water Management. Verne Alexander, March 1970.
- WBTM CR 35 A Note on the Categorical Verification of Probability Forecasts. Lawrence A. Hughes and Wayne E. Sangster, August 1970.
- WBTM CR 36 A Comparison of Observed and Calculated Urban Mixing Depths. Donald E. Wuerch, August 1970.

NOAA Technical Memoranda NWS

- NWS CR 37 Forecasting Maximum and Minimum Surface Temperatures at Topeka, Kansas, Using Guidance from the PE Numerical Prediction Model (FOUS). Morris S. Webb, Jr., November 1970 (COM 71 00118).
- NWS CR 38 Snow Forecasting for Southeastern Wisconsin. Rheinhart W. Harms, November 1970 (COM 71-00019).
- NWS CR 39 A Synoptic Climatology of Blizzards on the North-Central Plains of the United States. Robert E. Black, February 1971 (COM 71-00369).
- NWS CR 40 Forecasting the Spring 1969 Midwest Snowmelt Floods. Herman F. Mondschein, February 1971 (COM 71-00489).
- NWS CR 41 The Temperature Cycle of Lake Michigan 1. (Spring and Summer). Lawrence A. Hughes, April 1971 (COM 71-00545).
- NWS CR 42 Dust Devil Meteorology. Jack R. Cooley, May 1971 (COM 71-00628).
- NWS CR 43 Summer Shower Probability in Colorado as Related to Altitude. Alois G. Topil, May 1971 (COM 71-00712).
- NWS CR 44 An Investigation of the Resultant Transport Wind Within the Urban Complex. Donald E. Wuerch, June 1971 (COM 71-00766).
- NWS CR 45 The Relationship of Some Cirrus Formations to Severe Local Storms. William E. Williams, July 1971 (COM 71-00844).
- NWS CR 46 The Temperature Cycle of Lake Michigan 2. (Fall and Winter). Lawrence A. Hughes, September 1971 (COM 71-01039).
- NWS CR 47 Practical Application of a Graphical Method of Geostrophic Wind Determination. C.B. Johnson, November 1971 (COM 71-01084).
- NWS CR 48 Manual of Great Lakes Ice Forecasting. C. Robert Snider, December 1971 (COM 72-10143).
- NWS CR 49 A Preliminary Transport Wind and Mixing Height Climatology, St. Louis, Missouri. Donald E. Wuerch, Albert J. Courtols, Carl Ewald, Gary Ernst, June 1972 (COM 72-10859).
- NWS CR 50 An Objective Forecast Technique for Colorado Downslope Winds. Wayne E. Sangster, December 1972 (COM 73-10280).
- NWS CR 51 Effect on Temperature and Precipitation of Observation Site Change at Columbia, Missouri. Warren M. Wisner, March 1973 (COM 73-10734).
- NWS CR 52 Cold Air Funnel Clouds. Jack R. Cooley and Marshall E. Soderberg, September 1973, (COM 73-11753/AS).
- NWS CR 53 The Frequency of Potentially Unfavorable Temperature Conditions in St. Louis, Missouri. Warren M. Wisner, October 1973.
- NWS CR 54 Objective Probabilities of Severe Thunderstorms Using Predictors from FOUS and Observed Surface Data. Clarence A. David, May 1974 (COM 74-11258/AS).

TABLE OF CONTENTS

	<u>Page No.</u>
LIST OF FIGURES	ii
ABSTRACT	iv
Chapter	
1. INTRODUCTION	1
2. THE PHYSICAL MODEL	4
3. THE NUMERICAL MODEL	23
Space Discretization	24
Time Discretization	55
Summary	63
4. BOUNDARY AND INITIAL CONDITIONS	64
5. MODEL IMPLEMENTATION AND DISCUSSION OF RESULTS	79
REFERENCES CITED	111
SELECTED BIBLIOGRAPHY	114

LIST OF FIGURES

<u>Figure</u>	<u>Page No.</u>
1. The distribution of variables over the grid domain (after Arakawa and Lamb, 1981).	25
2. Computational stencils. A) eqn. (3.43); B) eqn. (3.44); C) eqn. (3.45).	55
3. Counties in Colorado. Important features in subsequent figures will refer to these.	87
4. Results after 10 minutes of simulated time using full, unscaled terrain (see text for details).	88
5. Initial test data wind field. Integration performed with flat bottom surface (no terrain).	90
6. Forecast wind field after 1 hour of simulated time using initial wind field in Figure 5.	91
7. Forecast wind field after 2 hours of simulated time using initial wind field in Figure 5.	92
8. Forecast wind field after 3 hours of simulated time using initial wind field in Figure 5.	93
9. Initial real data wind field. Bottom surface is scaled topography (see text for details).	95
10. Forecast wind field after 1 hour of simulated time using initial data shown in Figure 9.	96
11. Forecast wind field after 2 hours of simulated time using initial data shown in Figure 9.	97
12. Forecast wind field after 3 hours of simulated time using initial data shown in Figure 9.	98
13. Initial real data wind field. Bottom surface is scaled topography (see text for details).	101
14. Forecast wind field after 1 hour of simulated time using initial data shown in Figure 13.	102
15. Forecast wind field after 2 hours of simulated time using initial data shown in Figure 13.	103
16. Forecast wind field after 3 hours of simulated time using initial data shown in Figure 13.	104

17.	Actual winds observed 1 hour after initial data in Figure 13. Compare with Figure 14.	105
18.	Actual winds observed 2 hours after initial data in Figure 13. Compare with Figure 15.	106
19.	Actual winds observed 3 hours after initial data in Figure 13. Compare with Figure 16.	107

NUMERICAL SOLUTIONS TO THE SHALLOW WATER EQUATIONS
AS APPLIED TO A LOCAL METEOROLOGICAL FORECAST PROBLEM¹

Eric R. Thaler

National Weather Service Forecast Office

Denver, Colorado

ABSTRACT

An initial-boundary value problem comprised of a coupled system of three nonlinear, nonhomogeneous, hyperbolic first order partial differential equations is solved by numerical methods. The equations arise in geophysical fluid dynamics and describe the two-dimensional flow of a shallow, inviscid, homogeneous, incompressible fluid which is in hydrostatic balance. Their solution is used to describe the time evolution of winds at the earth's surface.

The solution is obtained numerically using a first order in time, second order in space finite difference scheme which is capable of simulating flow over steep topography. Initial conditions for

¹ This is a reprint of Mr. Thaler's Masters Thesis for the Colorado School of Mines.

the integrations are obtained from a recently developed analysis scheme which provides high temporal and spatial resolution wind fields.

Results indicate that the model produces satisfying mathematical solutions to the problem. However, since the physical model is very elementary, it has difficulty producing useful meteorological wind forecasts when the flow is dominated by factors not included in it, most notably thermal and frictional effects. If these forces are secondary, the model is capable of providing useful wind forecasts.

CHAPTER 1
INTRODUCTION

The surface winds along the Front Range of the Colorado Rockies and over the adjacent plains to the east, coupled with the highly varying terrain in this area, play a very prominent role in the local meteorology. For example, winds blowing from the mountains onto the plains usually bring warm and dry weather conditions, while winds blowing upslope from east to west, under proper conditions, can lead to clouds and precipitation.

Thus, by increasing the accuracy of the surface wind forecasts for this area, better forecasts of the actual weather conditions can be made. Unfortunately, extrapolation of current conditions, extremely rough numerical guidance from large scale models, climatology, and forecaster experience have been the sole means of producing surface wind predictions. Numerical modeling on small scales, which takes local effects such as topography into account, is currently being done, (see for example Abbs and Pielke 1986, Wilczak and Glendening 1988) but for the most part is confined to the research community. (Note also that these models have not had access to the high resolution data set described below.)

Within the last five years or so, a new analysis scheme has been devised (McGinley 1989) which produces, on an hourly basis, a very fine spatial resolution gridpoint analysis of surface winds over a large portion of Colorado. This data set has proven to be very useful in diagnosing current weather conditions. Could it now be taken one step further and used to help obtain forecasted weather conditions?

Numerical prediction of the wind involves a great deal of mathematics. A numerical wind forecast, in theory, requires the solution of an initial-boundary value problem consisting of a coupled system of nonlinear, nonhomogeneous, hyperbolic, first order partial differential equations derived from the laws of geophysical fluid dynamics. Since this problem cannot be solved analytically, numerical methods must be employed to find a solution.

This thesis will describe a rather novel approach to this formidable problem. By using a selection of methods from various sources, a simple physical and numerical model, one based on techniques normally reserved for modelling larger scale atmospheric processes, is developed which solves this mathematical problem and produces real time surface wind forecasts that can be used in day-to-day weather prediction operations.

The thesis is divided into five chapters. Chapter 2 develops the differential equations which describe the physics of the problem. Chapter 3 then transforms the differential equations into difference equations capable of being solved on a computer, subject to proper initial and boundary conditions which are discussed in Chapter 4. Chapter 5 covers the actual implementation of the model and discusses the results obtained from it.

Chapter 2

THE PHYSICAL MODEL

Three dimensional motion in the atmosphere is governed by a complicated set of nonlinear, nonhomogeneous partial differential equations (see Holton 1979). Since analytic solutions to this set of equations are not known, one must resort to numerical methods in order to solve them.

Including all of the physical processes that occur in the atmosphere in a numerical model requires an enormous amount of effort and computing power. In this study, we would like to use a physical model (set of differential equations) which retains most of the important physics of the motion (including nonlinear effects) while requiring only modest computing resources for its numerical solution. The simplest physical model satisfying the above requirements is the primitive equation barotropic model, also known as the shallow-water model. This model governs the motion of an inviscid, homogeneous, incompressible fluid with a free surface which is in hydrostatic equilibrium.

The model equations, which represent conservation of fluid mass and horizontal momentum, are derived from the complete set of governing equations through scale analysis. Scale analysis is performed by substituting into the equa-

tions characteristic values of each of the variables and then comparing the magnitude of each term. Those with small magnitude are disregarded and the simplified equations are then assumed to sufficiently describe the motion.

As the name implies, scale analysis uses characteristic values for the variables based on a certain scale of the motion. Scales of atmospheric motion range from several thousand kilometers for large planetary wave motions down to just a few millimeters for minute turbulent eddies (Holton 1979). The scale used to derive the shallow-water equations is on the order of 1000 km, or roughly the size of a major midlatitude weather system.

In this study we are dealing with a square domain roughly 500 km on a side. Thus, the physical model will not be totally representative of motions in this domain. The choice of the shallow-water model was based on its mathematical and physical simplicity with the implicit assumption that it should be sufficient to describe at least the basic flow pattern in the domain.

Along with the assumptions used in the scale analysis of the complete governing equations (Pedlosky 1987), the following assumptions concerning the fluid (air in this case) are made:

1. The fluid is inviscid, so that no frictional effects are involved.
2. The fluid is homogeneous, meaning it has constant and uniform density which for convenience, will be set equal to unity. Since spatial gradients in the density field are absent, the fluid is termed barotropic. From this assumption it will be shown that the fluid is incompressible.
3. The fluid is in hydrostatic equilibrium, that is, the vertical pressure gradient force per unit mass exactly balances the acceleration of gravity. The main implication of this is that if the horizontal velocity is initially independent of height, it will remain so for all time. This in turn implies that the fluid moves as a set of vertical columns.
4. The fluid is situated on a plane tangent to the earth's surface and is rotating at the constant angular velocity of the earth. This eliminates all effects of the earth's sphericity.
5. The vertical component of the earth's vorticity vector, the Coriolis parameter, is assumed constant. In reality it is a function of latitude.

6. The fluid is considered to be shallow, that is, the fluid depth is assumed to be much smaller than the scale of horizontal motions in the fluid.

The complete derivation of the equations will not be presented here but may be found in Pedlosky (1987), upon which much of the following is based.

The differential equations are written in a Cartesian coordinate system with the unit vectors i , j , k pointing east along the x -axis, north along the y -axis and vertically up along the z -axis respectively. The variable t stands for time.

The horizontal momentum conservation equations governing the motion can be written in component form as

$$\frac{\partial u}{\partial t} + u \frac{\partial u}{\partial x} + v \frac{\partial u}{\partial y} + \frac{\partial \phi}{\partial x} - fv = 0, \quad (2.1)$$

$$\frac{\partial v}{\partial t} + u \frac{\partial v}{\partial x} + v \frac{\partial v}{\partial y} + \frac{\partial \phi}{\partial y} + fu = 0, \quad (2.2)$$

or in vector form as

$$\frac{\partial \mathbf{v}}{\partial t} + (\mathbf{v} \cdot \nabla) \mathbf{v} + f \mathbf{k} \times \mathbf{v} + \nabla \phi = \mathbf{0}, \quad (2.3)$$

where:

- $u(x,y,t) = \frac{dx}{dt}$ is the east-west wind component,
 positive for a west wind;
- $v(x,y,t) = \frac{dy}{dt}$ is the north-south wind component,
 positive for a south wind;
- $\mathbf{V}(x,y,t) = u\mathbf{i}+v\mathbf{j}$ is the horizontal velocity vector;
- $\nabla = \mathbf{i}\frac{\partial}{\partial x} + \mathbf{j}\frac{\partial}{\partial y}$ is the horizontal gradient operator;
- $f = \text{constant}$ is the Coriolis parameter;
- $\Phi(x,y,t) = g[h(x,y,t)+h_S(x,y)]$

is the geopotential of the free surface, with g the constant acceleration of gravity, $h(x,y,t)$ the height (above the ground) of the free surface of the fluid (the fluid depth), and $h_S(x,y)$ the height of the terrain above sea-level ($z=0$).

The usual form of the mass continuity equation for a fluid with no mass sources or sinks can be written as

$$\frac{\partial \rho}{\partial t} + \mathbf{V}_3 \cdot \nabla_3 \rho + \rho \nabla_3 \cdot \mathbf{V}_3 = \frac{\partial \rho}{\partial t} + \nabla_3 \cdot (\rho \mathbf{V}_3) = 0, \quad (2.4)$$

where $\rho(x,y,z,t)$ is the density of the fluid and \mathbf{V}_3 is the three dimensional velocity vector ($=u\mathbf{i}+v\mathbf{j}+w\mathbf{k}$ with $w=\frac{dz}{dt}$ the

vertical velocity, positive for upward motion; also $v_3 = \mathbf{v} \cdot \mathbf{k} \frac{\partial}{\partial z}$). Since we are dealing with a homogeneous fluid in this model, ρ is a constant and (2.4) becomes

$$\nabla_3 \cdot \nabla_3 = \frac{\partial u}{\partial x} + \frac{\partial v}{\partial y} + \frac{\partial w}{\partial z} = 0, \quad (2.5)$$

the incompressibility condition. This is not a very useful form of the continuity equation but can be transformed into an equation for the depth of the fluid as follows.

Since the horizontal velocity is assumed independent of height, (2.5) can be integrated over the depth of the fluid to get

$$\int_{h_s}^{h+h_s} \frac{\partial w}{\partial z} dz = - \int_{h_s}^{h+h_s} \left[\frac{\partial u}{\partial x} + \frac{\partial v}{\partial y} \right] dz$$

$$w(x, y, h+h_s, t) - w(x, y, h_s, t) = -h \left[\frac{\partial u}{\partial x} + \frac{\partial v}{\partial y} \right]. \quad (2.6)$$

At the free surface of the fluid $z=h(x, y, t)+h_s(x, y)$ and by requiring this to be a material surface (fluid particles once on the surface remain there for all time) implies

$$\left. \frac{dz}{dt} \right|_{h+h_s} = w(x, y, h+h_s, t) = \frac{d}{dt} [h+h_s]$$

$$= \frac{\partial}{\partial t} [h+h_s] + \mathbf{v} \cdot \nabla (h+h_s). \quad (2.7)$$

In addition, at the ground $z=h_s(x,y)$ and since no fluid can flow into the ground, the velocity vector must be tangent to the terrain. Mathematically, this condition is represented by letting $F(x,y,z)=z-h_s(x,y)=0$ describe the terrain and requiring $\mathbf{V}_3 \cdot \nabla_3 F = 0$. This gives

$$(\mathbf{u}\mathbf{i} + \mathbf{v}\mathbf{j} + \mathbf{w}\mathbf{k}) \cdot \left[-\mathbf{i} \frac{\partial h_s}{\partial x} - \mathbf{j} \frac{\partial h_s}{\partial y} + \mathbf{k} \right] = 0$$

implying

$$\left. \frac{dz}{dt} \right|_{h_s} = w(x,y,h_s,t) = \mathbf{V} \cdot \nabla h_s. \quad (2.8)$$

Substituting (2.7) and (2.8) into (2.6) yields

$$\frac{\partial}{\partial t} (h+h_s) + \mathbf{V} \cdot \nabla (h+h_s) - \mathbf{V} \cdot \nabla h_s + h \left[\frac{\partial u}{\partial x} + \frac{\partial v}{\partial y} \right] = 0,$$

or

$$\frac{\partial h}{\partial t} + \mathbf{V} \cdot \nabla h + h \mathbf{V} \cdot \nabla = \frac{\partial h}{\partial t} + \nabla \cdot (h \mathbf{V}) = 0, \quad (2.9)$$

which is the mass continuity equation for this shallow-water model.

Note that this equation is completely analogous to (2.4) with ρ being replaced by h and \mathbf{V}_3 replaced with \mathbf{V} . In fact, since we are considering the fluid density to be one, multiplying (2.9) by this density gives h the units of mass per unit area.

To see that (2.9) does indeed describe mass continuity, assume for the moment that the flow is nondivergent in a neighborhood of a point P_0 , but that a spatial gradient in the fluid depth (mass per unit area) exists. Then equation (2.9) becomes

$$\frac{\partial h}{\partial t} = -\mathbf{v} \cdot \nabla h,$$

showing that the local change in the depth of the fluid is equal to the horizontal advection of fluid depth. Thus, if deeper fluid is upstream from P_0 , the fluid depth at P_0 must increase with time in order to balance the equation. Since no fluid can flow into the ground, this depth increase comes about by a rise in the free surface of the fluid. Looked at another way, if more mass per unit area is upstream from P_0 , the mass per unit area at P_0 must increase with time since there are no mass sinks.

Next assume that the flow is divergent in a neighborhood of P_0 but that the fluid has uniform depth in this neighborhood. In this case (2.9) becomes

$$\frac{\partial h}{\partial t} = -h \nabla \cdot \mathbf{v},$$

showing that the local change in the fluid depth is proportional to the divergence of the flow. Since $\nabla \cdot \mathbf{v}$ and h are both positive the local fluid depth at P_0 must decrease with

time. Again since there can be no flow into the ground, this depth decrease comes about through a fall in the height of the free surface. In terms of mass, if fluid is diverging from the neighborhood of P_0 , the mass per unit area at P_0 must decrease with time.

The equations of horizontal momentum conservation, (2.1) and (2.2), and the mass continuity equation (2.9) are known as the shallow-water equations or barotropic primitive equations (primitive meaning u and v are dependent variables). However, the equations in this form are not the ones used in the numerical integrations. Further manipulations of the equations are now undertaken to bring them into a form suitable for numerical integration. These transformations (Pedlosky 1987; Arakawa and Lamb 1981) will also yield important physical properties of the fluid which will be exploited in the development of the numerical scheme.

A quantity of utmost importance in meteorology is the vorticity of the wind. Vorticity is a vector and is defined mathematically as the curl of the velocity vector, in two dimensions

$$\nabla \times \mathbf{V} = \mathbf{k} \left[\frac{\partial v}{\partial x} - \frac{\partial u}{\partial y} \right].$$

For convenience let $\zeta = \mathbf{k} \cdot \nabla \times \mathbf{V} = \frac{\partial v}{\partial x} - \frac{\partial u}{\partial y}$.

ζ is called the relative vorticity, since it describes the rotation of the wind field relative to the earth's surface. However, since the fluid is rotating with the earth, there is another contribution to the vorticity, namely the Coriolis parameter f , which is the vertical component of the earth's vorticity vector. Combining these two gives $\zeta+f$, the vertical component of the absolute vorticity (hereafter referred to simply as absolute vorticity).

With vorticity now defined, an equation is derived describing the absolute vorticity dynamics of the shallow-water model. Taking the partial derivative with respect to x of equation (2.2) and subtracting from it the partial derivative with respect to y of equation (2.1) (assuming the proper continuity requirements to assure the reordering of partial derivatives) gives

$$\frac{\partial}{\partial x} \left[\frac{\partial v}{\partial t} + u \frac{\partial v}{\partial x} + v \frac{\partial v}{\partial y} + \frac{\partial \phi}{\partial y} + fu = 0 \right]$$

$$\frac{\partial}{\partial t} \frac{\partial v}{\partial x} + u \frac{\partial}{\partial x} \frac{\partial v}{\partial x} + \frac{\partial u}{\partial x} \frac{\partial v}{\partial x} + v \frac{\partial}{\partial y} \frac{\partial v}{\partial x} + \frac{\partial v}{\partial x} \frac{\partial v}{\partial y}$$

$$+ \frac{\partial^2 \phi}{\partial x \partial y} + f \frac{\partial u}{\partial x} = 0;$$

and for (2.1)

$$\frac{\partial}{\partial y} \left[\frac{\partial u}{\partial t} + u \frac{\partial u}{\partial x} + v \frac{\partial u}{\partial y} + \frac{\partial \phi}{\partial x} - fv = 0 \right]$$

$$\begin{aligned} \frac{\partial}{\partial t} \frac{\partial u}{\partial y} + u \frac{\partial}{\partial x} \frac{\partial u}{\partial y} + \frac{\partial u}{\partial y} \frac{\partial u}{\partial x} + v \frac{\partial}{\partial y} \frac{\partial u}{\partial y} + \frac{\partial v}{\partial y} \frac{\partial u}{\partial y} \\ + \frac{\partial^2 \phi}{\partial x \partial y} - f \frac{\partial v}{\partial y} = 0; \end{aligned}$$

hence, the subtraction yields

$$\begin{aligned} \frac{\partial}{\partial t} \left[\frac{\partial v}{\partial x} - \frac{\partial u}{\partial y} + f \right] + u \frac{\partial}{\partial x} \left[\frac{\partial v}{\partial x} - \frac{\partial u}{\partial y} + f \right] + v \frac{\partial}{\partial y} \left[\frac{\partial v}{\partial x} - \frac{\partial u}{\partial y} + f \right] \\ + \left[\frac{\partial u}{\partial x} + \frac{\partial v}{\partial y} \right] \left[\frac{\partial v}{\partial x} - \frac{\partial u}{\partial y} + f \right] = 0 \end{aligned}$$

or in vector form

$$\begin{aligned} \frac{\partial (\zeta + f)}{\partial t} + \mathbf{v} \cdot \nabla (\zeta + f) + (\zeta + f) \nabla \cdot \mathbf{v} \\ = \frac{\partial (\zeta + f)}{\partial t} + \nabla \cdot [(\zeta + f) \mathbf{v}] = 0. \end{aligned} \quad (2.10)$$

Equation (2.10) is the vorticity equation for the shallow-water model. It states that absolute vorticity at a point can change through advection of absolute vorticity by the wind or through divergence/convergence of the wind.

Another useful quantity is the (absolute) potential vorticity q , defined as

$$q = \frac{(\zeta + f)}{h}.$$

Using this quantity to combine equations (2.9) and (2.10) yields a very interesting property of this model which serves as a basis for the numerical scheme. Equation (2.10) can be written as

$$\frac{\partial(hq)}{\partial t} + q\mathbf{v}\cdot\nabla h + h\mathbf{v}\cdot\nabla q + hq\mathbf{v}\cdot\nabla = 0, \quad (2.11)$$

while multiplication of (2.9) by q gives

$$q\frac{\partial h}{\partial t} + q\mathbf{v}\cdot\nabla h + qh\mathbf{v}\cdot\nabla = 0. \quad (2.12)$$

Subtracting (2.12) from (2.11) and noting that $\frac{\partial(hq)}{\partial t} - q\frac{\partial h}{\partial t} =$

$h\frac{\partial q}{\partial t}$ we get, after division by nonzero h ,

$$\frac{\partial q}{\partial t} + \mathbf{v}\cdot\nabla q = \frac{dq}{dt} = 0, \quad (2.13)$$

showing that the potential vorticity of the fluid is conserved following the motion or, at a point, the potential vorticity can change only through advection. Thus if there are no spatial gradients in the potential vorticity field, it cannot change with time. Looked at another way, if a fluid column stretches (shrinks) as it is flowing along, its absolute vorticity must increase (decrease) so as to keep its potential vorticity constant. An important consequence of this is that absolute vorticity can be generated by the movement of fluid columns over uneven terrain.

To conclude this chapter, several important integral constraints on the fluid (conservation laws) will be derived. Some of these will be used to test the numerical model, while others actually form the basis for the finite difference scheme.

A vector identity that is quite useful in these derivations states that for any two dimensional vector \mathbf{v}

$$\frac{d\mathbf{v}}{dt} = \frac{\partial\mathbf{v}}{\partial t} + (\mathbf{v}\cdot\nabla)\mathbf{v} = \frac{\partial\mathbf{v}}{\partial t} + \nabla\frac{1}{2}|\mathbf{v}|^2 + (\mathbf{k}\cdot\nabla\times\mathbf{v})[\mathbf{k}\times\mathbf{v}]$$

With this definition, equation (2.3) can be written as

$$\frac{\partial\mathbf{v}}{\partial t} + \nabla\frac{1}{2}|\mathbf{v}|^2 + \nabla\phi + (\zeta+f)(\mathbf{k}\times\mathbf{v}) = \mathbf{0}. \quad (2.14)$$

Since $h\mathbf{v}\cdot\frac{\partial\mathbf{v}}{\partial t} = h\frac{\partial}{\partial t}[\frac{1}{2}\mathbf{v}\cdot\mathbf{v}] = h\frac{\partial}{\partial t}[\frac{1}{2}|\mathbf{v}|^2]$ and $(\zeta+f)h\mathbf{v}\cdot(\mathbf{k}\times\mathbf{v}) = -(\zeta+f)h\mathbf{k}\cdot(\nabla\times\mathbf{v}) = 0$, the scalar product of $h\mathbf{v}$ and (2.14) is

$$h\frac{\partial}{\partial t}[\frac{1}{2}|\mathbf{v}|^2] + h\mathbf{v}\cdot\nabla(\frac{1}{2}|\mathbf{v}|^2) + h\mathbf{v}\cdot\nabla\phi = 0. \quad (2.15)$$

Noting that $\nabla\cdot(\frac{1}{2}h|\mathbf{v}|^2\mathbf{v}) = \frac{1}{2}h|\mathbf{v}|^2\nabla\cdot\mathbf{v} + h\mathbf{v}\cdot\nabla\frac{1}{2}|\mathbf{v}|^2 + \frac{1}{2}h|\mathbf{v}|^2\nabla\cdot\mathbf{v}$, we add $\frac{1}{2}h|\mathbf{v}|^2$ times equation (2.9) to (2.15) yielding

$$\frac{\partial}{\partial t}[\frac{1}{2}h|\mathbf{v}|^2] + \nabla\cdot(\frac{1}{2}h|\mathbf{v}|^2\mathbf{v}) + h\mathbf{v}\cdot\nabla\phi = 0. \quad (2.16)$$

Furthermore, $\nabla\cdot(h\phi\mathbf{v}) = h\mathbf{v}\cdot\nabla\phi + \phi\nabla\cdot(h\mathbf{v})$, which with (2.9) and the fact that $\phi\frac{\partial h}{\partial t} = \frac{\partial}{\partial t}[g(\frac{1}{2}h^2+hh_s)]$ gives

$$h\nabla \cdot \nabla \phi = \nabla \cdot (h\nabla \phi) + \frac{\partial}{\partial t} [g(\frac{1}{2}h^2 + hh_s)].$$

Substituting this into (2.15) we obtain

$$\frac{\partial}{\partial t} [\frac{1}{2}h|\nabla|^2 + g(\frac{1}{2}h^2 + hh_s)] + \nabla \cdot [(\frac{1}{2}|\nabla|^2 + \phi)h\nabla] = 0 \quad (2.17)$$

Since h can be interpreted as the mass per unit area, and $\frac{1}{2}|\nabla|^2$ is the kinetic energy per unit mass, $\frac{1}{2}h|\nabla|^2$ is the kinetic energy per unit area.

Moreover, $g(\frac{1}{2}h^2 + hh_s)$ is the potential energy per unit area. To see this, consider a column in the fluid which extends from the surface ($z=h_s$) to the top of the fluid ($z=h+h_s$). Within the column, suppose there is a slab of thickness dz' located at a height $z=z'$ above sea-level. Since the fluid in the slab has unit density, its potential energy per unit area is $gz'dz'$. Hence the potential energy per unit area of the entire column is

$$\int_{h_s}^{h+h_s} gz'dz' = \frac{1}{2}g(h^2 + 2hh_s) = g(\frac{1}{2}h^2 + hh_s).$$

Consequently, equation (2.17) gives the local time rate of change of the total mechanical energy of the fluid.

For the integrations that follow, let R be a fixed, closed, finite, rectangular region in the xy -plane which has

boundary ∂R . Let \mathbf{n} be the outward pointing normal (unit) vector to the region and let ds be a vector line element on ∂R . Furthermore, assume that the boundary of the region is impermeable to fluid motion so that $\mathbf{v} \cdot \mathbf{n} = 0$ everywhere on ∂R .

Integrating (2.17) over R , applying Gauss' divergence theorem and recalling that R is fixed in time gives

$$\iint_R \frac{\partial}{\partial t} [\frac{1}{2} \rho |\mathbf{v}|^2 + g(\frac{1}{2} \rho h^2 + \rho h h_s)] dx dy = - \iint_R \nabla \cdot [(\frac{1}{2} \rho |\mathbf{v}|^2 + \rho h \phi) \mathbf{v}] dx dy$$

$$\frac{\partial}{\partial t} \iint_R [\frac{1}{2} \rho |\mathbf{v}|^2 + g(\frac{1}{2} \rho h^2 + \rho h h_s)] dx dy = - \oint_{\partial R} [(\frac{1}{2} \rho |\mathbf{v}|^2 + \rho h \phi)] \mathbf{v} \cdot \mathbf{n} ds.$$

Since

$$- \oint_{\partial R} [(\frac{1}{2} \rho |\mathbf{v}|^2 + \rho h \phi)] \mathbf{v} \cdot \mathbf{n} ds = 0,$$

$$\frac{\partial}{\partial t} \overline{[\frac{1}{2} \rho |\mathbf{v}|^2 + g(\frac{1}{2} \rho h^2 + \rho h h_s)]} = 0, \quad (2.18)$$

where the overbar indicates the area averaged total mechanical energy over the domain R . Equation (2.18) says that if no fluid is allowed to pass into or out of a given fixed domain, the average value of the total mechanical energy of the fluid, kinetic plus potential, is constant with time.

Next, multiplying (2.13) by hq , (2.9) by κq^2 and adding the results yields

$$\begin{aligned} & hq \frac{\partial q}{\partial t} + hq \nabla \cdot \nabla q + \kappa q^2 \frac{\partial h}{\partial t} + \kappa q^2 \nabla \cdot (h \nabla) \\ &= \frac{\partial}{\partial t} (\kappa h q^2) + \nabla \cdot (\kappa h q^2 \nabla) = 0. \end{aligned} \quad (2.19)$$

Integrating this equation in the same manner as for the energy equation gives

$$\begin{aligned} \iint_R \frac{\partial}{\partial t} (\kappa h q^2) dx dy &= - \iint_R \nabla \cdot (\kappa h q^2 \nabla) dx dy \\ \frac{\partial}{\partial t} \iint_R (\kappa h q^2) dx dy &= - \oint_{\partial R} \kappa h q^2 \nabla \cdot \mathbf{n} ds = 0 \end{aligned}$$

so that

$$\frac{\partial}{\partial t} \overline{(\kappa h q^2)} = 0. \quad (2.20)$$

Thus the area averaged value of the quantity $\kappa h q^2$, called the potential enstrophy, over the domain is conserved.

Performing an analogous procedure on equation (2.9) shows the obvious conclusion that

$$\frac{\partial}{\partial t} \iint_R h dx dy = 0,$$

stating that the total mass of fluid in the domain remains constant if none leaves or enters.

Finally, taking the scalar product of (2.14) with ds and integrating around ∂R gives

$$\begin{aligned} & \oint_{\partial R} \left[\frac{\partial \mathbf{v}}{\partial t} + \nabla(\chi|\mathbf{v}|^2 + \phi) + (\zeta + f)(\mathbf{k} \times \mathbf{v}) \right] \cdot d\mathbf{s} \\ &= \frac{\partial}{\partial t} \oint_{\partial R} \mathbf{v} \cdot d\mathbf{s} = 0. \end{aligned} \quad (2.21)$$

The gradient term vanishes since it is a perfect differential integrated around a closed curve. The last term in the integrand vanishes because the velocity is parallel to the boundary ($\mathbf{v} \cdot \mathbf{n} = 0$) so that $(\mathbf{k} \times \mathbf{v}) \cdot d\mathbf{s} = \mathbf{k} \cdot (\mathbf{v} \times d\mathbf{s}) = 0$.

Equation (2.21) shows that the circulation of the velocity vector around the boundary of the domain is independent of time.

Applying Stokes' theorem to (2.21) we have

$$\frac{\partial}{\partial t} \oint_{\partial R} \mathbf{v} \cdot d\mathbf{s} = \frac{\partial}{\partial t} \iint_R \mathbf{k} \cdot (\nabla \times \mathbf{v}) \, dx \, dy = \frac{\partial}{\partial t} \iint_R \zeta \, dx \, dy = \frac{\partial \bar{\zeta}}{\partial t} = 0$$

which states that the area averaged relative vorticity in the domain is constant with time. Since the Coriolis parameter is constant (in time and space), we also have

$$\overline{\frac{\partial(\zeta+f)}{\partial t}} = 0,$$

or the area averaged absolute vorticity over the domain is independent of time.

In summary then, the physical model we have developed can be described by the following equations:

$$\frac{\partial u}{\partial t} + u \frac{\partial u}{\partial x} + v \frac{\partial u}{\partial y} + \frac{\partial \phi}{\partial x} - fv = 0,$$

$$\frac{\partial v}{\partial t} + u \frac{\partial v}{\partial x} + v \frac{\partial v}{\partial y} + \frac{\partial \phi}{\partial y} + fu = 0,$$

$$\frac{\partial h}{\partial t} + \nabla \cdot (h\nabla) = 0,$$

which collectively are the shallow-water equations and describe conservation of mass and horizontal momentum;

$$\frac{dq}{dt} = \frac{\partial q}{\partial t} + \nabla \cdot \nabla q = 0,$$

which is the conservation of potential vorticity, and

$$\frac{\partial}{\partial t} \overline{[\frac{1}{2}h|\nabla|^2 + g(\frac{1}{2}h^2 + hh_s)]} = 0, \quad \frac{\partial}{\partial t} \iint_R h dx dy = 0,$$

$$\frac{\partial}{\partial t} \overline{(\frac{1}{2}hq^2)} = 0,$$

$$\overline{\frac{\partial(\zeta+f)}{\partial t}} = 0,$$

which state, respectively, that area averaged total mechanical energy, total mass, area averaged potential enstrophy and absolute vorticity are conserved if the fluid is confined to an area with solid walls.

In the next chapter we derive the numerical scheme used to integrate the shallow-water equations. These conservation laws play an important role in the formulation of the finite difference approximations used in the integration.

CHAPTER 3

THE NUMERICAL MODEL

During the relatively short history of numerical weather prediction, numerous methods of finite differencing the barotropic primitive equations in both time and space have been developed (see for example Grammelvedt 1969). Most of these methods were created for atmospheric models without terrain effects, that is, free-surface models where the fluid was overlying a flat domain.

For the study undertaken here however, terrain effects play a major role in determining the flow. For example, as pointed out in Chapter 2, conservation of potential vorticity dictates that if fluid columns are stretched, then absolute vorticity must increase. Thus, if fluid is flowing over a mountain range, its vorticity must decrease on ascent and increase again as it descends on the lee side. This phenomenon is responsible for the development of the "lee trough", an area of low pressure often observed along the east slopes of the Rocky Mountains.

Consequently, most of the finite difference methods in the literature that deal with the shallow-water model are of no use here. In fact, using some of the standard finite differencing schemes in the presence of high terrain can lead to useless results due to large truncation errors.

Furthermore, schemes which don't retain the conservation properties possessed by the original differential equations can exhibit nonlinear computational instability, whereby, through nonlinear interactions, energy cascades into wavelengths too small to be represented on the finite difference grid, ultimately causing the integration to become unstable.

However, a scheme has been developed by Arakawa and Lamb (1981) which can be used with terrain. Like the differential equations themselves, the scheme conserves potential enstrophy and total energy and is immune to nonlinear computational instability. This scheme differences the space derivatives in the shallow-water equations while leaving the time derivatives in continuous form. This has the added advantage of allowing one to independently choose a time differencing scheme which possesses desirable properties.

SPACE DISCRETIZATION

The discretization in space of the shallow-water equations is now presented and follows the development in Arakawa and Lamb (1981).

The (spatial) finite difference approximations are developed on what is known in the meteorology literature as the C grid (Arakawa and Lamb 1977) which defines the variables over the gridpoints as shown in Figure 1. The grid-

length d is the distance between two gridpoints carrying the same variable.

•q	...	•q	•v	•q	•v	•q	...	•q	2L
•	•	•	•	•	•	•	•	•	•
•q	...	•q	•v	•q	•v	•q	...	•q	2n+2
•u	...	•u	•h	•u	•h	•u	...	•u	2n+1
•q	...	•q	•v	•q	•v	•q	...	•q	2n
•u	...	•u	•h	•u	•h	•u	...	•u	2n-1
•q	...	•q	•v	•q	•v	•q	...	•q	2n-2
•	•	•	•	•	•	•	•	•	•
•q	...	•q	•v	•q	•v	•q	...	•q	0
0	...	2m-2	2m-1	2m	2m+1	2m+2	...	2L	

Figure 1. The distribution of variables over the grid domain (after Arakawa and Lamb 1981).

The variables h , u , v , and q were defined in Chapter 2. Note from the figure that h is defined only at gridpoints where i and j are both odd, q only at gridpoints where i and j are both even, etc.

The equations to be differenced on the grid are equations (2.9) and (2.14) written in slightly different form as follows. Let $\mathbf{v}^* = h\mathbf{v} = hu\mathbf{i} + hv\mathbf{j} = u^*\mathbf{i} + v^*\mathbf{j}$, $K = \frac{1}{2}|\mathbf{v}^*|^2$ (kinetic energy per unit mass) and recall that $hq = \zeta + f$. Then equation (2.9) can be written as

$$\frac{\partial h}{\partial t} + \nabla \cdot \mathbf{v}^* = 0, \quad (3.1)$$

and (2.14) as

$$\frac{\partial \mathbf{v}}{\partial t} + \nabla(K+\Phi) + \mathbf{qk} \times \mathbf{v}^* = 0,$$

or in component form as

$$\frac{\partial u}{\partial t} - \mathbf{q} \mathbf{v}^* + \frac{\partial}{\partial x}(K+\Phi) = 0 \quad (3.2)$$

$$\frac{\partial v}{\partial t} + \mathbf{q} u^* + \frac{\partial}{\partial y}(K+\Phi) = 0. \quad (3.3)$$

Throughout the derivation, all space derivatives will be approximated using standard second order centered differences. Thus, equation (3.1) is approximated by

$$\frac{\partial}{\partial t} h_{2m+1, 2n+1} + (\nabla \cdot \mathbf{v}^*)_{2m+1, 2n+1} = 0 \quad (3.4)$$

where

$$\begin{aligned} (\nabla \cdot \mathbf{v}^*)_{2m+1, 2n+1} = & \frac{1}{d} \left[u_{2m+2, 2n+1}^* - u_{2m, 2n+1}^* \right. \\ & \left. + v_{2m+1, 2n+2}^* - v_{2m+1, 2n}^* \right] \end{aligned} \quad (3.5)$$

and

$$u_{2m, 2n+1}^* \equiv [h^{(u)} u]_{2m, 2n+1} ; v_{2m+1, 2n}^* \equiv [h^{(v)} v]_{2m+1, 2n} \quad (3.6)$$

$h^{(u)}$ and $h^{(v)}$ are h values at the u and v points respectively. Their form will be obtained later by requiring energy conservation in the scheme.

A general approximation to (3.2) and (3.3) can be written as

$$\begin{aligned}
 & \frac{\partial}{\partial t} u_{2m,2n+1} - \alpha_{2m,2n+1} v_{2m+1,2n+2}^* - \beta_{2m,2n+1} v_{2m-1,2n+2}^* \\
 & - \gamma_{2m,2n+1} v_{2m-1,2n}^* - \delta_{2m,2n+1} v_{2m+1,2n}^* \\
 & + \epsilon_{2m+1,2n+1} u_{2m+2,2n+1}^* - \epsilon_{2m-1,2n+1} u_{2m-2,2n+1}^* \\
 & + \frac{1}{d} \left[(K+\Phi)_{2m+1,2n+1} - (K+\Phi)_{2m-1,2n+1} \right] = 0 \quad (3.7)
 \end{aligned}$$

and

$$\begin{aligned}
 & \frac{\partial}{\partial t} v_{2m+1,2n} + \gamma_{2m+2,2n+1} u_{2m+2,2n+1}^* + \delta_{2m,2n+1} u_{2m,2n+1}^* \\
 & + \alpha_{2m,2n-1} u_{2m,2n-1}^* + \beta_{2m+2,2n-1} u_{2m+2,2n-1}^* \\
 & + \psi_{2m+1,2n+1} v_{2m+1,2n+2}^* - \psi_{2m+1,2n-1} v_{2m+1,2n-2}^* \\
 & + \frac{1}{d} \left[(K+\Phi)_{2m+1,2n+1} - (K+\Phi)_{2m+1,2n-1} \right] = 0, \quad (3.8)
 \end{aligned}$$

where the various weighting factors ($\alpha, \beta, \gamma, \delta, \epsilon, \psi$) are linear combinations of q values to be specified later by requiring the scheme to conserve potential enstrophy.

Before finding expressions for the as yet undefined

variables in (3.6), (3.7), and (3.8), a lemma will be stated without proof (the conclusions are just summation by parts or variations thereof) which will be very useful in the subsequent analysis.

LEMMA 3.1

Let the variables a_{2k} ($0 \leq k \leq L$) and b_{2k+1} ($0 \leq k \leq L-1$) be defined on a set of gridpoints. If $a_0 = a_{2L} = 0$ then

$$\sum_{k=1}^{L-1} a_{2k} (b_{2k+1} - b_{2k-1}) = - \sum_{k=0}^{L-1} b_{2k+1} (a_{2k+2} - a_{2k}); \quad (3.9)$$

$$\sum_{k=1}^{L-1} a_{2k} (a_{2k+2} b_{2k+1} - a_{2k-2} b_{2k-1}) = 0; \quad (3.10)$$

$$\sum_{k=1}^{L-1} a_{2k} (b_{2k+1} + b_{2k-1}) = \sum_{k=0}^{L-1} b_{2k+1} (a_{2k} + a_{2k+2}). \quad (3.11)$$

Throughout what follows, it will be assumed that the finite difference grid has rigid walls as boundaries. Thus all normal velocities will be zero at their respective boundary gridpoints implying that u^* and v^* vanish as well, regardless of how $h^{(u)}$ and $h^{(v)}$ are defined.

The first constraint imposed on the finite difference

equations is that they conserve total mechanical energy when there is no flow into or out of the grid, analogous to what was done using the differential equations. Recall that the differential form of this conservation law is

$$\frac{\partial}{\partial t} \iint_R [\frac{1}{2}h(u^2+v^2) + g(\frac{1}{2}h^2 + hh_s)] dx dy = 0. \quad (3.12)$$

We now derive the discrete version of (3.12), and in doing so will obtain expressions for $h^{(u)}$, $h^{(v)}$, and K . To start, multiply (3.7) by $u_{2m,2n+1}^*$ and sum the product over all of the interior u points in the grid. This gives

$$\begin{aligned} & \sum_{n=0}^{L-1} \sum_{m=1}^{L-1} \left\{ \left[u_{2m,2n+1}^* \frac{\partial}{\partial t} u_{2m,2n+1} \right] + \left[u_{2m,2n+1}^* \right. \right. \\ & \times \left[\epsilon_{2m+1,2n+1} u_{2m+2,2n+1}^* - \epsilon_{2m-1,2n+1} u_{2m-2,2n+1}^* \right] \\ & + \frac{1}{d} \left\{ u_{2m,2n+1}^* \left[(K+\phi)_{2m+1,2n+1} - (K+\phi)_{2m-1,2n+1} \right] \right\} \\ & + \left[u_{2m,2n+1}^* \left[-\alpha_{2m,2n+1} v_{2m+1,2n+2}^* - \beta_{2m,2n+1} v_{2m-1,2n+2}^* \right. \right. \\ & \left. \left. - \gamma_{2m,2n+1} v_{2m-1,2n}^* - \delta_{2m,2n+1} v_{2m+1,2n}^* \right] \right\} = 0. \quad (3.13) \end{aligned}$$

Application of (3.10) with $a=u^*$ and $b=\epsilon$ shows that the term in brackets involving ϵ is zero since u^* vanishes at all boundary gridpoints where it is defined. Using (3.9) to rewrite the $K+\phi$ terms along with the fact that $\left[u^* \frac{\partial u}{\partial t}\right] =$

$\frac{\partial}{\partial t} \left[\frac{1}{2} h(u) u^2 \right] - \left[\frac{1}{2} u \frac{\partial h(u)}{\partial t} \right]$, equation (3.13) becomes

$$\begin{aligned} & \sum_{n=0}^{L-1} \sum_{m=1}^{L-1} \left\{ \frac{\partial}{\partial t} \left[\frac{1}{2} h(u) u^2 \right]_{2m, 2n+1} - \left[\frac{1}{2} u \frac{\partial h(u)}{\partial t} \right]_{2m, 2n+1} \right. \\ & + \left[u^*_{2m, 2n+1} \left(-\alpha_{2m, 2n+1} v^*_{2m+1, 2n+2} - \beta_{2m, 2n+1} v^*_{2m-1, 2n+2} \right. \right. \\ & \left. \left. - \gamma_{2m, 2n+1} v^*_{2m-1, 2n} - \delta_{2m, 2n+1} v^*_{2m+1, 2n} \right) \right] \left. \right\} \\ & - \frac{1}{d} \sum_{n=0}^{L-1} \sum_{m=0}^{L-1} (K+\phi)_{2m+1, 2n+1} \left[u^*_{2m+2, 2n+1} - u^*_{2m, 2n+1} \right] = 0. \end{aligned} \tag{3.14}$$

Next multiply (3.8) by $v^*_{2m+1, 2n}$ and sum this product over all the interior v points. Then using (3.9) and (3.10) in Lemma 3.1 to rearrange the $K+\phi$ and eliminate the ψ terms and recalling that v^* is zero at boundary gridpoints where it is defined gives

$$\begin{aligned}
& \sum_{m=0}^{L-1} \sum_{n=1}^{L-1} \left\{ \frac{\partial}{\partial t} \left[\frac{1}{2} h(v) v^2 \right]_{2m+1, 2n} - \left[\frac{1}{2} v \frac{2\partial h(v)}{\partial t} \right]_{2m+1, 2n} \right. \\
& + \left[v_{2m+1, 2n}^* \left(\gamma_{2m+2, 2n+1} u_{2m+2, 2n+1}^* + \delta_{2m, 2n+1} u_{2m, 2n+1}^* \right. \right. \\
& \left. \left. + \alpha_{2m, 2n-1} u_{2m, 2n-1}^* + \beta_{2m+2, 2n-1} u_{2m+2, 2n-1}^* \right) \right] \left. \right\} \\
& - \frac{1}{d} \sum_{m=0}^{L-1} \sum_{n=0}^{L-1} (K+\Phi)_{2m+1, 2n+1} \left[v_{2m+1, 2n+2}^* - v_{2m+1, 2n}^* \right] = 0.
\end{aligned} \tag{3.15}$$

Since u^* and v^* are assumed to vanish at all boundary gridpoints where they are defined, we can add the $m=0$ and $n=0$ terms to the first sums in (3.14) and (3.15) respectively. The indices of the resulting sums then run over the same values so that (3.14) and (3.15) may be added together to obtain

$$\begin{aligned}
& \sum_{n=0}^{L-1} \sum_{m=0}^{L-1} \left\{ \frac{\partial}{\partial t} \left[\frac{1}{2} h(u) u^2 \right]_{2m, 2n+1} + \frac{\partial}{\partial t} \left[\frac{1}{2} h(v) v^2 \right]_{2m+1, 2n} \right. \\
& \left. - \left[\frac{1}{2} u \frac{2\partial h(u)}{\partial t} \right]_{2m, 2n+1} - \left[\frac{1}{2} v \frac{2\partial h(v)}{\partial t} \right]_{2m+1, 2n} \right\}
\end{aligned}$$

$$- \frac{1}{d} \left[(K+\Phi)_{2m+1,2n+1} \left(u_{2m+2,2n+1}^* - u_{2m,2n+1}^* + v_{2m+1,2n+2}^* - v_{2m+1,2n}^* \right) \right] = 0.$$

Note that the $\alpha, \beta, \gamma, \delta$ terms have exactly cancelled since they are equal but oppositely signed in (3.14) and (3.15). Furthermore, using (3.4) and (3.5) this becomes

$$\begin{aligned} & \sum_{n=0}^{L-1} \sum_{m=0}^{L-1} \left[\frac{\partial}{\partial t} \left\{ \left[\frac{1}{2} h^{(u)} u^2 \right]_{2m,2n+1} + \left[\frac{1}{2} h^{(v)} v^2 \right]_{2m+1,2n} \right\} \right. \\ & \left. - \left[\Phi(\nabla \cdot \mathbf{v}^*) \right]_{2m+1,2n+1} \right] = \sum_{n=0}^{L-1} \sum_{m=0}^{L-1} \left\{ \left[K(\nabla \cdot \mathbf{v}^*) \right]_{2m+1,2n+1} \right. \\ & \left. + \left[\frac{1}{2} u \frac{2\partial h^{(u)}}{\partial t} \right]_{2m,2n+1} + \left[\frac{1}{2} v \frac{2\partial h^{(v)}}{\partial t} \right]_{2m+1,2n} \right\} \quad (3.16) \end{aligned}$$

Now $\frac{\partial}{\partial t} \left[\frac{1}{2} gh^2 + gh h_s \right] = \Phi \frac{\partial h}{\partial t}$. Multiplying (3.4) by $\Phi_{2m+1,2n+1}$ and summing the resulting product over all the h points yields

$$\sum_{n=0}^{L-1} \sum_{m=0}^{L-1} \left[\frac{\partial}{\partial t} \left[\frac{1}{2} gh^2 + gh h_s \right] + \Phi \nabla \cdot \mathbf{v}^* \right]_{2m+1,2n+1} = 0. \quad (3.17)$$

Next, adding (3.16) to (3.17), gives

$$\begin{aligned}
& \frac{\partial}{\partial t} \sum_{n=0}^{L-1} \sum_{m=0}^{L-1} \left\{ \left[\frac{1}{2} h^{(u)} u^2 \right]_{2m, 2n+1} + \left[\frac{1}{2} h^{(v)} v^2 \right]_{2m+1, 2n} \right. \\
& \quad \left. + \left[g \left(\frac{1}{2} h^2 + h h_s \right) \right]_{2m+1, 2n+1} \right\} \\
& = \sum_{n=0}^{L-1} \sum_{m=0}^{L-1} \left\{ \left[K(\mathbf{v} \cdot \mathbf{v}^*) \right]_{2m+1, 2n+1} + \left[\frac{1}{2} u^2 \frac{\partial h^{(u)}}{\partial t} \right]_{2m, 2n+1} \right. \\
& \quad \left. + \left[\frac{1}{2} v^2 \frac{\partial h^{(v)}}{\partial t} \right]_{2m+1, 2n} \right\}. \tag{3.18}
\end{aligned}$$

The left hand side of (3.18) is the discrete version of the left hand side of (3.12), that is, the local time change of the total mechanical energy in the grid. Thus the necessary and sufficient condition for this quantity to be conserved in the finite difference scheme is that the right hand side of (3.18) vanish identically. To achieve this make the following definitions:

$$\begin{aligned}
h_{2m, 2n+1}^{(u)} & \equiv \frac{1}{2} \left[h_{2m+1, 2n+1} + h_{2m-1, 2n+1} \right] = \bar{h}_{2m, 2n+1}^i \\
h_{2m+1, 2n}^{(v)} & \equiv \frac{1}{2} \left[h_{2m+1, 2n+1} + h_{2m+1, 2n-1} \right] = \bar{h}_{2m+1, 2n}^j
\end{aligned} \tag{3.19}$$

(Note that $\bar{\cdot}_i$ and $\bar{\cdot}_j$ are just averaging operators using the two surrounding points in the x and y directions respectively.)

Use of equations (3.19) and (3.4) allows the right hand side of (3.18) to be written as

$$\sum_{n=0}^{L-1} \sum_{m=0}^{L-1} \left\{ \left[\frac{1}{2} u^2 \frac{\partial}{\partial t} \left[\bar{h}^i \right] \right]_{2m, 2n+1} + \left[\frac{1}{2} v^2 \frac{\partial}{\partial t} \left[\bar{h}^j \right] \right]_{2m+1, 2n} - \left[K \frac{\partial h}{\partial t} \right]_{2m+1, 2n+1} \right\}. \quad (3.20)$$

Using (3.11) in Lemma 3.1 and recalling that $u_{0, 2n+1} = 0$, the first term in (3.20) becomes

$$\begin{aligned} & \sum_{n=0}^{L-1} \sum_{m=0}^{L-1} \frac{1}{2} u^2_{2m, 2n+1} \frac{\partial}{\partial t} \left[\bar{h}^i \right]_{2m, 2n+1} \\ &= \sum_{n=0}^{L-1} \sum_{m=0}^{L-1} \frac{1}{4} u^2_{2m, 2n+1} \left[\frac{\partial}{\partial t} \left[h_{2m+1, 2n+1} \right] + \frac{\partial}{\partial t} \left[h_{2m-1, 2n+1} \right] \right] \\ &= \sum_{n=0}^{L-1} \sum_{m=0}^{L-1} \frac{\partial}{\partial t} \left[h_{2m+1, 2n+1} \right] \times \frac{1}{2} \left[\frac{1}{2} u^2_{2m, 2n+1} + \frac{1}{2} u^2_{2m+2, 2n+1} \right] \\ &= \sum_{n=0}^{L-1} \sum_{m=0}^{L-1} \frac{\partial}{\partial t} \left[h_{2m+1, 2n+1} \right] \times \left(\frac{1}{2} u^2 \right)^i_{2m+1, 2n+1}. \end{aligned}$$

With an analogous argument for the second term, equation (3.20) becomes

$$\sum_{n=0}^{L-1} \sum_{m=0}^{L-1} \frac{\partial}{\partial t} h_{2m+1, 2n+1} \left[\overline{(ku^2)^i} + \overline{(kv^2)^j} - K \right]_{2m+1, 2n+1}.$$

This sum will vanish identically if and only if

$$K_{2m+1, 2n+1} \equiv \left[\overline{(ku^2)^i} + \overline{(kv^2)^j} \right]_{2m+1, 2n+1}. \quad (3.21)$$

Hence, using the definitions in (3.19) and (3.21), the right hand side of (3.18) is zero, and the numerical scheme disallows (in exact arithmetic) any increase or decrease in the total mechanical energy over the grid as long as the quantities u and v vanish at boundary gridpoints where they are defined. Note that $\alpha, \beta, \gamma, \delta, \epsilon, \psi$ did not enter into this part of the derivation. They will be determined next by requiring the difference scheme to conserve potential enstrophy, $\frac{1}{2} h q^2$.

We begin by recalling that the differential form of the absolute vorticity is

$$\zeta + f = \frac{\partial v}{\partial x} - \frac{\partial u}{\partial y} + f.$$

Define the absolute vorticity at q points in the gridded domain using centered differences as

$$(\zeta+f)_{2m,2n} = \frac{1}{d} \left[v_{2m+1,2n} - v_{2m-1,2n} - u_{2m,2n+1} + u_{2m,2n-1} \right] + f_{2m,2n} \quad (3.22)$$

where $f_{2m,2n}$ = constant for all m and n (see Chapter 4 for definition). The potential vorticity is then defined as

$$q_{2m,2n} = \frac{(\zeta+f)_{2m,2n}}{h_{2m,2n}^{(q)}}, \quad (3.23)$$

where $h_{2m,2n}^{(q)}$ is the value of h at a q point in the grid and is a linear combination of the surrounding h 's, to be prescribed later.

To derive the finite difference vorticity equation we use (3.23) to write

$$(\zeta+f)_{2m,2n} = \left[h^{(q)} q \right]_{2m,2n}$$

and then take the partial time derivative of (3.22) yielding

$$\frac{\partial}{\partial t} \left[h^{(q)} q \right]_{2m,2n} = \frac{1}{d} \left[\frac{\partial}{\partial t} v_{2m+1,2n} - \frac{\partial}{\partial t} v_{2m-1,2n} - \frac{\partial}{\partial t} u_{2m,2n+1} + \frac{\partial}{\partial t} u_{2m,2n-1} \right]. \quad (3.24)$$

We now substitute the appropriate forms of (3.7) and (3.8) into (3.24) to obtain the vorticity equation for the scheme:

$$\begin{aligned}
\frac{\partial}{\partial t} [h^{(q)} q]_{2m, 2n} &= \frac{1}{d} \left[v_{2m+1, 2n}^* \left[\alpha_{2m, 2n-1} - \delta_{2m, 2n+1} \right] \right. \\
&+ v_{2m-1, 2n}^* \left[\beta_{2m, 2n-1} - \gamma_{2m, 2n+1} \right] + v_{2m+1, 2n-2}^* \left[\delta_{2m, 2n-1} \right. \\
&+ \psi_{2m+1, 2n-1} \left. \right] - v_{2m+1, 2n+2}^* \left[\psi_{2m+1, 2n+1} + \alpha_{2m, 2n+1} \right] \\
&- v_{2m-1, 2n+2}^* \left[\beta_{2m, 2n+1} - \psi_{2m-1, 2n+1} \right] + v_{2m-1, 2n-2}^* \\
&\times \left[\gamma_{2m, 2n-1} - \psi_{2m-1, 2n-1} \right] - u_{2m+2, 2n+1}^* \left[\gamma_{2m+2, 2n+1} \right. \\
&- \epsilon_{2m+1, 2n+1} \left. \right] - u_{2m+2, 2n-1}^* \left[\epsilon_{2m+1, 2n-1} + \beta_{2m+2, 2n-1} \right] \\
&+ u_{2m-2, 2n+1}^* \left[\delta_{2m-2, 2n+1} - \epsilon_{2m-1, 2n+1} \right] + u_{2m-2, 2n-1}^* \\
&\times \left[\epsilon_{2m-1, 2n-1} + \alpha_{2m-2, 2n-1} \right] - u_{2m, 2n+1}^* \left[\delta_{2m, 2n+1} \right. \\
&\left. - \gamma_{2m, 2n+1} \right] - u_{2m, 2n-1}^* \left[\alpha_{2m, 2n-1} - \beta_{2m, 2n-1} \right] \left. \right]. \quad (3.25)
\end{aligned}$$

Note that the $(K+\phi)$ terms are absent from (3.25) which is consistent with the differential equation, since they appear there as a gradient vector which vanishes under the curl operator.

Recalling that $\alpha, \beta, \gamma, \delta, \epsilon, \psi$ are linear combinations of q values, we can write them in a general form as

$$\begin{aligned} \alpha_{2m, 2n+1} &= \hat{\alpha}_1 q_{2m+2, 2n+2} + \hat{\alpha}_2 q_{2m, 2n+2} \\ &+ \hat{\alpha}_3 q_{2m, 2n} + \hat{\alpha}_4 q_{2m+2, 2n} \end{aligned} \quad (3.26a)$$

$$\begin{aligned} \beta_{2m, 2n+1} &= \hat{\beta}_1 q_{2m, 2n+2} + \hat{\beta}_2 q_{2m-2, 2n+2} \\ &+ \hat{\beta}_3 q_{2m-2, 2n} + \hat{\beta}_4 q_{2m, 2n} \end{aligned} \quad (3.26b)$$

$$\begin{aligned} \gamma_{2m, 2n+1} &= \hat{\gamma}_1 q_{2m, 2n+2} + \hat{\gamma}_2 q_{2m-2, 2n+2} \\ &+ \hat{\gamma}_3 q_{2m-2, 2n} + \hat{\gamma}_4 q_{2m, 2n} \end{aligned} \quad (3.26c)$$

$$\begin{aligned} \delta_{2m, 2n+1} &= \hat{\delta}_1 q_{2m+2, 2n+2} + \hat{\delta}_2 q_{2m, 2n+2} \\ &+ \hat{\delta}_3 q_{2m, 2n} + \hat{\delta}_4 q_{2m+2, 2n} \end{aligned} \quad (3.26d)$$

$$\begin{aligned} \epsilon_{2m+1, 2n+1} &= \hat{\epsilon}_1 q_{2m+2, 2n+2} + \hat{\epsilon}_2 q_{2m, 2n+2} \\ &+ \hat{\epsilon}_3 q_{2m, 2n} + \hat{\epsilon}_4 q_{2m+2, 2n} \end{aligned} \quad (3.26e)$$

$$\begin{aligned} \psi_{2m+1, 2n+1} &= \hat{\psi}_1 q_{2m+2, 2n+2} + \hat{\psi}_2 q_{2m, 2n+2} \\ &+ \hat{\psi}_3 q_{2m, 2n} + \hat{\psi}_4 q_{2m+2, 2n} \end{aligned} \quad (3.26f)$$

Also let

$$\begin{aligned}
 A &= \sum_{k=1}^4 \hat{\alpha}_k, & B &= \sum_{k=1}^4 \hat{\beta}_k, & C &= \sum_{k=1}^4 \hat{\gamma}_k, \\
 D &= \sum_{k=1}^4 \hat{\delta}_k, & E &= \sum_{k=1}^4 \hat{\epsilon}_k, & F &= \sum_{k=1}^4 \hat{\psi}_k.
 \end{aligned} \tag{3.27}$$

Recall that in the physical model potential vorticity is conserved, that is, $\frac{dq}{dt} = \frac{\partial q}{\partial t} + \mathbf{v} \cdot \nabla q = 0$. If q were constant in space this would require that $\frac{\partial q}{\partial t} = 0$. Imposing this constraint on (3.25), noting that

$$\frac{\partial}{\partial t} [h(q)q]_{2m,2n} = q_{2m,2n} \frac{\partial h(q)}{\partial t} + h(q) \frac{\partial q}{\partial t}$$

and using equations (3.26) and (3.27) gives

$$\begin{aligned}
 \frac{\partial h(q)}{\partial t} &= \frac{1}{d} \left[(A-D)v_{2m+1,2n}^* + (B-C)v_{2m-1,2n}^* \right. \\
 &+ (D+F)v_{2m+1,2n-2}^* - (F+A)v_{2m+1,2n+2}^* - (B-F)v_{2m-1,2n+2}^* \\
 &+ (C-F)v_{2m-1,2n-2}^* - (C-E)u_{2m+2,2n+1}^* - (E+B)u_{2m+2,2n-1}^* \\
 &+ (D-E)u_{2m-2,2n+1}^* + (E+A)u_{2m-2,2n-1}^* - (D-C)u_{2m,2n+1}^* \\
 &\left. - (A-B)u_{2m,2n-1}^* \right]. \tag{3.28}
 \end{aligned}$$

Now (3.28) gives an expression for the local time rate of change of the fluid depth at a q point, which must be consistent with (3.4) no matter how we define $h^{(q)}$. For simplicity and geometric symmetry choose

$$h_{2m,2n}^{(q)} \equiv \frac{1}{4} \left[h_{2m+1,2n+1} + h_{2m-1,2n+1} + h_{2m-1,2n-1} + h_{2m+1,2n-1} \right]. \quad (3.29)$$

Taking the local time derivative of (3.29) and using (3.4) and (3.5) yields

$$\begin{aligned} \frac{\partial}{\partial t} h_{2m,2n}^{(q)} = & - \frac{1}{4d} \left[u_{2m+2,2n+1}^* + v_{2m+1,2n+2}^* - u_{2m-2,2n+1}^* \right. \\ & + v_{2m-1,2n+2}^* - u_{2m-2,2n-1}^* - v_{2m-1,2n-2}^* \\ & \left. + u_{2m+2,2n-1}^* - v_{2m+1,2n-2}^* \right]. \quad (3.30) \end{aligned}$$

Thus, equating like coefficients in (3.28) and (3.30),

$$\begin{aligned} A-D &= 0 ; & B-C &= 0 ; & C-D &= 0 ; & B-A &= 0 ; \\ D+F &= \frac{1}{4} ; & D-E &= \frac{1}{4} ; & A+E &= \frac{1}{4} ; & C-F &= \frac{1}{4} ; \\ C-E &= \frac{1}{4} ; & E+B &= \frac{1}{4} ; & F+A &= \frac{1}{4} ; & B-F &= \frac{1}{4} ; \end{aligned}$$

from which we conclude that $A = B = C = D = \frac{1}{4}$ and $E = F = 0$.

Next, substituting (3.26) into (3.25) and gathering like terms of the q 's yields

$$\begin{aligned}
\frac{\partial}{\partial t} [h^{(q)} q]_{2m, 2n} &= \frac{1}{d} \left\{ q_{2m, 2n} \left[-[\hat{\psi}_3 + \hat{\alpha}_3] v_{2m+1, 2n+2}^* \right. \right. \\
&- [\hat{\beta}_4 - \hat{\psi}_4] v_{2m-1, 2n+2}^* + [\hat{\alpha}_2 - \hat{\delta}_3] v_{2m+1, 2n}^* \\
&+ [\hat{\beta}_1 - \hat{\gamma}_4] v_{2m-1, 2n}^* + [\hat{\delta}_2 + \hat{\psi}_2] v_{2m+1, 2n-2}^* \\
&+ [\hat{\gamma}_1 - \hat{\psi}_1] v_{2m-1, 2n-2}^* - [\hat{\gamma}_3 - \hat{\epsilon}_3] u_{2m+2, 2n+1}^* \\
&- [\hat{\delta}_3 - \hat{\gamma}_4] u_{2m, 2n+1}^* + [\hat{\delta}_4 - \hat{\epsilon}_4] u_{2m-2, 2n+1}^* \\
&- [\hat{\epsilon}_2 + \hat{\beta}_2] u_{2m+2, 2n-1}^* - [\hat{\alpha}_2 - \hat{\beta}_1] u_{2m, 2n-1}^* \\
&\left. + [\hat{\epsilon}_1 + \hat{\alpha}_1] u_{2m-2, 2n-1}^* \right] \\
&+ q_{2m+2, 2n} \left[-[\hat{\psi}_4 + \hat{\alpha}_4] v_{2m+1, 2n+2}^* + [\hat{\alpha}_1 - \hat{\delta}_4] v_{2m+1, 2n}^* \right. \\
&+ [\hat{\delta}_1 + \hat{\psi}_1] v_{2m+1, 2n-2}^* - [\hat{\gamma}_4 - \hat{\epsilon}_4] u_{2m+2, 2n+1}^* \\
&\left. - \hat{\delta}_4 u_{2m, 2n+1}^* - [\hat{\epsilon}_1 + \hat{\beta}_1] u_{2m+2, 2n-1}^* - \hat{\alpha}_1 u_{2m, 2n-1}^* \right]
\end{aligned}$$

$$\begin{aligned}
& + q_{2m-2, 2n} \left[-\left[\hat{\beta}_3 - \hat{\psi}_3\right] v_{2m-1, 2n+2}^* + \left[\hat{\beta}_2 - \hat{\gamma}_3\right] v_{2m-1, 2n}^* \right. \\
& \quad + \left[\hat{\gamma}_2 - \hat{\psi}_2\right] v_{2m-1, 2n-2}^* + \left[\hat{\delta}_3 - \hat{\epsilon}_3\right] u_{2m-2, 2n+1}^* \\
& \quad \left. + \left[\hat{\epsilon}_2 + \hat{\alpha}_2\right] u_{2m-2, 2n-1}^* + \hat{\gamma}_3 u_{2m, 2n+1}^* + \hat{\beta}_2 u_{2m, 2n-1}^* \right] \\
& + q_{2m, 2n+2} \left[-\left[\hat{\psi}_2 + \hat{\alpha}_2\right] v_{2m+1, 2n+2}^* - \left[\hat{\beta}_1 - \hat{\psi}_1\right] v_{2m-1, 2n+2}^* \right. \\
& \quad - \hat{\delta}_2 v_{2m+1, 2n}^* - \hat{\gamma}_1 v_{2m-1, 2n}^* - \left[\hat{\delta}_2 - \hat{\gamma}_1\right] u_{2m, 2n+1}^* \\
& \quad \left. - \left[\hat{\gamma}_2 - \hat{\epsilon}_2\right] u_{2m+2, 2n+1}^* + \left[\hat{\delta}_1 - \hat{\epsilon}_1\right] u_{2m-2, 2n+1}^* \right] \\
& + q_{2m, 2n-2} \left[\hat{\alpha}_3 v_{2m+1, 2n}^* + \hat{\beta}_4 v_{2m-1, 2n}^* - \left[\hat{\alpha}_3 - \hat{\beta}_4\right] u_{2m, 2n-1}^* \right. \\
& \quad + \left[\hat{\delta}_3 + \hat{\psi}_3\right] v_{2m+1, 2n-2}^* + \left[\hat{\gamma}_4 - \hat{\psi}_4\right] v_{2m-1, 2n-2}^* \\
& \quad \left. - \left[\hat{\epsilon}_3 + \hat{\beta}_3\right] u_{2m+2, 2n-1}^* + \left[\hat{\epsilon}_4 + \hat{\alpha}_4\right] u_{2m-2, 2n-1}^* \right] \\
& + q_{2m+2, 2n+2} \left[-\left[\hat{\psi}_1 + \hat{\alpha}_1\right] v_{2m+1, 2n+2}^* - \hat{\delta}_1 v_{2m+1, 2n}^* \right. \\
& \quad \left. - \left[\hat{\gamma}_1 - \hat{\epsilon}_1\right] u_{2m+2, 2n+1}^* - \hat{\delta}_1 u_{2m, 2n+1}^* \right]
\end{aligned}$$

$$\begin{aligned}
& + q_{2m-2, 2n-2} \left[\hat{\beta}_3 v_{2m-1, 2n}^* + \left[\hat{\gamma}_3 - \hat{\psi}_3 \right] v_{2m-1, 2n-2}^* \right. \\
& \quad \left. + \hat{\beta}_3 u_{2m, 2n-1}^* + \left[\hat{\alpha}_3 + \hat{\epsilon}_3 \right] u_{2m-2, 2n-1}^* \right] \\
& + q_{2m-2, 2n+2} \left[- \left[\hat{\beta}_2 - \hat{\psi}_2 \right] v_{2m-1, 2n+2}^* - \hat{\gamma}_2 v_{2m-1, 2n}^* \right. \\
& \quad \left. + \hat{\gamma}_2 u_{2m, 2n+1}^* + \left[\hat{\delta}_2 - \hat{\epsilon}_2 \right] u_{2m-2, 2n+1}^* \right] \\
& + q_{2m+2, 2n-2} \left[\hat{\alpha}_4 v_{2m+1, 2n}^* + \left[\hat{\delta}_4 + \hat{\psi}_4 \right] v_{2m+1, 2n-2}^* \right. \\
& \quad \left. - \left[\hat{\epsilon}_4 + \hat{\beta}_4 \right] u_{2m+2, 2n-1}^* - \hat{\alpha}_4 u_{2m, 2n-1}^* \right] \Big\}. \quad (3.31)
\end{aligned}$$

Letting $b_{2m, 2n}$ be the coefficient of $q_{2m, 2n}$ and $a_{2m+2i', 2n+2j'}$ the coefficient of $q_{2m+2i', 2n+2j'}$, equation (3.31) can be written as

$$\begin{aligned}
\frac{\partial}{\partial t} [h^{(q)} q]_{2m, 2n} &= \frac{1}{d} \left[\sum' \left[a_{2m, 2n}^{2m+2i', 2n+2j'} q_{2m+2i', 2n+2j'} \right] \right. \\
& \quad \left. + b_{2m, 2n} q_{2m, 2n} \right], \quad (3.32)
\end{aligned}$$

where \sum' = $\sum_{i'=-1}^1 \sum_{j'=-1}^1$ excluding the term $i'=j'=0$.

If q is constant over the entire grid, (3.32) becomes

$$\frac{\partial}{\partial t} h_{2m,2n}(q) = \frac{1}{d} \left[b_{2m,2n} + \sum' a_{2m,2n}^{2m+2i', 2n+2j'} \right] \quad (3.33)$$

Multiplication of (3.33) by $-q_{2m,2n}$ and addition of this result to (3.32) gives

$$\begin{aligned} & \frac{\partial}{\partial t} \left[h(q) q \right]_{2m,2n} - q_{2m,2n} \frac{\partial}{\partial t} h_{2m,2n}(q) \\ &= \frac{1}{d} \left[\sum' \left[a_{2m,2n}^{2m+2i', 2n+2j'} q_{2m+2i', 2n+2j'} \right. \right. \\ & \quad \left. \left. - a_{2m,2n}^{2m+2i', 2n+2j'} q_{2m,2n} \right] \right] \quad (3.34) \end{aligned}$$

Noting that the left hand side of (3.34) is equivalent to $h_{2m,2n}(q) \frac{\partial}{\partial t} q_{2m,2n}$, we multiply (3.34) by $q_{2m,2n}$ and add it to

$\frac{1}{2} q_{2m,2n}^2$ times (3.33) to obtain

$$\begin{aligned}
\frac{\partial}{\partial t} \left[\frac{1}{2} h^{(q)} q^2 \right]_{2m, 2n} &= \frac{1}{2} q_{2m, 2n}^2 \frac{\partial h^{(q)}}{\partial t} + \left[h^{(q)} q \right]_{2m, 2n} \\
\times \frac{\partial q}{\partial t} &= \frac{1}{d} \left[\sum' \left[a_{2m, 2n}^{2m+2i', 2n+2j'} q_{2m+2i', 2n+2j'} q_{2m, 2n} \right. \right. \\
&\quad \left. \left. - \frac{1}{2} a_{2m, 2n}^{2m+2i', 2n+2j'} q_{2m, 2n}^2 \right] + \frac{1}{2} b_{2m, 2n} q_{2m, 2n}^2 \right] \quad (3.35)
\end{aligned}$$

Since the left hand side of (3.35) is the local time rate of change of potential enstrophy at a q point in the grid, summing this equation over all q points gives the local time rate of change of the (discrete) total potential enstrophy over the grid. Conservation of this value is expressed as

$$\frac{\partial}{\partial t} \sum_{n=1}^{L-1} \sum_{m=1}^{L-1} \left[\frac{1}{2} h^{(q)} q^2 \right]_{2m, 2n} = 0$$

requiring

$$\begin{aligned}
&\sum_{n=1}^{L-1} \sum_{m=1}^{L-1} \left[\sum' \left[a_{2m, 2n}^{2m+2i', 2n+2j'} q_{2m+2i', 2n+2j'} q_{2m, 2n} \right] \right. \\
&\quad \left. + \frac{1}{2} q_{2m, 2n}^2 \left[b_{2m, 2n} - \sum' a_{2m, 2n}^{2m+2i', 2n+2j'} \right] \right] = 0,
\end{aligned}$$

which will be satisfied by forcing

$$\sum_{n=1}^{L-1} \sum_{m=1}^{L-1} \sum' a_{2m,2n}^{2m+2i', 2n+2j'} q_{2m+2i', 2n+2j'} q_{2m,2n} \quad (3.36)$$

and

$$\sum_{n=1}^{L-1} \sum_{m=1}^{L-1} \left[\frac{1}{2} q_{2m,2n}^2 \left[b_{2m,2n} - \sum' a_{2m,2n}^{2m+2i', 2n+2j'} \right] \right] \quad (3.37)$$

to vanish for arbitrary u^* and v^* .

Due to the nature of the sum in (3.36), the q terms will appear twice but with different "a" coefficients each time. For example, at the $(2m,2n)$ gridpoint, the term involving the $(2m+2i', 2n+2j')$ coefficient will be

$$a_{2m,2n}^{2m+2i', 2n+2j'} q_{2m+2i', 2n+2j'} q_{2m,2n}$$

Furthermore, at the $(2m+2i', 2n+2j')$ gridpoint, the term involving the $(2m,2n) = [(2m+2i')-2i', (2n+2j')-2j']$ coefficient will be

$$a_{2m+2i', 2n+2j'}^{2m, 2n} q_{2m,2n} q_{2m+2i', 2n+2j'}$$

By choosing these "a" coefficients to be equal but oppositely signed, when summing over all the q gridpoints (3.36) will vanish. Thus we require

$$a_{2m,2n}^{2m+2i',2n+2j'} = -a_{2m+2i',2n+2j'}^{2m,2n}.$$

First, with $i'=-1$ and $j'=0$ we want $a_{2m-2,2n}^{2m,2n} = -a_{2m,2n}^{2m-2,2n}$.

The terms involving $a_{2m-2,2n}^{2m,2n}$ in equation (3.31) are

$$\begin{aligned} & - \left[\hat{\psi}_4 + \hat{\alpha}_4 \right] v_{2m-1,2n+2}^* + \left[\hat{\alpha}_1 - \hat{\delta}_4 \right] v_{2m-1,2n}^* \\ & + \left[\hat{\delta}_1 + \hat{\psi}_1 \right] v_{2m-1,2n-2}^* - \left[\hat{\gamma}_4 - \hat{\epsilon}_4 \right] u_{2m,2n+1}^* \\ & - \hat{\delta}_4 u_{2m-2,2n+1}^* - \left[\hat{\epsilon}_1 + \hat{\beta}_1 \right] u_{2m,2n-1}^* - \hat{\alpha}_1 u_{2m-2,2n-1}^* \end{aligned}$$

while those involving $a_{2m,2n}^{2m-2,2n}$ are

$$\begin{aligned} & - \left[\hat{\beta}_3 - \hat{\psi}_3 \right] v_{2m-1,2n+2}^* + \left[\hat{\beta}_2 - \hat{\gamma}_3 \right] v_{2m-1,2n}^* \\ & + \left[\hat{\gamma}_2 - \hat{\psi}_2 \right] v_{2m-1,2n-2}^* + \hat{\gamma}_3 u_{2m,2n+1}^* + \hat{\beta}_2 u_{2m,2n-1}^* \\ & + \left[\hat{\delta}_3 - \hat{\epsilon}_3 \right] u_{2m-2,2n+1}^* + \left[\hat{\epsilon}_2 + \hat{\alpha}_2 \right] u_{2m-2,2n-1}^* \end{aligned}$$

Equating like coefficients yields the following seven equations

$$\begin{aligned} \hat{\delta}_4 + \hat{\epsilon}_3 - \hat{\delta}_3 &= 0 & \hat{\delta}_1 + \hat{\gamma}_2 + \hat{\psi}_1 - \hat{\psi}_2 &= 0 \\ \hat{\beta}_1 + \hat{\epsilon}_1 - \hat{\beta}_2 &= 0 & \hat{\beta}_3 + \hat{\psi}_4 + \hat{\alpha}_4 - \hat{\psi}_3 &= 0 \end{aligned} \tag{3.38}$$

$$\begin{aligned}
\hat{\gamma}_4 - \hat{\epsilon}_4 - \hat{\gamma}_3 &= 0 & \hat{\beta}_2 - \hat{\gamma}_3 + \hat{\alpha}_1 - \hat{\delta}_4 &= 0 \\
\hat{\alpha}_1 - \hat{\alpha}_2 - \hat{\epsilon}_2 &= 0 & &
\end{aligned}
\tag{cont'd} \tag{3.38}$$

Next, with $j'=1$ and $i'=0$ we want $a_{2m,2n+2}^{2m,2n} = -a_{2m,2n}^{2m,2n+2}$.

Following a similar procedure as above gives

$$\begin{aligned}
\hat{\psi}_2 + \hat{\alpha}_2 - \hat{\alpha}_3 &= 0 & \hat{\epsilon}_3 + \hat{\beta}_3 - \hat{\epsilon}_2 + \hat{\gamma}_2 &= 0 \\
\hat{\beta}_1 - \hat{\psi}_1 - \hat{\beta}_4 &= 0 & \hat{\alpha}_3 - \hat{\beta}_4 + \hat{\delta}_2 - \hat{\gamma}_1 &= 0 \\
\hat{\delta}_2 - \hat{\psi}_3 - \hat{\delta}_3 &= 0 & \hat{\epsilon}_4 + \hat{\alpha}_4 - \hat{\epsilon}_1 + \hat{\delta}_1 &= 0 \\
\hat{\psi}_4 - \hat{\gamma}_4 + \hat{\gamma}_1 &= 0 & &
\end{aligned}
\tag{3.39}$$

Next, with $i'=1$ and $j'=1$ we want $a_{2m+2,2n+2}^{2m,2n} = -a_{2m,2n}^{2m+2,2n+2}$.

As before we get

$$\begin{aligned}
\hat{\psi}_1 + \hat{\alpha}_1 - \hat{\beta}_3 &= 0 & \hat{\delta}_1 - \hat{\gamma}_3 + \hat{\psi}_3 &= 0 \\
\hat{\gamma}_1 - \hat{\epsilon}_1 - \hat{\beta}_3 &= 0 & \hat{\delta}_1 - \hat{\alpha}_1 - \hat{\epsilon}_3 &= 0
\end{aligned}
\tag{3.40}$$

Last, with $i'=-1$ and $j'=1$ we want $a_{2m-2,2n-2}^{2m,2n} = -a_{2m,2n}^{2m-2,2n-2}$.

Thus,

$$\begin{aligned}
 \hat{\beta}_2 - \hat{\psi}_2 - \hat{\alpha}_4 &= 0 & \hat{\gamma}_2 - \hat{\delta}_4 - \hat{\psi}_4 &= 0 \\
 \hat{\gamma}_2 - \hat{\epsilon}_4 - \hat{\beta}_4 &= 0 & \hat{\delta}_2 - \hat{\epsilon}_2 - \hat{\alpha}_4 &= 0
 \end{aligned}
 \tag{3.41}$$

To force (3.37) to vanish, it is sufficient to have

$$b_{2m,2n} = \sum' a_{2m,2n}^{2m+2i', 2n+2j'}$$

Thus we set the coefficient of $q_{2m,2n}$ equal to the sum of the coefficients of the remaining q terms in (3.31), recalling that the condition is to hold for arbitrary u^* and v^* . This yields, upon using (3.27) and the known values of A, B, C, D, E , and F :

$$\begin{aligned}
 \hat{\alpha}_2 - \hat{\delta}_3 &= \hat{\beta}_1 - \hat{\gamma}_4 = 0 & \hat{\delta}_3 - \hat{\gamma}_4 &= \hat{\alpha}_2 - \hat{\beta}_1 = 0 \\
 \hat{\delta}_2 + \hat{\psi}_2 &= \hat{\gamma}_1 - \hat{\psi}_1 = \frac{1}{8} & \hat{\alpha}_3 + \hat{\psi}_3 &= \hat{\beta}_4 - \hat{\psi}_4 = \frac{1}{8} \\
 \hat{\gamma}_3 - \hat{\epsilon}_3 &= \hat{\delta}_4 - \hat{\epsilon}_4 = \frac{1}{8} & \hat{\beta}_2 + \hat{\epsilon}_2 &= \hat{\alpha}_1 + \hat{\epsilon}_1 = \frac{1}{8}
 \end{aligned}
 \tag{3.42}$$

Equations (3.38)-(3.42) form a nonhomogeneous linear system of 34 algebraic equations in 24 unknowns. Gaussian elimination reduces this system to the following under-determined system of 20 equations in 24 unknowns:

$$\begin{aligned}
\hat{\alpha}_1 + \hat{\epsilon}_1 &= \frac{1}{8} ; & \hat{\alpha}_2 - \hat{\beta}_1 &= 0 ; & \hat{\beta}_1 - \hat{\delta}_3 &= 0 ; \\
\hat{\beta}_2 + \hat{\epsilon}_2 &= \frac{1}{8} ; & \hat{\beta}_4 - \hat{\psi}_4 &= \frac{1}{8} ; & \hat{\gamma}_1 - \hat{\psi}_1 &= \frac{1}{8} ; \\
\hat{\gamma}_3 - \hat{\epsilon}_3 &= \frac{1}{8} ; & \hat{\delta}_3 - \hat{\gamma}_4 &= 0 ; & \hat{\delta}_2 + \hat{\psi}_2 &= \frac{1}{8} ; \\
\hat{\delta}_4 - \hat{\epsilon}_4 &= \frac{1}{8} ; & \hat{\epsilon}_3 + \hat{\epsilon}_4 &= \frac{-1}{12} ; & \hat{\psi}_2 + \hat{\psi}_3 &= \frac{1}{12} ; \\
\hat{\alpha}_3 + \hat{\psi}_3 &= \frac{1}{8} ; & \hat{\alpha}_4 + \hat{\beta}_3 - \hat{\psi}_3 + \hat{\psi}_4 &= 0 ; \\
\hat{\delta}_1 - \hat{\epsilon}_3 + \hat{\psi}_3 &= \frac{1}{8} ; & \hat{\delta}_3 - \hat{\epsilon}_3 - \hat{\epsilon}_4 &= \frac{1}{8} ; \\
\hat{\beta}_3 + \hat{\gamma}_2 - \hat{\epsilon}_2 + \hat{\epsilon}_3 &= 0 ; & \hat{\gamma}_2 + \hat{\delta}_1 + \hat{\psi}_1 - \hat{\psi}_2 &= 0 ; \\
\hat{\epsilon}_1 + \hat{\epsilon}_2 + \hat{\epsilon}_3 + \hat{\epsilon}_4 &= 0 ; & -\hat{\psi}_1 + \hat{\psi}_2 + \hat{\psi}_3 - \hat{\psi}_4 &= \frac{1}{6} ,
\end{aligned}$$

which can be solved in terms of $\hat{\epsilon}_1$, $\hat{\epsilon}_3$, $\hat{\psi}_1$, and $\hat{\psi}_3$ to obtain

$$\begin{aligned}
\hat{\alpha}_1 &= \frac{1}{8} - \hat{\epsilon}_1 ; & \hat{\alpha}_2 &= \frac{1}{24} ; & \hat{\alpha}_3 &= \frac{1}{8} - \hat{\psi}_3 ; & \hat{\alpha}_4 &= \frac{-1}{24} + \hat{\epsilon}_1 + \hat{\psi}_3 \\
\hat{\beta}_1 &= \frac{1}{24} ; & \hat{\beta}_2 &= \frac{1}{24} + \hat{\epsilon}_1 ; & \hat{\beta}_3 &= \frac{1}{8} + \hat{\psi}_1 - \hat{\epsilon}_1 ; & \hat{\beta}_4 &= \frac{1}{24} - \hat{\psi}_1 \\
\hat{\gamma}_1 &= \frac{1}{8} + \hat{\psi}_1 ; & \hat{\gamma}_2 &= \frac{-1}{24} - \hat{\psi}_1 - \hat{\epsilon}_3 ; & \hat{\gamma}_3 &= \frac{1}{8} + \hat{\epsilon}_3 ; & \hat{\gamma}_4 &= \frac{1}{24} \\
\hat{\delta}_1 &= \frac{1}{8} + \hat{\epsilon}_3 - \hat{\psi}_3 ; & \hat{\delta}_2 &= \frac{1}{24} + \hat{\psi}_3 ; & \hat{\delta}_3 &= \frac{1}{24} ; & \hat{\delta}_4 &= \frac{1}{24} - \hat{\epsilon}_3 \\
\hat{\epsilon}_2 &= \frac{1}{12} - \hat{\epsilon}_1 ; & \hat{\epsilon}_4 &= \frac{-1}{12} - \hat{\epsilon}_3 ; & \hat{\psi}_2 &= \frac{1}{12} - \hat{\psi}_3 ; & \hat{\psi}_4 &= \frac{-1}{12} - \hat{\psi}_1 .
\end{aligned}$$

To keep ϵ and ψ symmetric, arbitrarily choose

$$\hat{\epsilon}_1 = \frac{1}{24}, \quad \hat{\epsilon}_3 = \frac{-1}{24}, \quad \hat{\psi}_1 = \frac{-1}{24}, \quad \hat{\psi}_3 = \frac{1}{24},$$

which allows complete specification of $\alpha, \beta, \gamma, \delta, \epsilon, \psi$ in (3.26) as

$$\alpha_{2m, 2n+1} = \frac{1}{24} \left[2q_{2m+2, 2n+2}^+ + q_{2m, 2n+2}^+ + 2q_{2m, 2n}^+ + q_{2m+2, 2n} \right]$$

$$\beta_{2m, 2n+1} = \frac{1}{24} \left[q_{2m, 2n+2}^+ + 2q_{2m-2, 2n+2}^+ + q_{2m-2, 2n}^+ + 2q_{2m, 2n} \right]$$

$$\gamma_{2m, 2n+1} = \frac{1}{24} \left[2q_{2m, 2n+2}^+ + q_{2m-2, 2n+2}^+ + 2q_{2m-2, 2n}^+ + q_{2m, 2n} \right]$$

$$\delta_{2m, 2n+1} = \frac{1}{24} \left[q_{2m+2, 2n+2}^+ + 2q_{2m, 2n+2}^+ + q_{2m, 2n}^+ + 2q_{2m+2, 2n} \right]$$

$$\epsilon_{2m+1, 2n+1} = \frac{1}{24} \left[q_{2m+2, 2n+2}^+ + q_{2m, 2n+2}^- + q_{2m, 2n}^- + q_{2m+2, 2n} \right]$$

$$\psi_{2m+1, 2n+1} = \frac{1}{24} \left[-q_{2m+2, 2n+2}^+ + q_{2m, 2n+2}^+ + q_{2m, 2n}^- + q_{2m+2, 2n} \right]$$

By substituting (3.19), (3.21) and the above expressions for $\alpha, \beta, \gamma, \delta, \epsilon$, and ψ into (3.4)-(3.8), we obtain the following system of ordinary differential equations:

$$\frac{\partial}{\partial t} h_{2m+1, 2n+1} = \frac{-1}{2d} \left[\left(h_{2m+1, 2n+1} + h_{2m+3, 2n+1} \right) u_{2m+2, 2n+1} \right.$$

$$\left. - \left(h_{2m-1, 2n+1} + h_{2m+1, 2n+1} \right) u_{2m, 2n+1} \right]$$

$$+ \left[\left(h_{2m+1, 2n+3} + h_{2m+1, 2n+1} \right) v_{2m+1, 2n+2} \right]$$

$$- \left[h_{2m+1,2n+1} + h_{2m+1,2m-1} \right] v_{2m+1,2n} \quad (3.43)$$

at the gridpoints $3 \leq 2m+1 \leq 2L-3$ and $3 \leq 2n+1 \leq 2L-3$;

$$\begin{aligned} \frac{\partial}{\partial t} u_{2m,2n+1} = & \frac{1}{48} \left[\left(2q_{2m+2,2n+2} + q_{2m,2n+2} + 2q_{2m,2n} \right. \right. \\ & + \left. \left. q_{2m+2,2n} \right) \left(h_{2m+1,2n+3} + h_{2m+1,2n+1} \right) v_{2m+1,2n+2} \right. \\ & + \left. \left(q_{2m,2n+2} + 2q_{2m-2,2n+2} + q_{2m-2,2n} + 2q_{2m,2n} \right) \right. \\ & \times \left. \left(h_{2m-1,2n+3} + h_{2m-1,2n+1} \right) v_{2m-1,2n+2} + \left(2q_{2m,2n+2} \right. \right. \\ & + \left. \left. q_{2m-2,2n+2} + 2q_{2m-2,2n} + q_{2m,2n} \right) \left(h_{2m-1,2n+1} \right. \right. \\ & + \left. \left. h_{2m-1,2n-1} \right) v_{2m-1,2n} + \left(q_{2m+2,2n+2} + 2q_{2m,2n+2} \right. \right. \\ & + \left. \left. q_{2m,2n} + 2q_{2m+2,2n} \right) \left(h_{2m+1,2n+1} + h_{2m+1,2n-1} \right) v_{2m+1,2n} \right. \\ & + \left. \left(q_{2m,2n+2} + q_{2m-2,2n+2} - q_{2m-2,2n} - q_{2m,2n} \right) \right. \\ & \times \left. \left(h_{2m-1,2n+1} + h_{2m-3,2n+1} \right) u_{2m-2,2n+1} - \left(q_{2m+2,2n+2} \right. \right. \\ & + \left. \left. q_{2m,2n+2} - q_{2m,2n} - q_{2m+2,2n} \right) \left(h_{2m+1,2n+1} \right. \right. \\ & + \left. \left. h_{2m+3,2n+1} \right) u_{2m+2,2n+1} \right] - \frac{1}{d} \left[\frac{1}{4} \left(u_{2m+2,2n+1}^2 + u_{2m,2n+1}^2 \right. \right. \\ & + \left. \left. v_{2m+1,2n+2}^2 + v_{2m+1,2n}^2 \right) + g \left(h + h_s \right)_{2m+1,2n+1} \right] \end{aligned}$$

$$\begin{aligned}
& + \frac{1}{d} \left[\frac{1}{4} \left(u_{2m-2, 2n+1}^2 + u_{2m, 2n+1}^2 + v_{2m-1, 2n+2}^2 + v_{2m-1, 2n}^2 \right) \right. \\
& \left. + g \left(h + h_s \right)_{2m-1, 2n+1} \right], \tag{3.44}
\end{aligned}$$

at the gridpoints $2 \leq 2m \leq 2L-2$ and $3 \leq 2n+1 \leq 2L-3$;

$$\begin{aligned}
\frac{\partial}{\partial t} v_{2m+1, 2n} &= \frac{-1}{48} \left[\left(2q_{2m+2, 2n+2} + q_{2m, 2n+2} + 2q_{2m, 2n} \right. \right. \\
& + \left. \left. q_{2m+2, 2n} \right) \left(h_{2m+1, 2n+1} + h_{2m+3, 2n+1} \right) u_{2m+2, 2n+1} \right. \\
& + \left. \left(q_{2m+2, 2n+2} + 2q_{2m, 2n+2} + q_{2m, 2n} + 2q_{2m+2, 2n} \right) \right. \\
& \times \left. \left(h_{2m+1, 2n+1} + h_{2m-1, 2n+1} \right) u_{2m, 2n+1} + \left(2q_{2m+2, 2n} \right. \right. \\
& + \left. \left. q_{2m, 2n} + 2q_{2m, 2n-2} + q_{2m+2, 2n-2} \right) \left(h_{2m-1, 2n-1} \right. \right. \\
& + \left. \left. h_{2m+1, 2n-1} \right) u_{2m, 2n-1} + \left(q_{2m+2, 2n} + 2q_{2m, 2n} + q_{2m, 2n-2} \right. \right. \\
& + \left. \left. 2q_{2m+2, 2n-2} \right) \left(h_{2m+1, 2n-1} + h_{2m+3, 2n-1} \right) u_{2m+2, 2n-1} \right. \\
& + \left. \left(-q_{2m+2, 2n+2} + q_{2m, 2n+2} + q_{2m, 2n} - q_{2m+2, 2n} \right) \right. \\
& \times \left. \left(h_{2m+1, 2n+3} + h_{2m+1, 2n+1} \right) v_{2m+1, 2n+2} - \left(-q_{2m+2, 2n} \right. \right. \\
& + \left. \left. q_{2m, 2n} + q_{2m, 2n-2} - q_{2m+2, 2n-2} \right) \left(h_{2m+1, 2n-1} \right. \right. \\
& + \left. \left. h_{2m+1, 2n-3} \right) v_{2m+1, 2n-2} \right] - \frac{1}{d} \left[\frac{1}{4} \left(u_{2m, 2n+1}^2 + u_{2m+2, 2n+1}^2 \right) \right.
\end{aligned}$$

$$\begin{aligned}
& + v_{2m+1,2n}^2 + v_{2m+1,2n+2}^2 + g[h + h_s]_{2m+1,2n+1} \\
& + \frac{1}{d} \left[\frac{1}{4} (u_{2m,2n-1}^2 + u_{2m+2,2n-1}^2 + v_{2m+1,2n}^2 + v_{2m+1,2n-2}^2) \right. \\
& \left. + g[h + h_s]_{2m+1,2n-1} \right], \tag{3.45}
\end{aligned}$$

at the gridpoints $3 \leq 2m+1 \leq 2L-3$ and $2 \leq 2n \leq 2L-2$.

Note that (3.43)-(3.45) are only defined at interior gridpoints, that is, the first row of each variable along all the boundaries are determined by the boundary conditions, to be discussed in Chapter 4. In addition, there is no forecast equation for the potential vorticity. Instead, the diagnostic equations (3.23) and (3.29) are used at each time step to determine these values.

Figure 2 shows the computational stencils for equations (3.43)-(3.45). As can be seen, quite a bit of smoothing in space is implicit in the equations, especially those for the u and v wind components. Actual experiments seem to suggest that this smoothing helps to damp unwanted computational noise without the use of an explicit space filtering scheme.

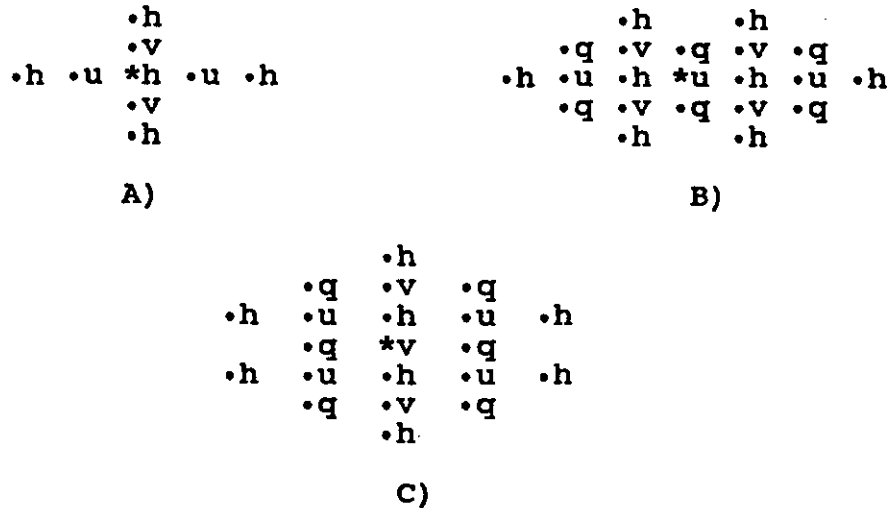


Figure 2. Computational stencils. A) eqn. (3.43);
B) eqn. (3.44); C) eqn. (3.45)

TIME DISCRETIZATION

With the original differential equations now discretized in space, it is necessary to find a proper time differencing scheme to perform the integrations. Since numerous methods are available (Kurihara 1965, Lilly 1965, Young 1968), the proper choice will depend on what properties we want the scheme to possess.

Initial experiments were conducted with the usual leap-frog or centered scheme. Results with rigid wall boundary conditions indicated that the computational mode quickly contaminated the physical solution near the boundaries, and lead to fairly rapid computational instability. Decreasing the timestep only served to delay the onset of the instabil-

ity. Applying an artificial filter kept the instability under control but dissipated the energy in the system unrealistically. Knowing that the terrain in the model would generate perturbations similar to those created by the rigid walls and thus possibly excite the computational mode, the idea of using a multistep method was abandoned.

Before describing the one step method that was implemented in this study (Kurihara and Tripoli 1976), note that equations (3.43)-(3.45) can be written symbolically as

$$y'(t) = F(y(t))$$

where y symbolizes the dependent variables u , v , or h and F represents the right hand sides.

Letting y_n denote the approximate value of $y(t_n)$, the method can be written as

$$Y_{n+1} = Y_n + \Delta t \left[(1-w)F(Y_n) + wF\left[Y_n + \Delta t F(Y_n)\right] \right], \quad (3.46)$$

where w is a weight parameter to be chosen later. Note that the method is an iterative scheme and requires two F evaluations per timestep. This is certainly a disadvantage when compared to the leapfrog scheme which only requires one F evaluation per timestep, but the scheme does possess other desirable properties, most notably no computational mode.

Equation (3.46) describes a first or second order time

differencing method depending on the choice of w . To see this, let τ_{n+1} be the local truncation error at the $(n+1)$ th time step. Then

$$\tau_{n+1} = \frac{y(t_{n+1}) - y(t_n)}{\Delta t} - (1-w)F(y(t_n)) - wF\left[y(t_n) + \Delta t F(y(t_n))\right].$$

Assuming that y and F are sufficiently smooth, we can expand the first and last terms in Taylor series about the points t_n and $y(t_n)$ respectively to obtain

$$\begin{aligned} \tau_{n+1} = & \frac{1}{\Delta t} \left[y(t_n) + y'(t_n)\Delta t + \frac{1}{2} y''(t_n)\Delta t^2 + O(\Delta t^3) \right. \\ & \left. - y(t_n) \right] - F(y(t_n)) + wF(y(t_n)) - w \left[F(y(t_n)) \right. \\ & \left. + F'(y(t_n))\Delta t + O(\Delta t^2) \right], \end{aligned}$$

which simplifies to

$$\tau_{n+1} = \left[\frac{1}{2} - w \right] F'(y(t_n))\Delta t + O(\Delta t^2).$$

Thus the time differencing scheme (3.46) is first order unless $w = 1/2$ (in which case the scheme becomes the modified Euler scheme).

To determine some of the properties of this time differencing scheme, consider the following Cauchy problem:

$$\frac{\partial z}{\partial t} + c \frac{\partial z}{\partial x} = 0, \quad z(x, 0) = e^{ikx} \quad (3.47)$$

where $c > 0$, the phase speed, is constant and $k = 2\pi/\lambda$ is the wavenumber (λ wavelength). By assuming a general solution of the form $z(x, t) = \xi(t)e^{ikx}$, substitution into (3.47) yields the following initial value problem

$$\frac{d\xi}{dt} = -ikc\xi, \quad \xi(0) = 1. \quad (3.48)$$

The exact solution to this problem is $\xi(t) = e^{-ikct}$ giving $z(x, t) = e^{ik(x-ct)}$ as the exact solution to equation (3.47), which describes a sinusoidal wave of constant amplitude 1 and wavenumber k moving to the right along the x -axis at constant phase speed c .

Now using (3.46) to approximate the solution to (3.48) yields

$$\xi_{n+1} = \xi_n + \Delta t \left[(1-w)(-ikc\xi_n) + w(-ikc)(\xi_n + \Delta t(-ikc\xi_n)) \right]$$

which can be written as

$$\xi_{n+1} = \xi_n \left[1 - ikc\Delta t - w(kc\Delta t)^2 \right],$$

where the expression in brackets is the amplification factor of the scheme.

Hence the approximate solution to equation (3.47) is

$$z(x, n\Delta t) = \left[1 - ikc\Delta t - w(kc\Delta t)^2 \right]^n e^{ikx} .$$

For discrete values of the variable t , the exact solution to equation (3.47) can be written as $z(x, n\Delta t) = \left[e^{-ikc\Delta t} \right]^n e^{ikx}$.

From this then we see that the time differencing scheme has just approximated the exponential term in parentheses by a weighted Taylor polynomial. Notice now that instead of having a constant amplitude of unity, the wave's amplitude will change with time and is dependent upon the timestep size and the weight parameter.

To keep the amplitude of the wave from growing arbitrarily large, and thus to insure stability of the difference scheme, the magnitude of the amplification factor must be bounded above by unity, that is,

$$\sqrt{1 + (1-2w)(kc\Delta t)^2 + w^2(kc\Delta t)^4} \leq 1 . \quad (3.49)$$

Ideally we would like to have the equality hold in (3.49) since the scheme would then be neutral, neither amplifying nor damping the wave solution of (3.47). For an equation as simple as (3.47) values of w and Δt could be found to make the time differencing scheme neutral for wavenumber k . Unfortunately, equations (3.43)-(3.45) are

not this simple since they may contain many wavenumbers and phase velocities and are nonlinear. Consequently, w and Δt cannot be chosen a priori but must be chosen experimentally based on the following arguments.

It can be shown (Haltiner and Williams 1980) that a linearized version of the shallow-water equations contains three different solutions: one slow moving, low frequency meteorological solution (the one of most importance), and two fast moving, high frequency waves known as inertial-gravity waves. These high frequency waves may at times play a relatively important role in determining the flow in a domain such as that used in this study, especially in the presence of high topography. However, since their amplitudes can become quite large, both in reality and more importantly in a numerical model, we must damp them in the model in order to assure computational stability.

Kurihara and Tripoli (1976) point out that the advection terms in the shallow-water equations are usually responsible for the meteorological solution, whereas the remaining terms in the equations (Coriolis, divergence, and geopotential gradient) produce the inertial-gravity wave solutions. Thus it would be desirable to have the time differencing scheme damp the high frequency waves but preserve the amplitude of the meteorologically significant waves as much as possible. To accomplish this task, the

scheme in (3.46) is modified and written as

$$y_{n+1} = y_n + \Delta t \left[(1-w_1)F_1(y_n) + w_1F_1[y_n + \Delta t F(y_n)] \right] \\ + \Delta t \left[(1-w_2)F_2(y_n) + w_2F_2[y_n + \Delta t F(y_n)] \right], \quad (3.50)$$

where F_1 represents the advection terms in equations (3.43)-(3.45), F_2 represents the remaining terms in the equations and $F=F_1+F_2$. Due to the nature of the space differencing scheme, the Coriolis terms are included in F_1 rather than F_2 . This does not appear to pose much of a problem since on the time and space scales dealt with in this study, Coriolis effects as they relate to inertial waves are not that important.

During the actual implementation of the scheme the following choice of the weight parameters was used: $w_2 = 1.0$ for all gridpoints and $w_1 = .5055$ for gridpoints away from the boundaries and $w_1 = 1.0$ for gridpoints near the boundaries (see Chapter 4). When $w_1 = w_2 = 1.0$, the scheme becomes what is known as the Matsuno (1966) scheme.

To get a rough idea of the damping characteristics of the actual time differencing scheme, and to show why the specific weights were chosen, consider the magnitude of the

amplification factor for the scheme (3.46), with $w=1.0$ and $w=.5055$, viz.,

$$A = \sqrt{1 - (kc\Delta t)^2 + (kc\Delta t)^4} \quad (3.51)$$

$$A = \sqrt{1 - .011(kc\Delta t)^2 + .25553025(kc\Delta t)^4} \quad (3.52)$$

respectively.

A in equation (3.51) is less than or equal to one and consequently the scheme is stable for $0 \leq kc\Delta t \leq 1$. The minimum value of A is .8660, occurring when $kc\Delta t=.7071$. Thus given a Δt , waves satisfying $kc=.7071/\Delta t$ will have their amplitude decreased by a factor of .8660 at each timestep with all other wavenumbers experiencing less damping.

For equation (3.52) stability is assured for $0 \leq kc\Delta t \leq .2075$ with the minimum value of A (maximum damping) occurring at $kc\Delta t=.1467$ and equal to .9999. In this case then, given a Δt , waves satisfying $kc=.1467/\Delta t$ will have their amplitude decreased by .9999 at each timestep with all other waves experiencing less damping.

With these results then it can be seen that the scheme defined by equation (3.50) should preserve the amplitude of waves associated with the advection terms in (3.43)-(3.45) quite well while strongly damping waves associated with the remaining terms in those equations.

SUMMARY

In conclusion, this chapter has described the method used to transform a coupled system of three partial differential equations into a set of algebraic equations through finite differencing in time and space. The discretization in space and time were done independently, yielding a first order in time, second order in space scheme. Finite differencing in space was accomplished by requiring the difference equations to retain some of the conservation properties of the original partial differential equations. Differencing in time was done in such a way as to control the noise inherent in the equations without adversely affecting the meteorological solution. The results of the discretization are equations (3.43), (3.44), (3.45) and (3.50).

Prior to actual implementation of these equations, initial and boundary conditions must be specified. This is the subject of the next chapter.

CHAPTER 4

BOUNDARY AND INITIAL CONDITIONS

The barotropic primitive equations ([2.1],[2.2],[2.9]) whose solutions we are seeking form a coupled system of three nonhomogeneous, nonlinear, hyperbolic, first order partial differential equations in the unknowns u , v , and h . Ideally, one would like to solve this set of equations on an infinite domain, giving rise to an initial value problem. Since this is often not feasible, artificial boundaries must be introduced to create a domain on which solutions can be found. This then requires the use of boundary conditions in addition to the initial conditions. From both a theoretical and practical standpoint this creates a number of difficulties. For example, how should the boundary conditions be chosen so as to make the problem well-posed? Can the boundary conditions which make the problem well-posed theoretically be implemented numerically? Should the artificial boundary physically be impermeable to the fluid (simple in theory but unrealistic for atmospheric problems) or should it be open, allowing air to flow freely through it?

Many authors, have provided theoretical solutions to this problem (Davies 1973; Elvius and Sundström 1973; Sundström 1977; Oliger and Sundström 1978). From a practical standpoint, however, a modification of the boundary con-

dition scheme developed by Perkey and Kreitzberg (1976) was chosen for this study.

Prior to implementation of this scheme, experiments were conducted using the rigid wall boundary conditions whereby the normal velocity was set to zero at all the boundary gridpoints. In addition, the potential vorticity at the boundary gridpoints was made zero. These boundary conditions very nicely proved the conservation properties of the space differencing scheme developed in Chapter 3. Stable integrations for over 30 hours of simulated time were made during which the total mass, and area averaged total energy, potential enstrophy and absolute vorticity were exactly conserved. Although the conservation properties of the finite difference scheme were displayed well using these boundary conditions, the rigid walls proved to be very effective but unrealistic reflectors of incident inertial-gravity waves.

The boundary scheme is designed to prohibit this unrealistic reflection and also to control other noise generated by the artificial boundaries. This is accomplished by creating a "sponge zone" near the edges of the domain which serves to absorb reflected waves and unwanted noise while allowing the low frequency solution to pass through relatively unimpeded.

Mathematically, the boundary conditions are implemented by modifying the time tendencies of the model prediction equations. To this end, equation (3.46) with $w=1$ is rewritten as

$$Y_{n+1} = Y_n + W(I)\Delta t \left[F(Y_n) + F\left[Y_n + W(I)\Delta t F(Y_n) \right] \right] \quad (4.1a)$$

where

$$W(I) = \begin{cases} 0.0 & \text{for } I = \text{boundary gridpoints} \\ 0.4 & \text{for } I = \text{boundary-1 gridpoints} \\ 0.7 & \text{for } I = \text{boundary-2 gridpoints} \\ 0.9 & \text{for } I = \text{boundary-3 gridpoints} \\ 1.0 & \text{for } I = \text{other interior gridpoints} \end{cases} \quad (4.1b)$$

Note that use of this scheme implies that the variables at all the boundary gridpoints remain constant throughout the integration. The boundary conditions are thus overspecified and the whole problem becomes ill-posed. This in itself leads to the creation of high frequency disturbances which propagate into the interior of the domain and can contaminate the solution. Consequently, a method of removing these disturbances as well as controlling reflected waves must be implemented to complete the boundary specification.

In their paper, Perkey and Kreitzberg (1976) suggest using a spatial smoother in the "sponge zone" to filter out

this high frequency noise before it can move into the interior of the domain. The modification of their original scheme, equation (4.1), appears to accomplish this task by exploiting the strong damping characteristics of the Matsuno (1966) time differencing scheme, thus eliminating the need for an artificial spatial smoothing device. (This is the reason for setting $w_1=w_2=1$ in equation (3.50) at grid-points near the boundary.)

With the boundary conditions now in place, it is necessary to determine the initial values of the variables before the time integration can begin. Phillips (1960) has pointed out that primitive equation models are very sensitive to the initial fields of wind and mass (equivalent to fluid depth h in our case). If these fields are not balanced at the beginning of the integration, they will try to obtain a balance during the integration through the development of high frequency inertial-gravity waves. In fact, even when the imbalance between these fields is small, these waves can completely mask the low frequency meteorological solution. Thus it is extremely important to properly initialize the model prior to beginning the integration.

Model initialization begins by placing the initial wind components (u and v) from the output of McGinley's (1989) analysis scheme onto the staggered grid (Figure 1). Initial values for the potential vorticity q are calculated through

the diagnostic equations (3.22), (3.23), and (3.29) after the initial mass field has been determined. The value of q at boundary gridpoints is zero throughout the integration.

Several methods for obtaining the initial mass field from the observed winds have been developed (e.g. Ellsaesser 1968). Many of these are quite complicated and require sophisticated procedures for their use. The method used in this study is very simple and is based on the assumption that the wind at initial time is in geostrophic balance, a steady-state flow in which the Coriolis force exactly balances the force produced by the geopotential gradient. Since we are also assuming a constant Coriolis parameter, this implies that the wind is initially nondivergent.

The assumption of geostrophic balance is not totally valid when considering motion on the space scale of this study. Other forces, not accounted for in the differential equations themselves (e.g. friction and thermal effects), can be acting on the fluid and at times can completely dominate the Coriolis force and geopotential gradient force. In addition, small scale divergence can be quite important. However, for large scale flows which are more accurately depicted by the shallow-water equations, the assumptions of nondivergence and geostrophic balance are quite good (Dutton 1986). Hence, their use here is consistent with the use of

the shallow-water model, and greatly simplify the initialization procedure.

A theorem of Helmholtz (Bourne and Kendall 1968) states that any two-dimensional vector field can be decomposed into the sum of a nondivergent part and an irrotational part, that is,

$$\mathbf{V} = (\mathbf{k} \times \nabla\psi) + \nabla\chi ,$$

where ψ is the streamfunction for the rotational part of the wind and χ is the velocity potential for the divergent portion of the wind. Since we are assuming the flow to be initially nondivergent, χ is set to zero. Thus the initial wind field can be written as

$$\mathbf{V} = u\mathbf{i} + v\mathbf{j} = \mathbf{k} \times \nabla\psi = -\mathbf{i}\frac{\partial\psi}{\partial y} + \mathbf{j}\frac{\partial\psi}{\partial x} , \quad (4.1)$$

with relative vorticity

$$\zeta = \frac{\partial v}{\partial x} - \frac{\partial u}{\partial y} = \frac{\partial^2\psi}{\partial x^2} + \frac{\partial^2\psi}{\partial y^2} = \nabla^2\psi . \quad (4.2)$$

From the geostrophic assumption, an expression for ψ is known, given by the poor man's balance equation (Elsaesser 1968) as

$$\psi = g(h+h_s)/f . \quad (4.3)$$

Here h_s is the height of the terrain above sea-level, $g = 9.8 \text{ m/sec}^2$ is the acceleration of gravity and f is the constant Coriolis parameter defined by

$$f = \frac{1}{\phi_n - \phi_s} \int_{\phi_s}^{\phi_n} 2\Omega \sin\phi \, d\phi \cong 9.2554 \times 10^{-5} \text{ sec}^{-1}.$$

ϕ_n and ϕ_s are, respectively, the latitude of the north and south boundary of the domain and Ω is the constant angular velocity of the earth.

Since the initial relative vorticity can be calculated from the initial winds, we need only find appropriate boundary conditions to solve the Poisson equation in (4.2) by a proper numerical scheme. Then, from (4.3), the initial mass field which will be in geostrophic balance with the initial winds can be found.

Perhaps the most natural boundary conditions to supplement equation (4.2) are the Neumann boundary conditions, whereby the normal derivative of ψ is prescribed. Since we are dealing with a rectangular domain, from (4.1) it is seen that this normal derivative is just equal to the tangential wind component along the boundary. However, there is a problem with this method. The Poisson equation with Neumann boundary conditions is subject to a compatibility condition,

namely, the line integral of the normal derivative of the streamfunction around the entire boundary of the domain must be equal to the double integral of the forcing function over the domain. In our case, this requires the line integral of the tangential wind component around the boundary of the domain to be equal to the double integral of the relative vorticity over the domain. With real data, this condition is not likely to be satisfied.

To avoid this difficulty we instead impose Dirichlet boundary conditions, whereby the actual value of ψ is prescribed along the boundary. This requires finding the streamfunction along the boundary prior to actually solving the Poisson equation (4.2)

Recalling that the u and v wind components are defined only at every other boundary gridpoint (see Figure 1), by using the average value at the two neighboring boundary gridpoints, we can obtain a u value for all the "missing" gridpoints (actually q gridpoints in Figure 1) along the left (west) and right (east) boundaries and a v value for all the "missing" boundary gridpoints along the top (north) and bottom (south) boundaries.

A value for $\psi_{0,0}$ is then guessed. Recalling that $u = -\frac{\partial\psi}{\partial y}$ and $v = \frac{\partial\psi}{\partial x}$, we use forward differences to calculate ψ along

the boundaries through the formulas

$$\begin{aligned}
 \psi_{0,j} &= \psi_{0,j-1} - u_{0,j-1} \Delta y && \text{west boundary} \\
 \psi_{i,2L} &= \psi_{i-1,2L} + v_{i-1,2L} \Delta x && \text{north boundary} \\
 \psi_{2L,j} &= \psi_{2L,j-1} - u_{2L,j-1} \Delta y && \text{east boundary} \\
 \psi_{i,0} &= \psi_{i-1,0} + v_{i-1,0} \Delta x && \text{south boundary}
 \end{aligned} \tag{4.4}$$

where $\Delta x = \Delta y$ is the distance between adjacent gridpoints (half the actual gridlength d on the staggered grid).

This method virtually guarantees a discontinuity in ψ along the boundary. To eliminate this discontinuity and the imbalances in the mass and wind fields that it would produce, the difference between the initial guess of $\psi_{0,0}$ and the final value of $\psi_{0,0}$ obtained after using (4.4) along the entire boundary is averaged over all the boundary gridpoints. This average is then evenly distributed among the ψ values on the boundary by executing equation (4.4) again, but this time subtracting this average difference from each calculation.

By removing the discontinuity in the streamfunction along the boundary, the original winds at boundary gridpoints are now out of balance with the streamfunction field. To correct this imbalance, the winds at boundary gridpoints are adjusted to the continuous streamfunction field by

applying the following equations along the west and east boundaries, respectively

$$u_{0,j} = \frac{\psi_{0,j-1} - \psi_{0,j+1}}{2\Delta y} ; \quad u_{2L,j} = \frac{\psi_{2L,j-1} - \psi_{2L,j+1}}{2\Delta y} ,$$

with

$$v_{i,0} = \frac{\psi_{i+1,0} - \psi_{i-1,0}}{2\Delta x} ; \quad v_{i,2L} = \frac{\psi_{i+1,2L} - \psi_{i-1,2L}}{2\Delta x}$$

applied along the south and north boundaries, respectively. The indices i and j run over the odd numbers from 1 to $2L-1$ since u and v values for the time integrations are needed at only odd grid points on the boundary.

With the appropriate boundary conditions now available, to solve equation (4.2) numerically we need only prescribe the forcing function at all the interior gridpoints. As previously mentioned, this can be done using the initial wind field. At q points in Figure 1, centered differences are used to approximate $(\partial v / \partial x - \partial u / \partial y)$. To obtain the relative vorticity at the interior u (v) gridpoints, the average value of ζ at the two nearest q points in the y (x) direction is used. At h points, the average of ζ at the four nearest q points is used.

By approximating the Laplacian with the usual centered finite differences, equation (4.2) can be written as

$$\psi_{i+1,j} + \psi_{i-1,j} + \psi_{i,j+1} + \psi_{i,j-1} - 4\psi_{i,j} = (d/2)^2 \zeta_{i,j} \quad (4.5)$$

Allowing i and j to run over all the interior gridpoints in Figure 1, and ordering the equations in the lexicographic manner from left to right and bottom to top transforms equation (4.2) into the following linear algebraic system:

$$Ax = b \quad (4.6)$$

where $x = [\psi_{1,1}, \psi_{2,1}, \dots, \psi_{2L-1,2L-1}]^t$, and b is a $(2L \times 1)$

column vector comprised of the right hand side of (4.5) and appropriate boundary values of ψ , and A is the $(2L-1) \times (2L-1)$ block tridiagonal matrix

$$\begin{bmatrix} -4 & 1 & 0 & 1 & 0 & & & \dots & & 0 \\ 1 & -4 & 1 & 0 & 1 & 0 & & \dots & & 0 \\ 0 & 1 & -4 & 1 & 0 & 1 & 0 & \dots & & 0 \\ 1 & 0 & 1 & -4 & 1 & 0 & 1 & 0 & \dots & 0 \\ 0 & 1 & 0 & 1 & -4 & 1 & 0 & 1 & 0 & \dots & 0 \\ 0 & 0 & 1 & 0 & 1 & -4 & 1 & 0 & 1 & 0 & \dots & 0 \\ 0 & & & \cdot & 0 \\ 0 & & & & \cdot & 0 \\ 0 & & & & & \cdot & \cdot & \cdot & \cdot & \cdot & \cdot & 1 \\ 0 & \dots & & & & \cdot & \cdot & \cdot & \cdot & \cdot & \cdot & 0 \\ 0 & \dots & & & & & 0 & 1 & 0 & 1 & -4 & 1 \\ 0 & \dots & & & & & & 0 & 1 & 0 & 1 & -4 \end{bmatrix} .$$

The initial approach to solving this linear system was a direct method based on fast Fourier transforms (IMSL 1987). Although extremely fast, this method proved unsuccessful. Numerical tests with very simple initial wind fields showed that unrealistic noise developed in the wind field after just a few time steps implying that the mass and wind fields were not properly balanced. For example, with an initial west wind ($u=5$ m/sec, $v=0$), the free surface of the fluid should be a plane sloping down from south to north on the grid. Using this direct method produced a plane which not only sloped down from south to north but also from east to west. Consequently, the initial mass and wind fields were out of balance and noise in the form of gravity waves developed almost immediately to try to overcome the imbalance.

The reasons for this poor performance were not clear. Roundoff error might have been the culprit based on the fact that if only half the gridpoints were used this method worked fine. Burden and Faires (1985) suggest that direct methods be replaced with iterative ones when the order of the system is greater than about 100. For the smaller systems, stability with respect to roundoff errors can be controlled by the positive definiteness and symmetry of the matrix A . Whether or not roundoff error was the cause of the problem, the direct method was abandoned and an iterative technique implemented.

The iterative technique used to solve (4.6) is the successive overrelaxation method, also known as extrapolated Liebmann relaxation (Frankel 1950). This method is very straightforward and since we are dealing with a rectangular domain, the theoretically optimum overrelaxation parameter which produces the most rapid convergence of the scheme is known.

The technique is implemented as follows. After finding ψ at all the boundary gridpoints, two dimensional linear interpolation is performed using the ψ values at the four corner boundary gridpoints to find a first guess ($n=0$) of the ψ field at interior gridpoints. The iteration process consists of finding a residual vector at the n^{th} iteration, defined by

$$\mathbf{r}^n = \mathbf{A}\mathbf{x}^n - \mathbf{b} ,$$

whose components, $r_{i,j}^n$, are computed through

$$\begin{aligned} \psi_{i+1,j}^{n-1} + \psi_{i-1,j}^n + \psi_{i,j+1}^{n-1} + \psi_{i,j-1}^n \\ - 4\psi_{i,j}^{n-1} - (d/2)^2 \zeta_{i,j} = r_{i,j}^n . \end{aligned} \quad (4.7)$$

The updated ψ values are then given by

$$\psi_{i,j}^n = \psi_{i,j}^{n-1} + \frac{\omega}{4} r_{i,j}^n,$$

where ω is the overrelaxation parameter.

It can be shown (Varga 1962) that the optimum overrelaxation parameter for this iteration is given by

$$\omega = \frac{2}{1 + \sqrt{1 - [\rho(B)]^2}},$$

where $\rho(B)$ is the spectral radius of the point Jacobi iteration matrix associated with A . In our case, $\rho(B) = \cos(\pi/110)$ so that

$$\omega = \frac{2}{1 + \sin(\pi/110)}.$$

The iteration is performed until the infinity norm of the residual vector is less than 10^{-8} , which requires around 640 iterations.

After the relaxation is complete, a ψ field is defined at all the gridpoints in Figure 1. The fluid depth is then determined at all the h points on this grid by using (4.3).

Upon completion of the above procedures, we have transformed the shallow-water equations into a set of difference equations, complete with initial and boundary conditions,

which can be numerically integrated. This integration will provide an approximate solution to the original partial differential equations, (2.1), (2.2), and (2.9).

CHAPTER 5

MODEL IMPLEMENTATION AND DISCUSSION OF RESULTS

The software developed to execute the model described in the previous chapters was written in FORTRAN-77. Excluding the graphics routines, it consists of one driver routine and 18 subprograms, for a total of just over 1200 lines of code. All calculations are performed using double precision arithmetic. A brief discussion of the execution sequence follows.

The first step in the execution is the input of the terrain. Values of the terrain height above sea level are available at all the h points on the staggered grid. There are 3025 such points. Unfortunately, using the actual terrain creates some computational instability problems which requires it to be smoothed prior to the integration. More will be said about this problem below.

After the terrain is entered, the initialization procedure discussed in Chapter 4 is executed. The value of 10^{-8} used as the stopping criteria in the relaxation routine was chosen because the initial wind data is only accurate to 7 decimal places. After the model is initialized, the actual integration is performed, using a timestep of $\Delta t=30$ seconds and a gridlength $d=10$ km. Thirty seconds was selected ex-

perimentally as the largest timestep that would allow a stable integration. Ten kilometers for the gridlength is inherent in McGinley's (1989) output. The actual grid (Figure 1) contains 111 gridpoints on a side or 12,321 total gridpoints. Since boundary values of each of the variables are held constant, we see that h is forecast at 2809 gridpoints, u and v both at 2862 gridpoints, while q is diagnosed at 2916 gridpoints. The equations are integrated for 3 hours of simulated time which amounts to 360 timesteps. Output in graphic form is produced at 1, 2, and 3 hours of simulated time. The whole numerical computation and post processing routine on a VAX 8800 computer requires about 15 minutes of real time, which is very much acceptable in an operational weather forecasting environment.

The three hour integration time was selected based on physical reasons and time constraints. Holding the boundary values of the variables constant throughout the integration is open to question. Since we have no way of updating these values during the integration, the integration period should be kept to a minimum. The lack of thermal affects in the model also suggests that the integration period be kept somewhat short. On the other hand, we would like to have a projection as far into the future as possible and would also like to have the forecast available in enough time to be used as a forecast. Execution time on the computer dictates

how far out we take the projection. Three hours seems to be an acceptable compromise between these opposing factors.

The computational instability problems concerning the terrain are now considered. The solution of equation (4.2) for the streamfunction and subsequent computation of the initial fluid depth from (4.3) will produce values of h which are negative even if the surface underlying the fluid is flat and at sea-level ($h_s(x,y) \equiv 0$). Negative values of h would imply that the atmosphere at those points is below ground, an obvious impossibility in reality. Consequently, the solution to (4.2) (which can be thought of as the free surface of the fluid) must be shifted up or down along the z -axis so as to create an atmosphere which is entirely above the ground. The amount we shift the solution up or down is determined from both physical and computational considerations as now shown.

Recall from Chapter 1 that the differential equations whose solutions we are approximating describe the motion of a shallow fluid. Pedlosky (1987) states that the term shallow implies that the ratio of the characteristic depth of the fluid to the characteristic length of horizontal motions within it (the aspect ratio) should be much less than 1. With a gridlength of 10 km, the smallest resolvable wavelength on the grid is 20 km. Using this value as the characteristic horizontal scale of motion implies that the

characteristic depth should be much less than 20 km. A 1 km depth would satisfy this constraint. Using a maximum depth of 1 km (taking into account the slope of the free surface) on test data with no terrain provided stable integrations. However, when the maximum depth was increased to 3 km the integration became unstable. Apparently a 3 km deep fluid on the horizontal scale used here is no longer shallow, implying that the physical model is no longer applicable. It would appear then that if we keep the maximum fluid depth at around 1 km, the shallowness assumption will hold, allowing stable integrations to be performed.

The actual terrain that exists on our grid ranges from over 4 km in the west central portion to around .85 km in the northeast and southeast part. If the atmosphere we create has a minimum depth of 1 km over the highest terrain, this implies that the depth over the lowest terrain is on the order of 4 km. Based on the results obtained with a 3 km maximum depth and no terrain we should expect the integration to become unstable, which is exactly what occurs. The instability occurs in the deep fluid, where high frequency gravity waves develop. From experimental evidence then, it is plausible to say that an aspect ratio "much less than 1" means that the characteristic depth here should be around 1 km.

The obvious method to alleviate this instability problem and keep the shallowness assumption valid would be to make the fluid depth over the highest terrain as small as possible. Doing this leads to two other problems. First, since the fluid depth is not constant with respect to time, in those areas where the free surface is very close to the terrain we run the risk of having the fluid depth become negative (the terrain pops out of the top of the fluid) during the time integration. Second, experiments showed that if the fluid was "too" shallow, a type of venturi effect developed in these areas and a fictitious increase in wind speed occurred. Note, in addition, that with the terrain values we have on the domain there is no way to satisfy the shallowness assumption (make the maximum fluid depth around 1 km) by vertically shifting the free surface height along the z-axis. Consequently, the terrain height has to be lowered. (If the gridlength were larger, we could use higher terrain since a deeper fluid would be allowed, but not without sacrificing horizontal resolution.)

Faced with the task of having to lower the terrain, the next concern is how to go about doing it. The use of smoothing operators (Shapiro 1970) will accomplish this task but not without detrimental side effects. To lower the terrain sufficiently requires several hundred applications of these smoothers, and while they lower the terrain, they also unrealistically change its shape by spreading it out.

Thus, some of the important terrain features which exist over short distances get spread out over larger areas, changing their effects on the flow. The method used in this study was a more shape preserving method: before placing the topography in the model, the value at each gridpoint is scaled by .4 . While lowering the terrain substantially and weakening the topography gradient (∇h_s), this method keeps the overall shape of the topography intact.

The scaled terrain ranges from roughly 1.6 km to .35 km. Assuming the free surface of the fluid is flat, setting the initial minimum fluid depth to .2 km gives a maximum depth of 1.45 km. Experiments verified that this maximum depth and scaled terrain was sufficient to satisfy the shallowness condition and also prevent computational instability under rather harsh test conditions (strong winds). The aforementioned venturi effect was minimized too. Hence, these are the values which are used in the actual integrations. Once equation (4.2) is solved for the streamfunction and the depth at all the h gridpoints is found via equation (4.3), a constant is added to all the h values which creates an initial atmosphere whose minimum depth is .2 km over the scaled terrain.

Further experimentation with the scaling factor and initial minimum fluid depth revealed that the model was quite sensitive to these parameters. For example, scaling the

terrain by .5 and making the minimum fluid .1 km led to an unstable integration.

A brief explanation of the form of the output graphics is now in order. Since the following discussion will reference the counties of Colorado, Figure 3 contains a map of Colorado with county names on it.

The dependent variables in the original partial differential equations we are solving are u , v , and h . Thus the output from the numerical integration consists of gridpoint data of these three variables on the domain shown in Figure 1. Meteorologically, this form of the solution is relatively useless. Instead, the graphical output shows gridpoint wind vectors derived as follows.

Recalling that the vector wind $\mathbf{V} = u\mathbf{i} + v\mathbf{j}$, we compute the wind vectors at every other h point in Figure 1 using

$$\mathbf{v}_{2m+1,2n+1} = iu_{2m,2n+1} + jv_{2m+1,2n}$$

The wind speed is then $|\mathbf{V}| = \sqrt{u^2 + v^2}$ and the wind direction is $\tan^{-1} \left[\frac{v}{u} \right] + c$, where c is a constant which converts the direction from mathematical polar coordinates to meteorological polar coordinates. These vectors are what appear in the output. The wind speed is determined by the number of barbs on the vectors. Each half barb represents 5 knots,

each full barb 10 knots and each flag constitutes 50 knots. A vector with no barbs indicates a wind speed less than 2.5 knots while small circles indicate wind speeds less than .5 knots. For example, a vector which contains two full barbs and one half barb would indicate a wind speed of 25 knots. The wind direction is determined by noting that the air flows along the vectors from the end with the barbs to the end without the barbs. The barbless end is positioned at the gridpoint where the wind is valid. Note that the routine used to create the graphics does not display the data for the 3 gridlines nearest all the boundaries.

An example of what occurs when the "full" terrain and an initial fluid depth of .1 km is used is shown in Figure 4. The initial wind field was a constant west wind of 20 knots over the entire grid with a minimum fluid depth of 100 meters. The figure gives the results after 10 minutes of simulated time (20 timesteps). The solution "blew up" shortly after this time. Note the fictitious increase in wind speed over eastern Grand county and western Clear Creek county. This is in the vicinity of the Continental Divide (the highest terrain on the grid) and is consequently where the fluid is most shallow. Furthermore, in the eastern part of the grid, where the fluid is the deepest, noise in the form of extremely strong winds has developed. Although not displayed, very sharp gradients in the fluid depth were

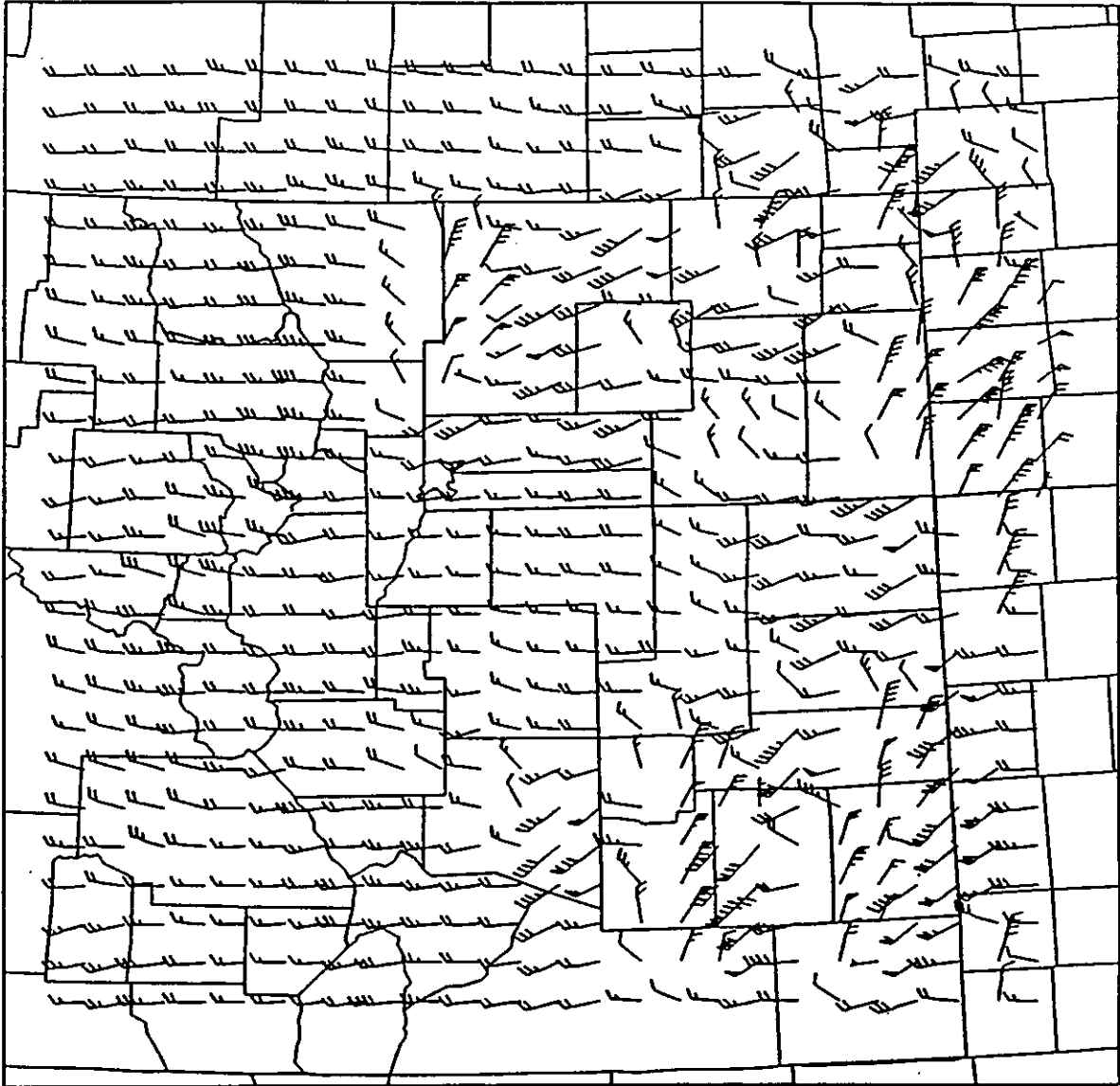


Figure 4. Results after 10 minutes of simulated time using full, unscaled terrain. See text for details.

present (inertial-gravity waves) here giving rise to the strong winds.

With the same initial wind field but the scaled terrain described above and a minimum fluid depth of .2 km, a stable integration for three hours of simulated time was carried out (not shown). The model even weakly developed the "lee trough" discussed in Chapter 3.

Figures 5-8 show integration of the equations with a well-behaved smooth initial wind field and no terrain. In Figure 5 the initial wind field is given by

$$u = 10 - (.0002y) \exp \left[\left[-.5 \times 10^{-10} \right] \left[x^2 + y^2 \right] \right]$$

$$v = (.0002x) \exp \left[\left[-.5 \times 10^{-10} \right] \left[x^2 + y^2 \right] \right] ,$$

which describes a cyclonic vortex embedded in a constant westerly flow of 20 knots. Cyclonic here means that the flow around the vortex is counterclockwise. Intuitively, since there is no friction or terrain, one would expect this vortex to propagate to the east with the mean flow and not change shape. Figures 6-8 show, respectively, the wind pattern after 1, 2, and 3 hours of simulated time. The numerical solution supports this intuition. The phase speed of the vortex is about 20 knots and its shape changes very lit-

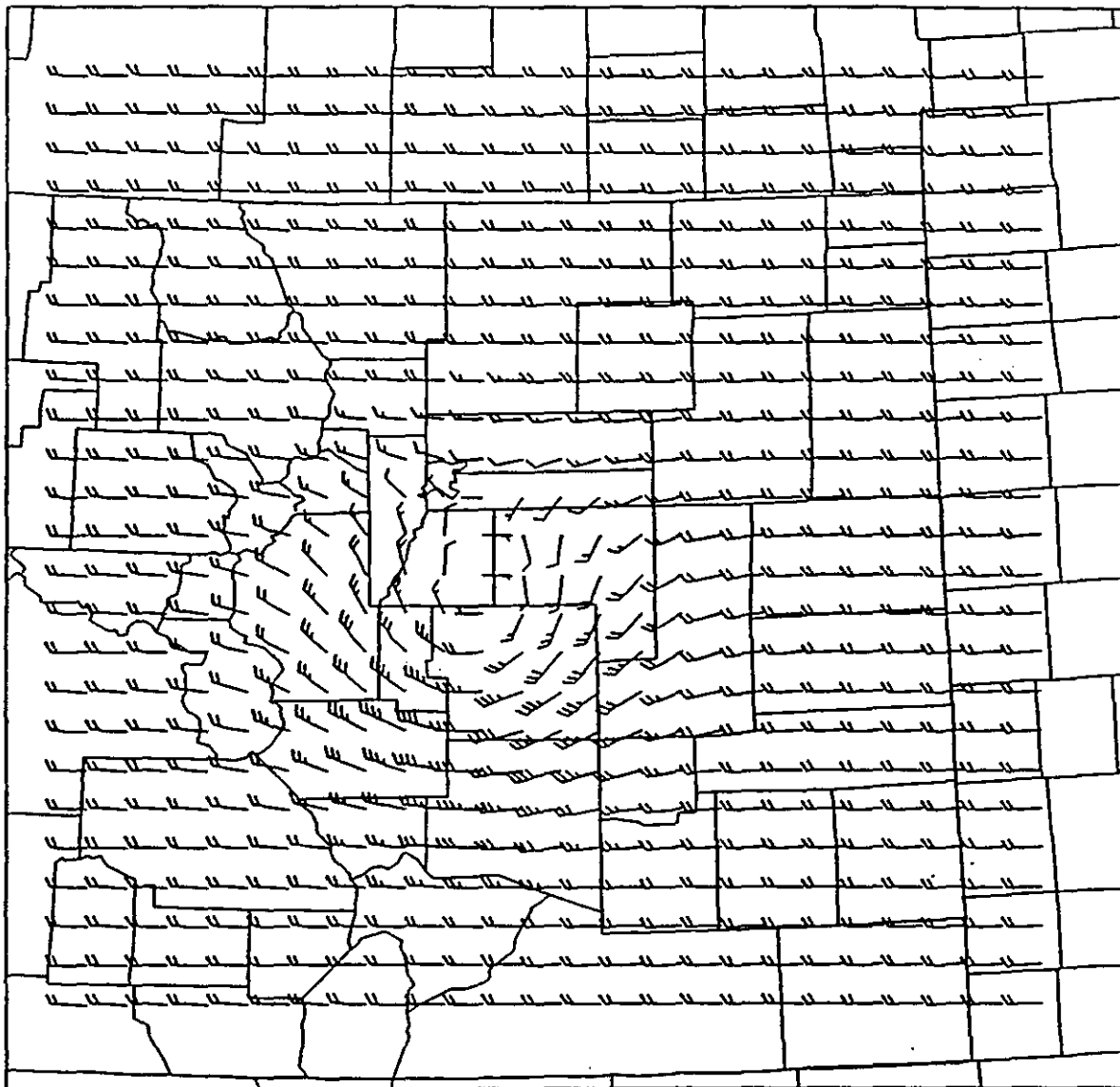


Figure 5. Initial test data wind field. Integration performed with flat bottom surface (no terrain).

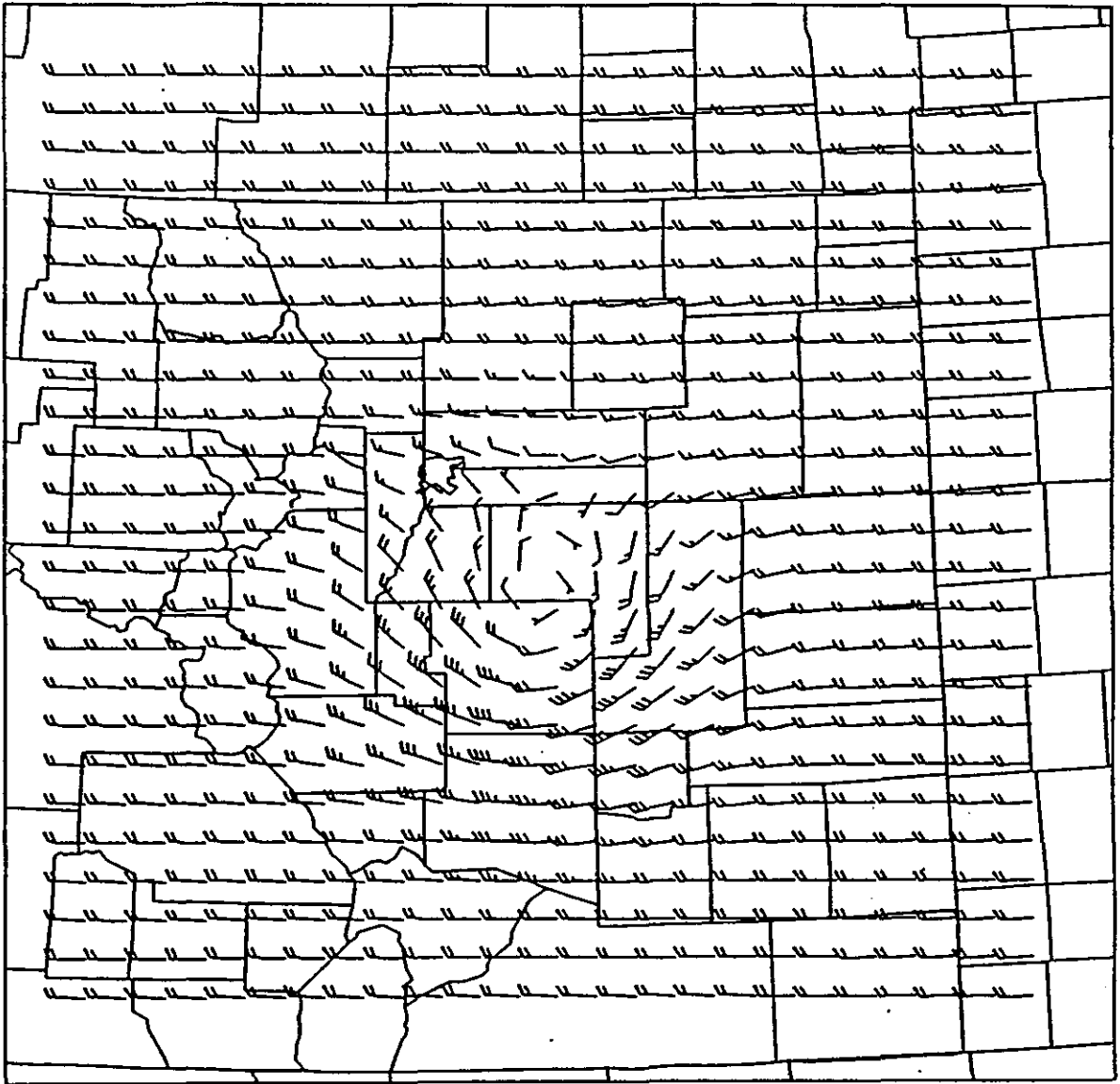


Figure 6. Forecast wind field after 1 hour of simulated time using initial wind field in Figure 5.

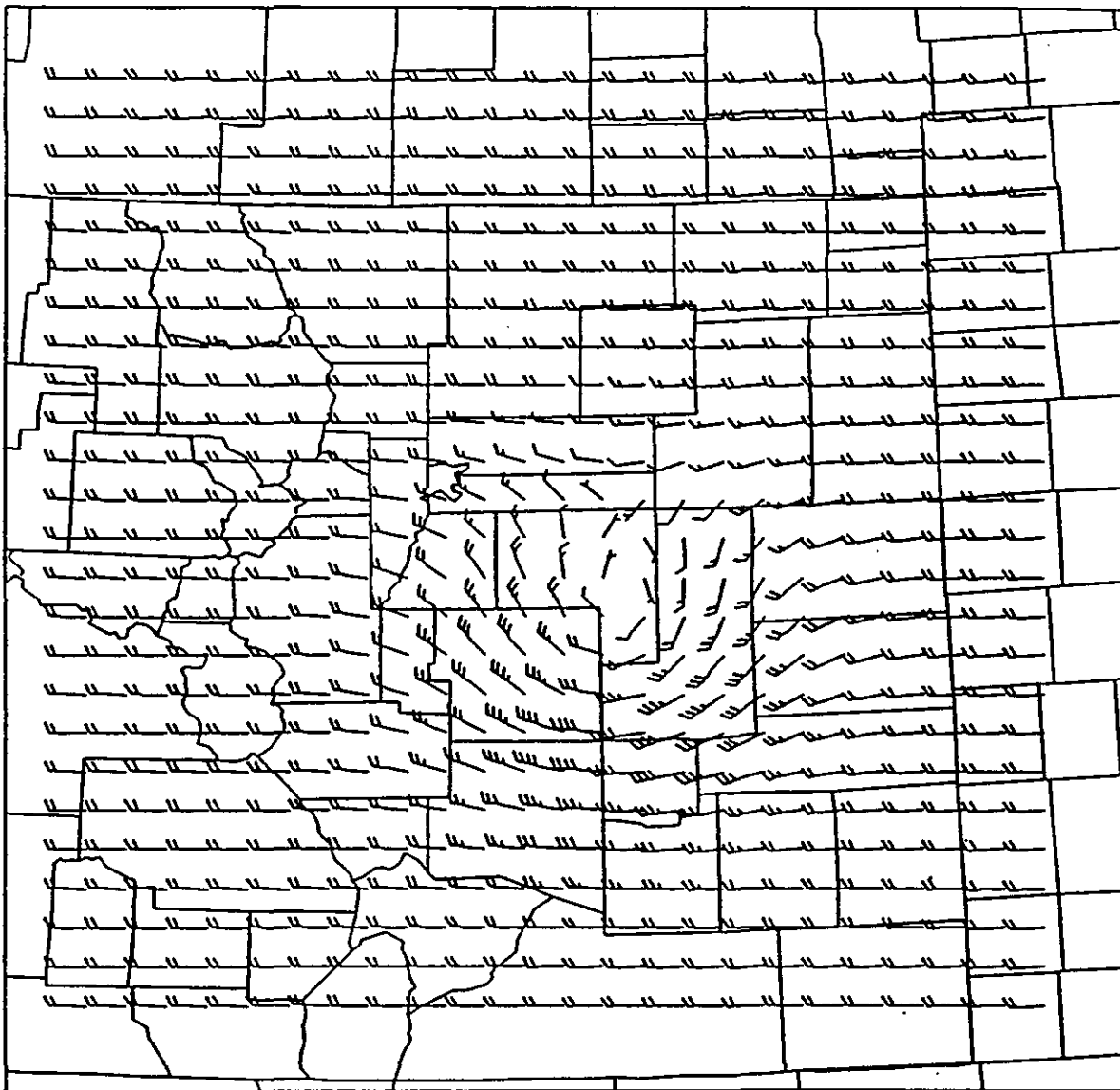


Figure 7. Forecast wind field after 2 hours of simulated time using initial wind field in Figure 5.

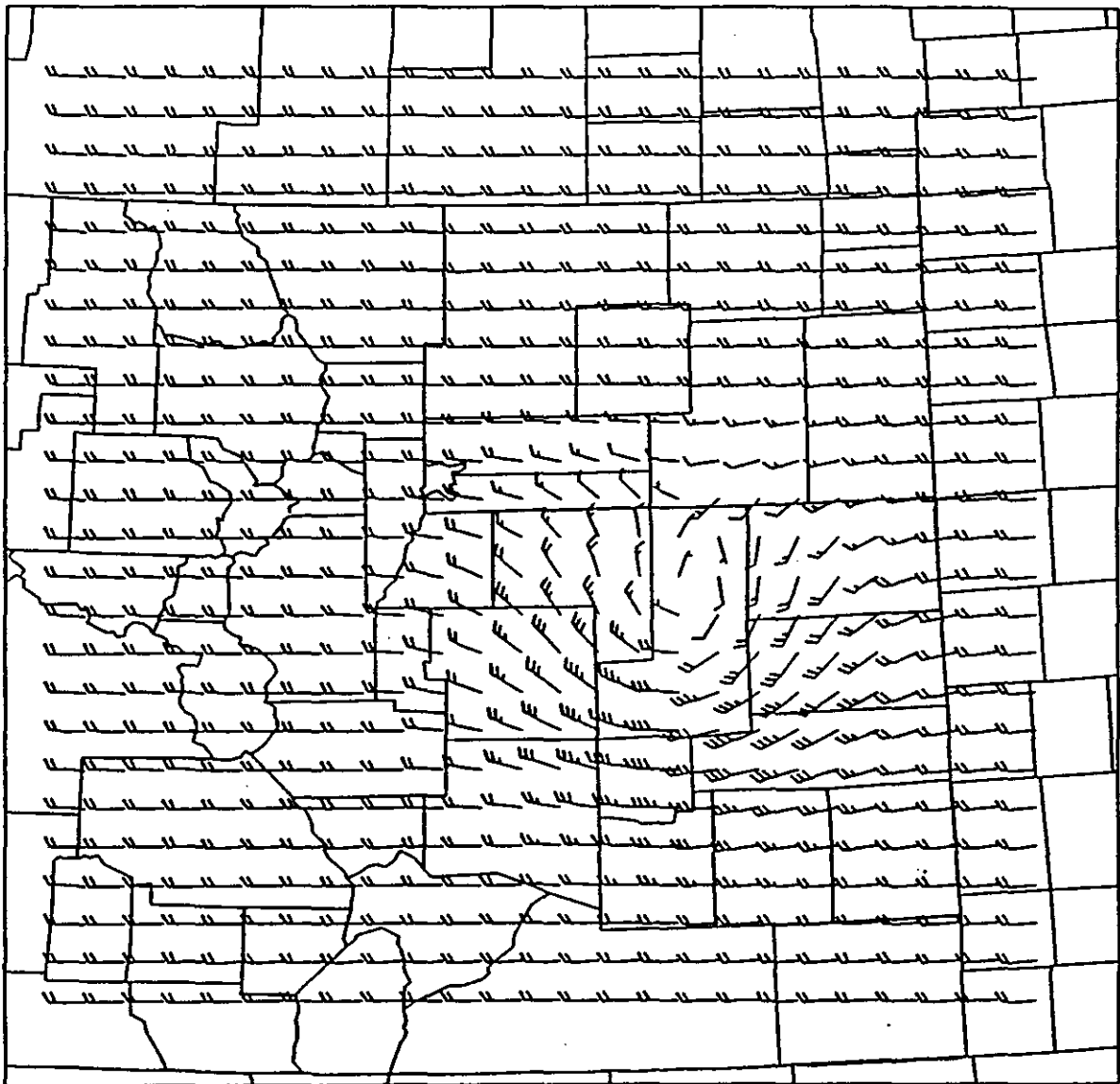


Figure 8. Forecast wind field after 3 hours of simulated time using initial wind field in Figure 5.

tle throughout the integration. Note that the wind speeds in the vortex and elsewhere remain nearly constant.

Figures 9-12 show an example of the integration with real data and the scaled terrain described above. Figure 9 depicts the initial conditions. A couple of features to note here include the weak anticyclonic vortex (clockwise circulation) just east of Yuma county in Kansas, the weak cyclonic vortex in northeast Pueblo county and the deformation zone (saddle point in the wind field) centered in northeast Bent county. Another weak anticyclonic vortex is apparent over southwest Park county.

Figures 10-12 show the results of the integration after 1, 2 and 3 hours of simulated time. The solutions here are quite satisfying mathematically. No sharp discontinuities develop, the wind directions and speeds evolve very smoothly with time, and the aforementioned features remain identifiable throughout the simulation. It also appears that the boundary conditions have not had any detrimental affect on the solution. From a meteorological standpoint, the solution appears to provide a reasonable forecast. The features do not jump around from one hour to the next and in fact move only very slowly, if at all, which would be expected under the generally light mean flow.

Unfortunately, when comparing this solution to the winds that were actually observed at the forecast valid

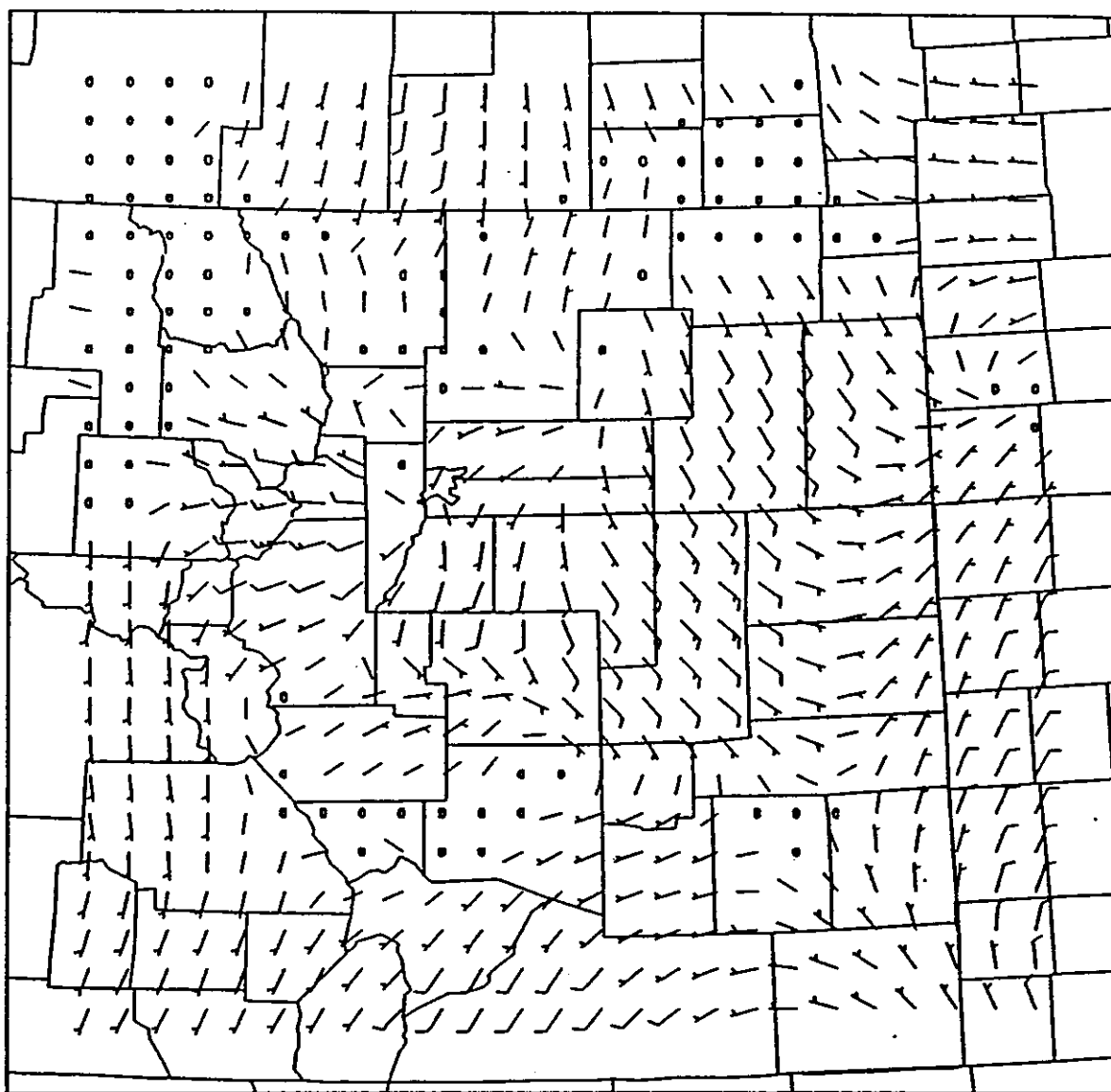


Figure 9. Initial real data wind field. Bottom surface is scaled topography. See text for details.

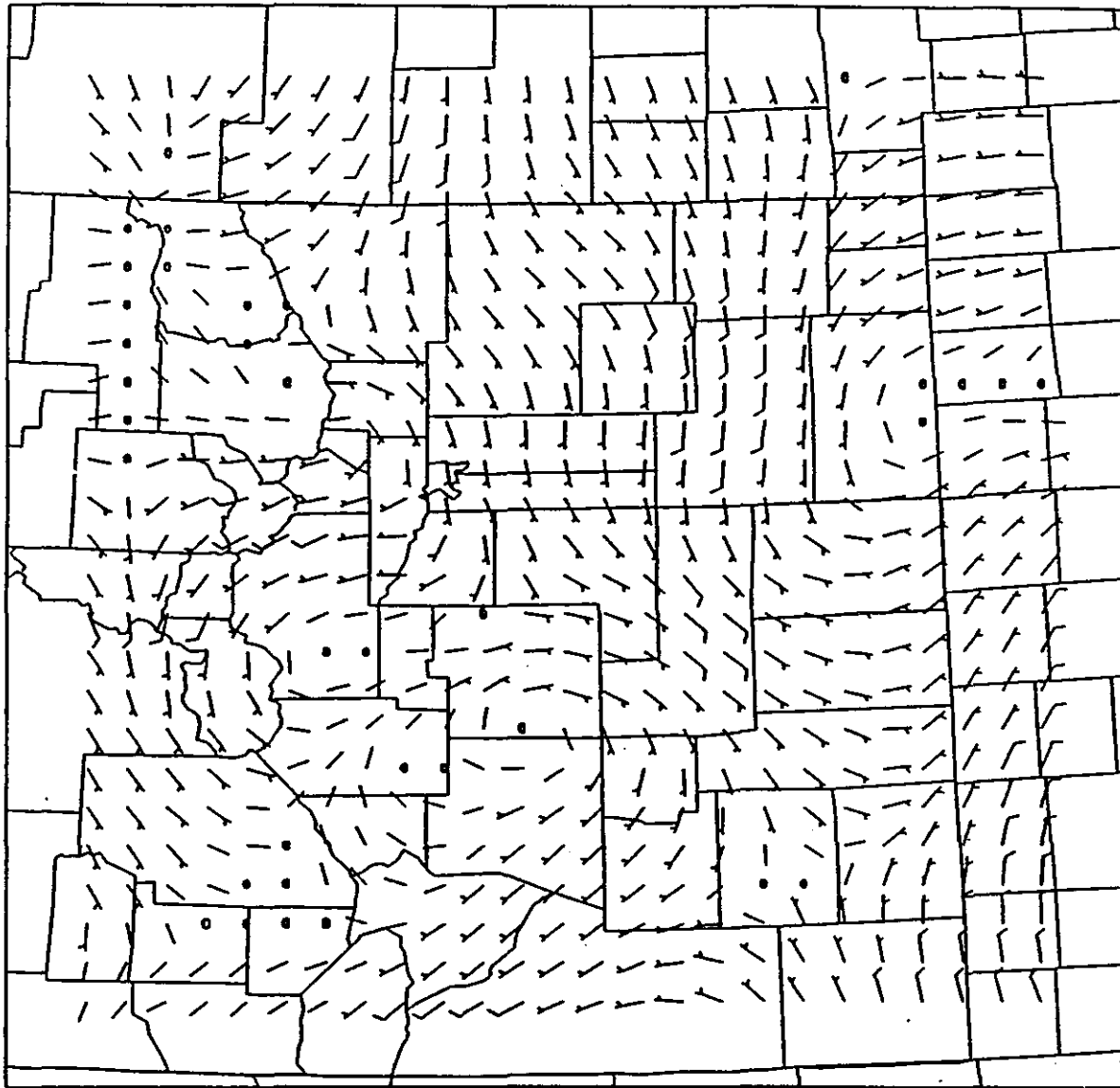


Figure 10. Forecast wind field after 1 hour of simulated time using initial data shown in Figure 9.

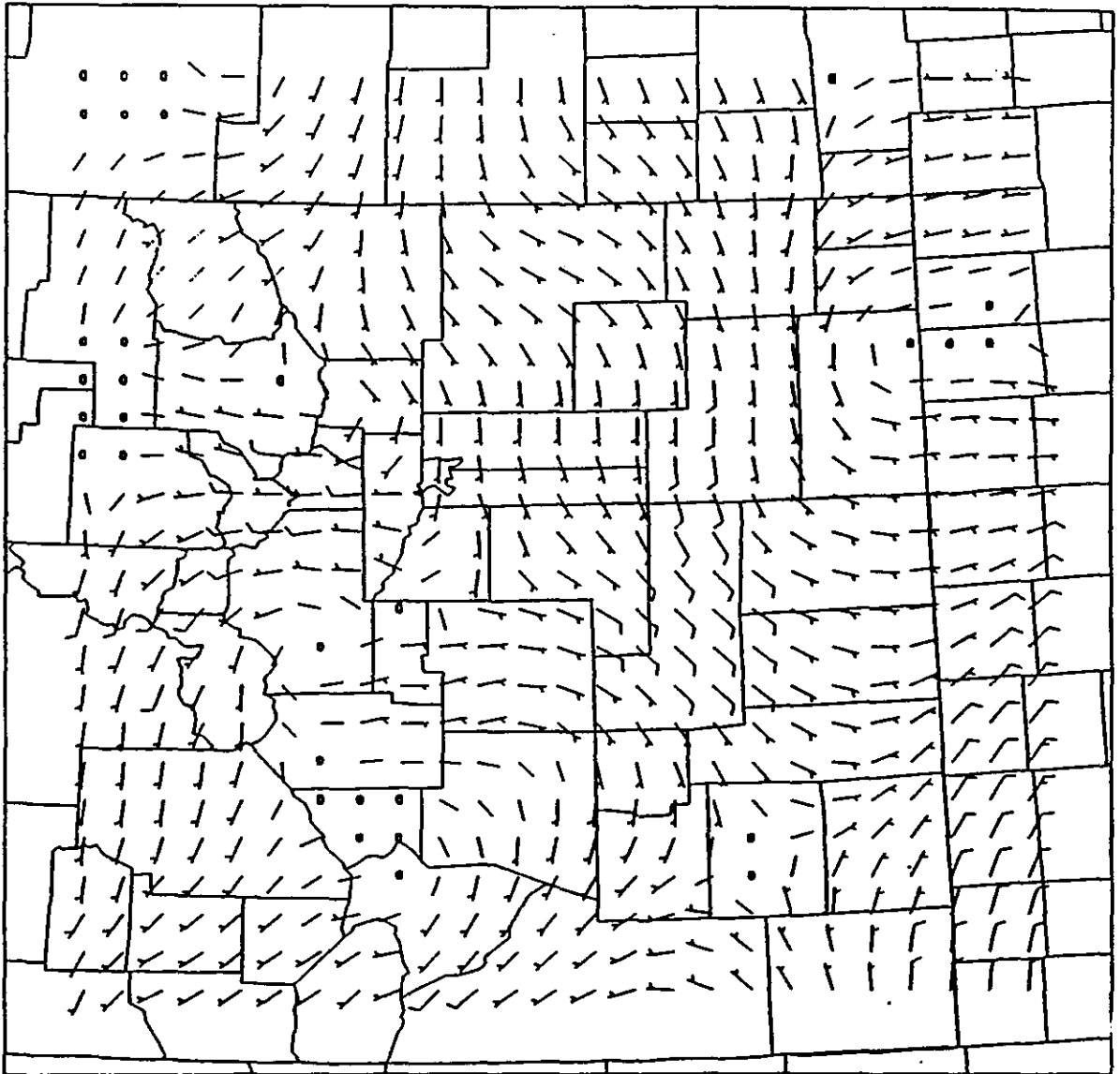


Figure 11. Forecast wind field after 2 hours of simulated time using initial data shown in Figure 9.

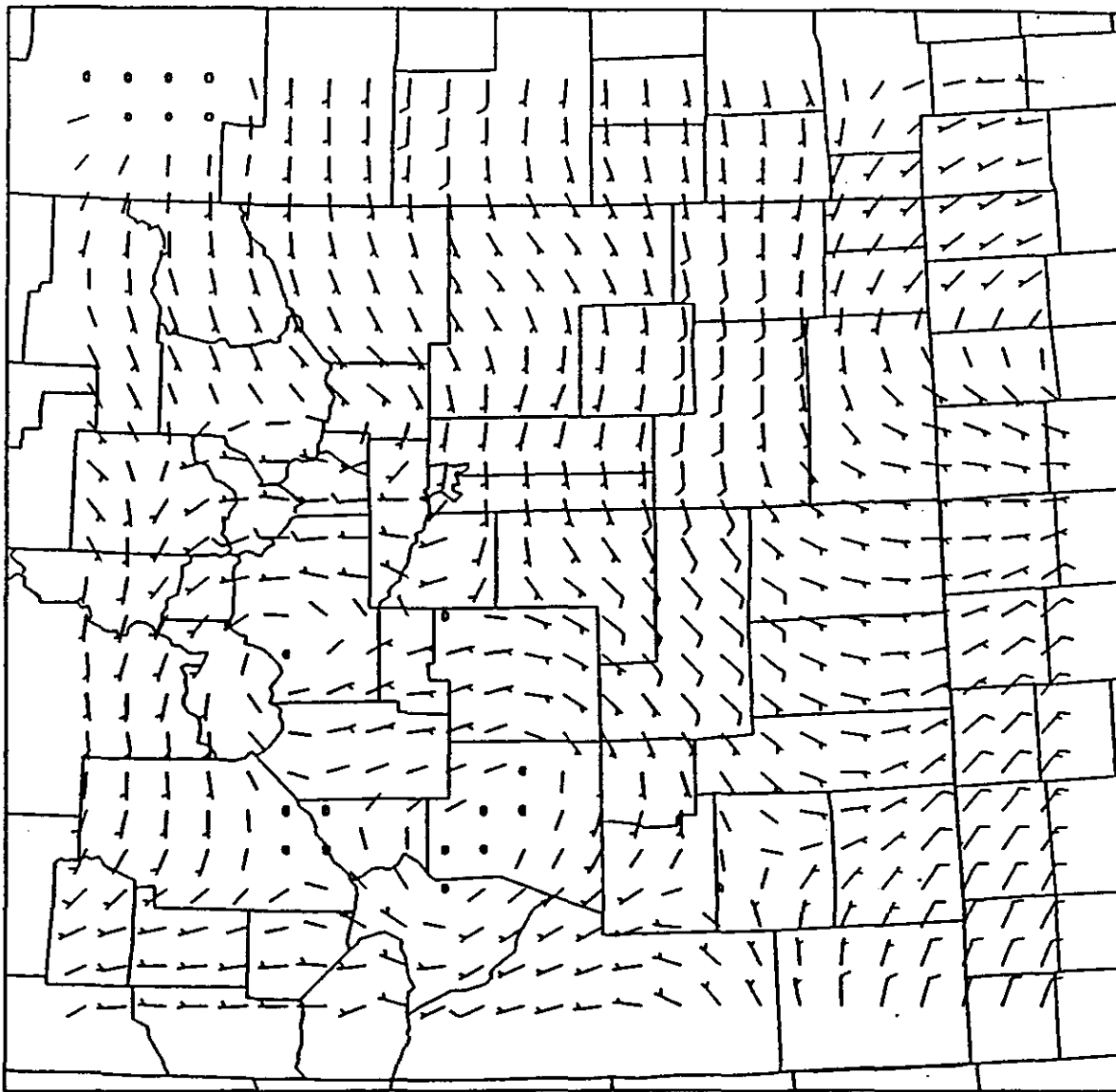


Figure 12. Forecast wind field after 3 hours of simulated time using initial data shown in Figure 9.

times (not shown), it was seen that the forecast was rather poor. Of the above noted features, only the deformation zone remained and even that dissipated after three hours. Winds in other portions of the domain were very poorly forecast.

One of the main reasons for the poor forecast in this case lies in the fact that the model has no thermal effects in it. In light flow situations such as this, local temperature (and hence density) differences, due mainly to the uneven terrain, tend to be the dominant forces in producing the winds. Thus, the assumption that the fluid is barotropic becomes invalid. Friction may be important here as well. Furthermore, the model assumes that the winds are in geostrophic balance and tends to preserve this balance throughout the integration. From this standpoint, the model did quite well, but in reality the winds departed substantially from geostrophic balance.

Figure 13 shows initial conditions for another simulation with real data and the scaled terrain. Note here the anticyclonic vortex over southwest Weld county and the hint of one over northwest El Paso county. The feature over Weld county is a common occurrence when northwest winds like this are occurring. Also note the fairly uniform north to northwest flow over the eastern portion of the domain which becomes easterly over the south central part of the grid.

This turning of the winds is due to the Palmer Divide, an area of higher terrain that runs roughly east-west from Teller county to Lincoln county. Figures 14-16 again show the 1, 2 and 3 hour forecasts based on this initial data. Figures 17, 18, and 19 contain the actual winds observed at 1, 2 and 3 hours after the initial time, respectively.

Again, a smooth mathematical solution is obtained from the model and this time the results are encouraging. Note that the vortex over southwest Weld county is forecast to remain there in the model and indeed does remain there in the observed winds, although its circulation center has shifted into southeast Larimer county after 3 hours. After 1 hour, the model strengthens the vortex over northwest El Paso county and the observed winds verify that this feature did develop although not as strong as forecast. The general turning of the winds from north or northwest to easterly south of the Palmer Divide was well forecast although the observed winds were more southeasterly, probably due to thermal affects. Observed winds over the northern and eastern part of the domain remained constant for the most part and this was forecast to occur in the model. Significant differences in wind speed between forecast and observed did occur however over Morgan, Washington and Lincoln counties.

Across the western part of the domain the forecast in

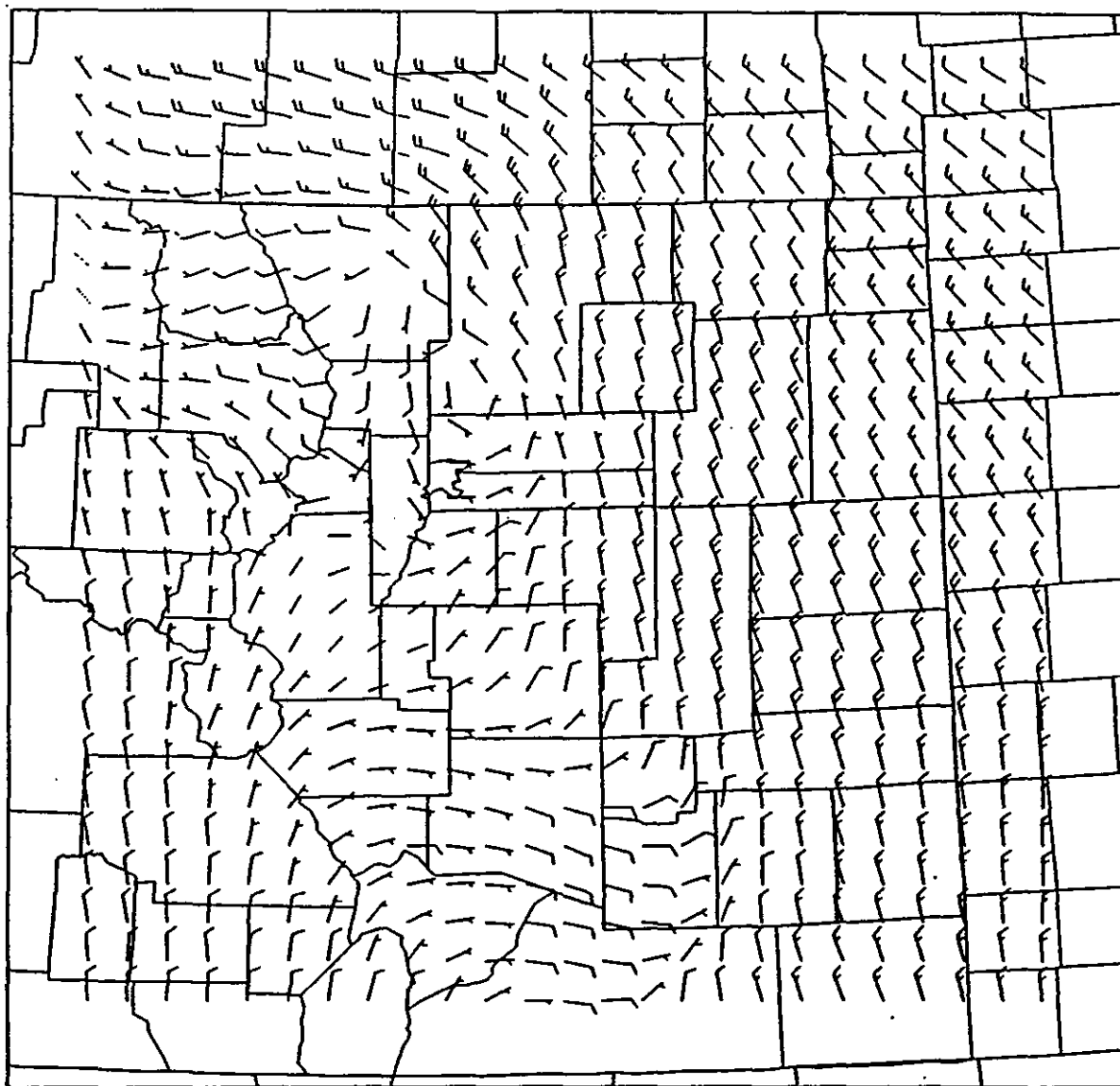


Figure 13. Initial real data wind field. Bottom surface is scaled topography. See text for details.

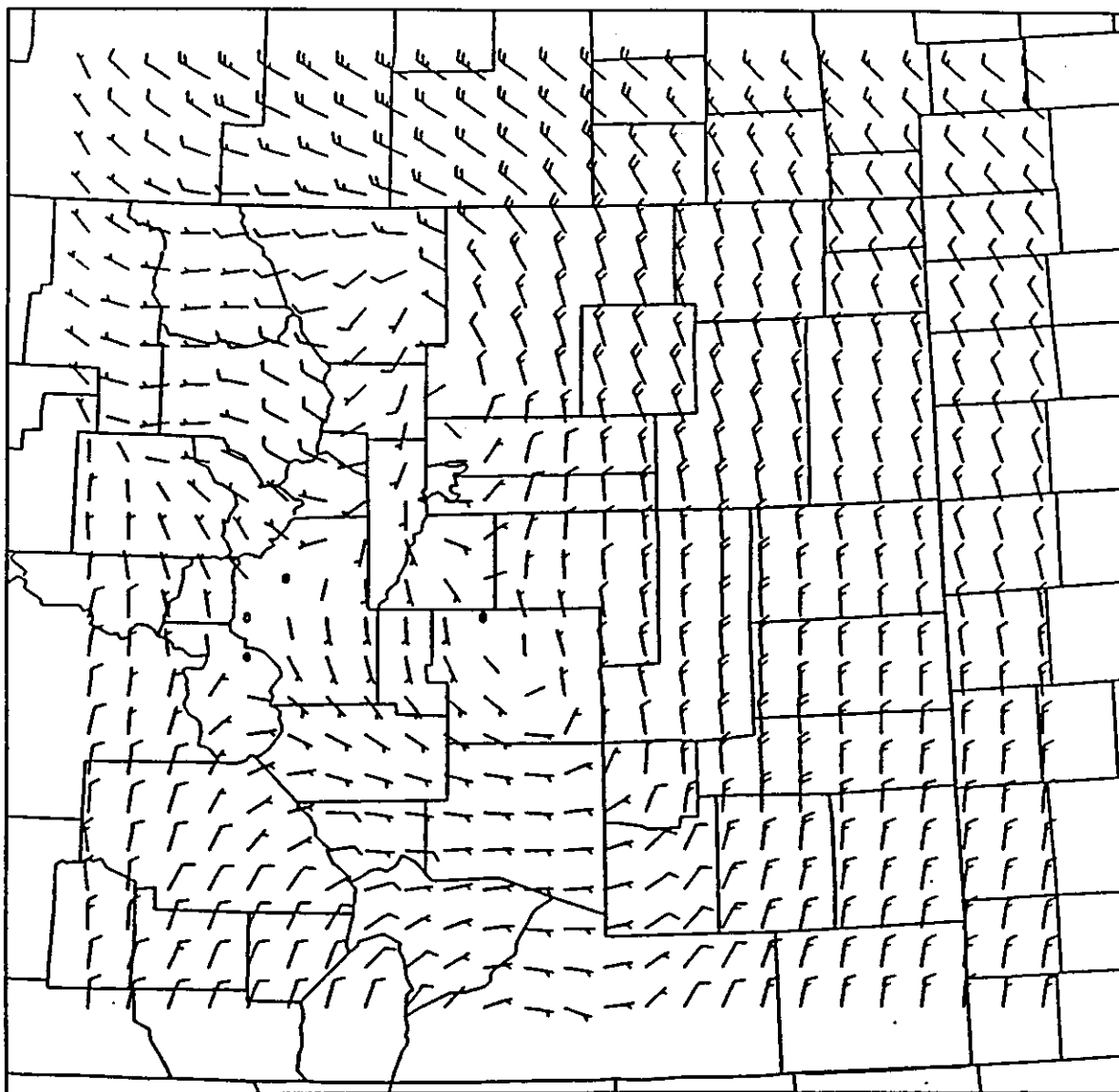


Figure 14. Forecast wind field after 1 hour of simulated time using initial data shown in Figure 13.

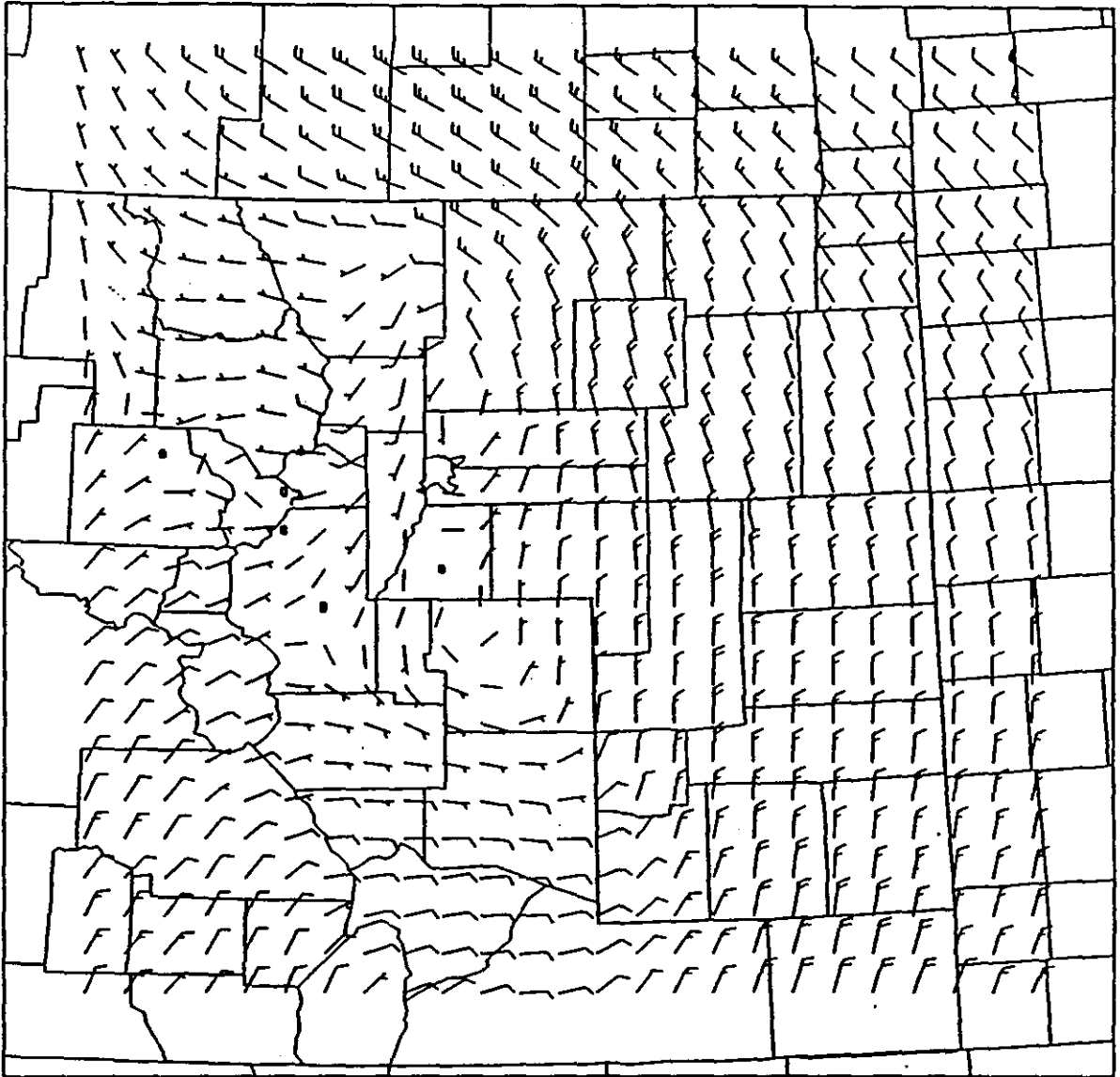


Figure 15. Forecast wind field after 2 hours of simulated time using initial data shown in Figure 13.

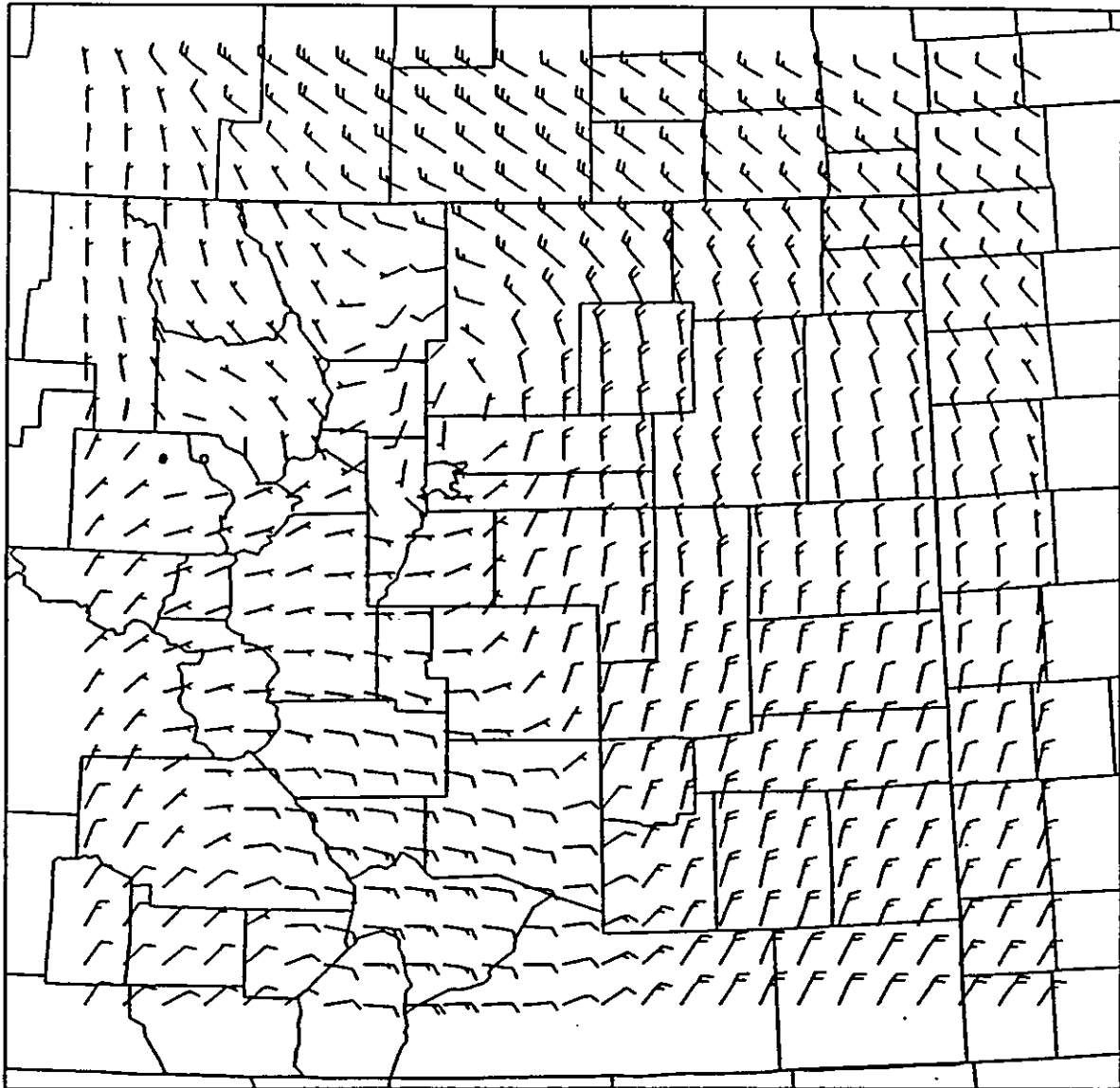


Figure 16. Forecast wind field after 3 hours of simulated time using initial data shown in Figure 13.

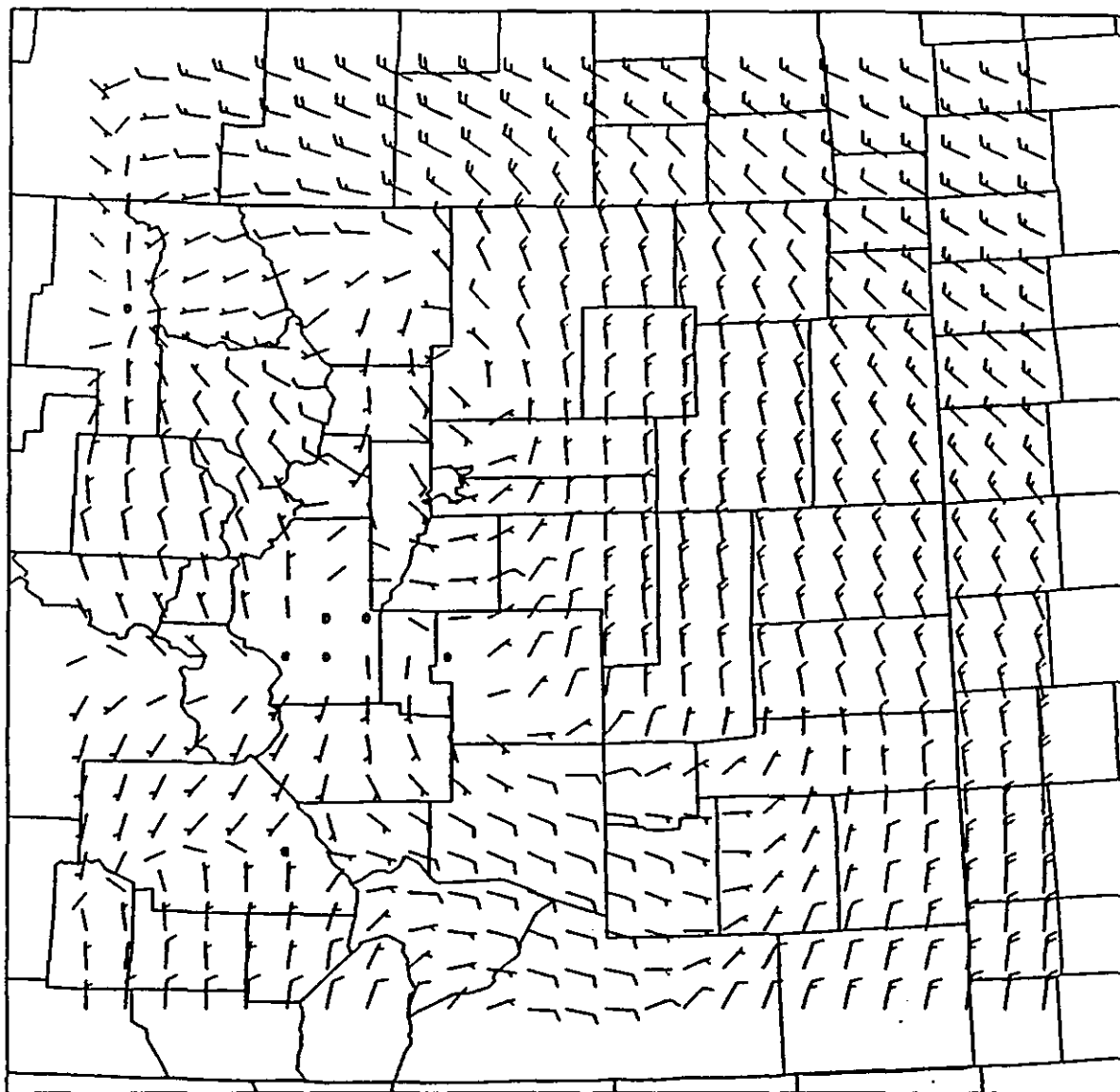


Figure 17. Actual winds observed 1 hour after initial data in Figure 13. Compare with Figure 14.

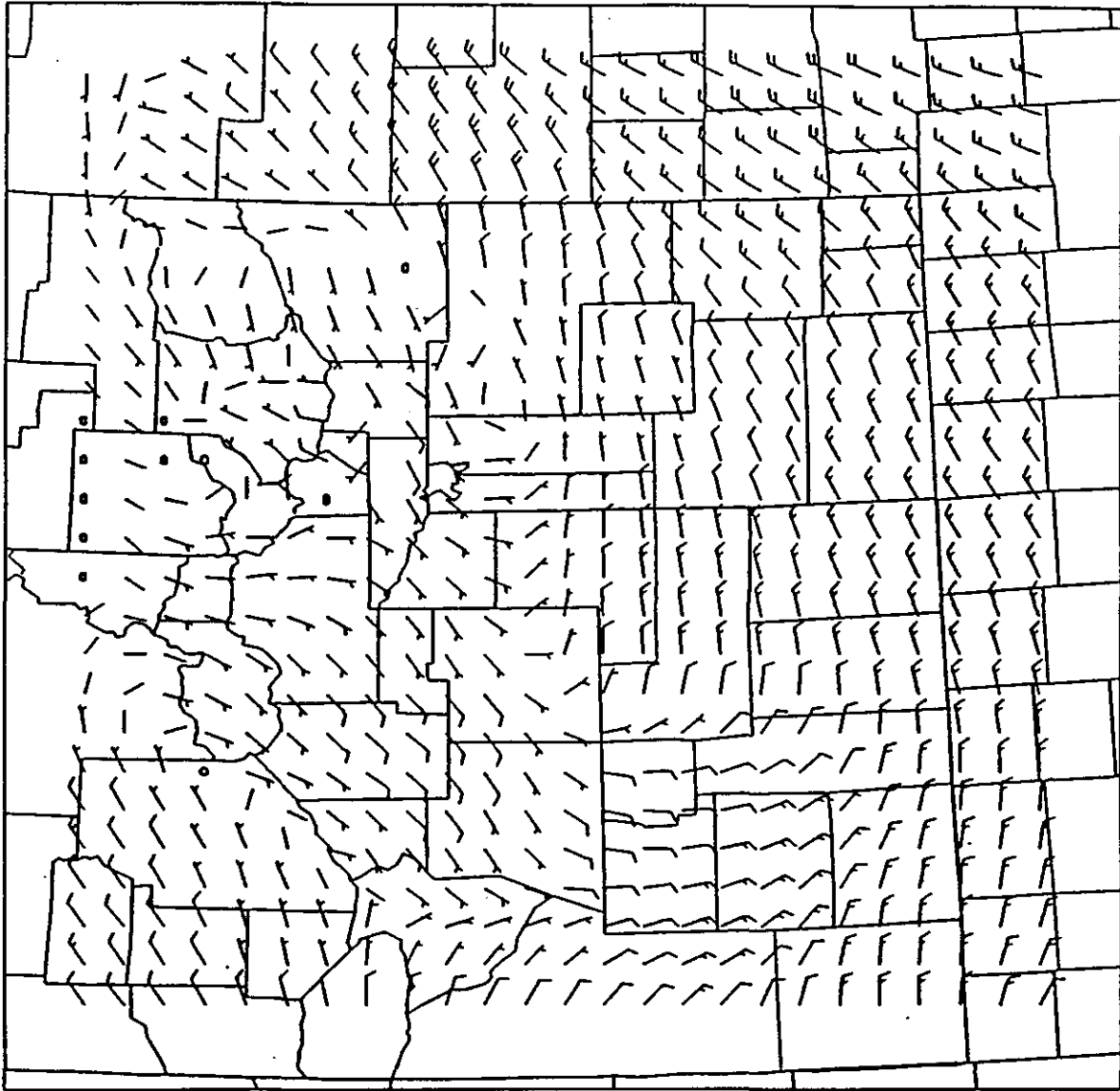


Figure 18. Actual winds observed 2 hours after initial data in Figure 13. Compare with Figure 15.

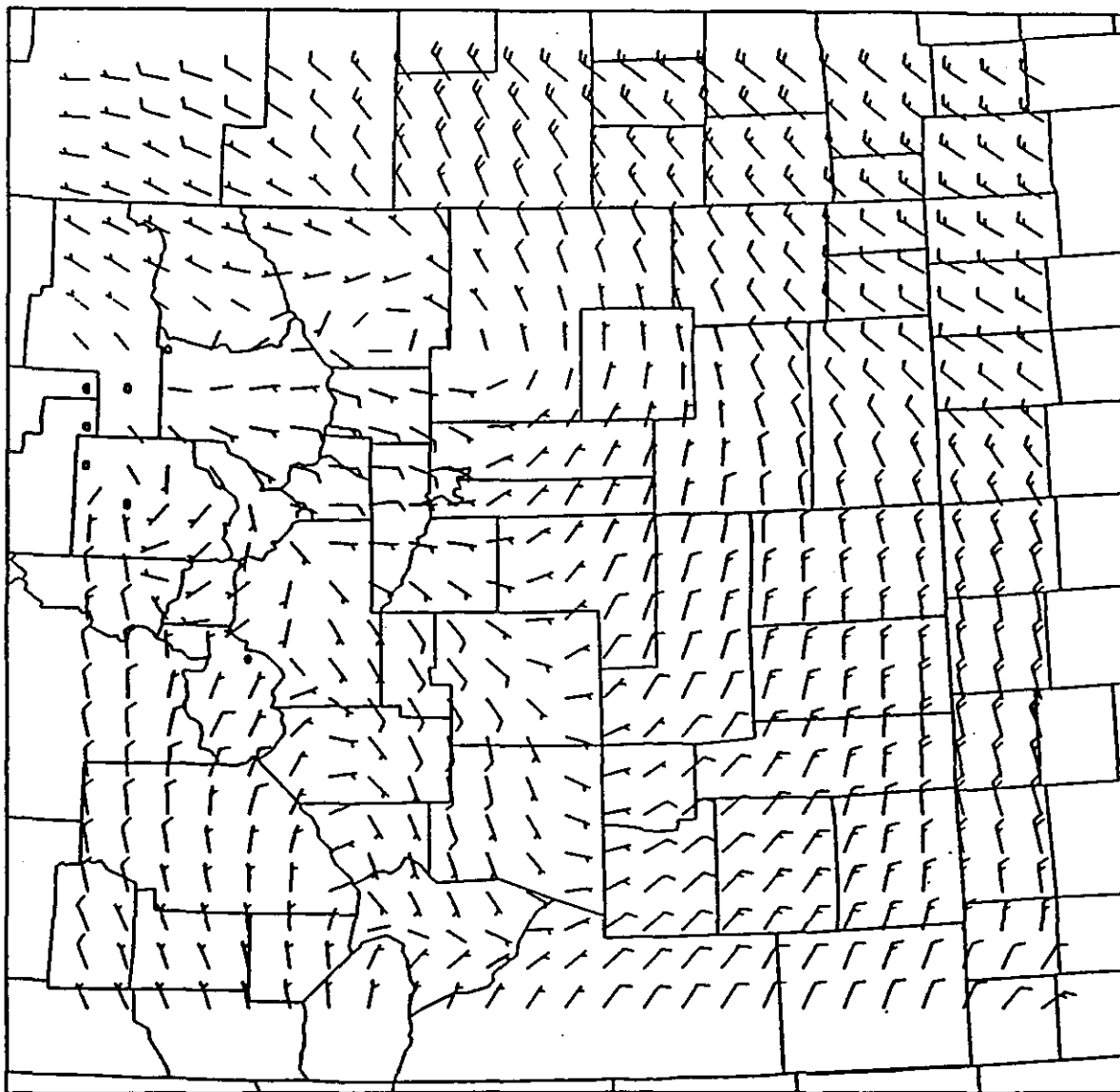


Figure 19. Actual winds observed 3 hours after initial data in Figure 13. Compare with Figure 16.

general was not as good as elsewhere. For example, the winds in the southwest part of the grid became more northwesterly with time in reality whereas the model predicted them to become northeasterly. This is likely due to the fact that this part of the grid contains the higher terrain and in this case the winds there came under the influence of the winds higher in the atmosphere. Recall that this model moves the air around as a set of columns with constant wind throughout the entire depth of the column. In reality winds from higher levels in the atmosphere can mix down to the surface, something this model is incapable of simulating. All in all though, this particular case shows that the model can produce useful wind forecasts.

It should be reiterated here that the conservation laws enjoyed by the differential and finite difference equations were guaranteed only in the case where no fluid was allowed across the boundary of the domain. With the boundary conditions used here, we expect that these conservation laws will not hold. This indeed is the case. However the changes in the "conserved" values throughout the three hour integrations were not, for the most part, extraordinary. Total mass and area averaged absolute vorticity and total mechanical energy changes were all less than about 5 percent in both the test cases and real data cases. Changes in the area-averaged potential enstrophy on the other hand varied widely, from 51% in one case to less than 1% in others (real

and test data). Interestingly enough, the 51% change occurred in the example shown in Figure 7. For the short term integrations we are considering, it appears that this should not be a problem.

To summarize then, this study has taken a very simple physical model from geophysical fluid dynamics, placed it in a mathematical framework as an initial-boundary value problem, and solved it by numerical techniques to produce the evolution of surface winds.

From a mathematical standpoint, the results are quite satisfying. Stable numerical integrations have been carried out on a number of cases using real data, yielding what appear to be very reasonable results based on the physics of the model. Smooth approximate solutions to the original partial differential equations have been obtained in each case.

From a meteorological standpoint, the solutions have been less pleasing. It is felt that this is due to the simplicity of the physics in the model and not the mathematics used for its solution. Admittedly, the physical model's validity on the scale used here is questionable. Since it is normally used to describe airflow on scales of about 1000 km, using it on a domain whose entire length is only on the order of 500 km perhaps may be asking more of it than it can handle.

The most notable deficiency in the model appears to be its inability to describe thermal effects. Under light flow conditions, the winds usually are more directly a result of thermal (and hence density) differences which are not included in the physical model. This, along with the assumption of geostrophic balance used to initialize the model and the model's tendency to keep the flow geostrophic, is least valid in these situations. However, under stronger flow regimes, thermal effects are not as important and the geostrophic assumption is not unreasonable. Results appear to indicate that useful surface wind forecasts can be had from the model under these conditions.

Current plans call for implementation of this model on an operational basis at the National Weather Service Forecast Office in Denver, Colorado in the near future. Since forecasters there have little in the way of objective wind forecasts to help in day-to-day weather predictions, it is hoped that the output from this model will serve as helpful guidance in their work. In addition, since the physics of the model are so simple, using the model on a routine basis may lead to a better understanding of the causes and evolution of wind patterns over its domain.

REFERENCES CITED

- Abbs, D. and R. Pielke. 1986. Thermally forced surface flow and convergence patterns over northeast Colorado. Monthly Weather Review 114: 2281-2296.
- Arakawa, A., and V. Lamb. 1977. Computational design of the basic dynamical processes of the UCLA general circulation model. In Methods in computational physics vol. 17, ed. J. Chang, 173-265. Academic Press, New York.
- Arakawa, A., and V. Lamb. 1981. A potential enstrophy and energy conserving scheme for the shallow water equations. Monthly Weather Review 109: 18-36.
- Bourne, D. and P. Kendall. 1968. Vector analysis. Boston: Allyn and Bacon.
- Burden, R. and J. Faires. 1985. Numerical analysis. 3d ed. Boston: PWS Publishers.
- Davies, H. 1973. On the initial-boundary value problem of some geophysical fluid flows. J. Computational Physics 13: 398-422.
- Dutton, J. 1986. The ceaseless wind - an introduction to the theory of atmospheric motion. Mineola, NY: Dover
- Ellsaesser, H. 1968. Comparative test of wind laws for numerical weather prediction. Monthly Weather Review 96: 277-285.
- Elvius, T. and A. Sundström. 1973. Computationally efficient schemes and boundary conditions for a fine-mesh barotropic model based on the shallow water equations. Tellus 25: 132-156.
- Frankel, S. 1950. Convergence rates of interative treatments of partial differential equations. Mathematical Tables and Other Aids to Computation 4: 65-75.
- Grammeltvedt, A. 1969. A survey of finite difference schemes for the primitive equations for a barotropic fluid. Monthly Weather Review 97: 384-404.
- Haltiner, G. and R. Williams. 1980. Numerical prediction and dynamic meteorology. 2d ed. New York: John Wiley and Sons.

- Holton, J. 1979. An introduction to dynamic meteorology. 2d ed. New York: Academic Press.
- International Mathematical and Statistical Library. 1987. User's manual, vol 3. Houston: IMSL, Inc.
- Kurihara, Y. 1965. On the use of implicit and iterative methods for the time integration of the wave equation. Monthly Weather Review 93: 33-46.
- Kurihara, Y. and G. Tripoli. 1976. An iterative time integration scheme designed to preserve a low frequency wave. Monthly Weather Review 104: 761-764.
- Lilly, D. 1965. On the computational stability of numerical solutions of time dependent nonlinear geophysical fluid dynamics problems. Monthly Weather Review 93: 11-26.
- Matsuno, T. 1966. Numerical integrations of the primitive equations by a simulated backward difference method. J. Meteorological Soc. Japan 44: 76-83.
- McGinley, J. 1989. The Local Analysis and Prediction System. In Preprints 12th Conference on Weather Analysis and Forecasting, 15-20. American Meteorological Society, Boston.
- Oliger, J. and A. Sundström. 1978. Theoretical and practical aspects of some initial-boundary value problems in fluid dynamics. SIAM J. Applied Math. 35: 419-446.
- Pedlosky, J. 1987. Geophysical Fluid Dynamics. 2d ed. New York: Springer-Verlag.
- Perkey, D. and C. Kreitzberg. 1976. A time dependent lateral boundary scheme for limited area primitive equation models. Monthly Weather Review 104: 744-755.
- Phillips, N. 1960. On the problem of initial data for the primitive equations. Tellus 12: 121-126.
- Shapiro, R. 1970. Smoothing, filtering, and boundary effects. Rev. Geophysics and Space Physics 8: 359-387.
- Sundström, A. 1977. Boundary conditions for limited-area integrations of the viscous forecast equations. Beiträge zur Physik der Atmosphäre 50: 218-224.
- Varga, R. 1962. Matrix iterative analysis. Englewood Cliffs, New Jersey: Prentice-Hall.

Wilczak, J. and J. Glendening. 1988. Observations and mixed layer modelling of a terrain induced mesoscale gyre: the Denver cyclone. Monthly Weather Review 116: 2688-2711.

Young, J. 1968. Comparative properties of some time differencing schemes for linear and nonlinear oscillations. Monthly Weather Review 96: 357-364.

SELECTED BIBLIOGRAPHY

- Ames, W. 1977. Numerical methods for partial differential equations. 2d ed. New York: Academic Press.
- Arakawa, A. 1966. Computational design for long-term numerical integration of the equations of motion: two dimensional incompressible flow. Part I. J. Computational Physics 1: 119-143.
- Baer, F. and J. Tribbia. 1977. On complete filtering of gravity modes thru nonlinear initialization. Monthly Weather Review 105: 1536-1539.
- Carnahan, B., H. Luther, and J. Wilkes. 1969. Applied numerical methods. New York: John Wiley and Sons.
- Davies, H. 1983. Limitations of some common lateral boundary schemes used in regional numerical weather prediction models. Monthly Weather Review 111: 1002-1012.
- Fischer, G. 1965. A survey of finite difference approximations to the primitive equations. Monthly Weather Review 93: 1-10.
- Fjortoft, R. 1953. On the changes in the spectral distribution of kinetic energy for two dimensional, non-divergent flow. Tellus 5: 225-230.
- Garabedian, P. 1964. Partial differential equations. New York: Wiley and Sons
- Gary, J. 1979. Nonlinear Instability. In Numerical methods used in atmospheric models. Global Atmospheric Research Program Publication Series no. 17, vol. 2 474-499. World Meteorological Organization.
- Gerrity, J. and R. McPherson. 1969. Development of a limited area fine-mesh prediction model. Monthly Weather Review 97: 665-669.
- Golub, G. and C. Van Loan. 1985. Matrix computations. Baltimore: Johns Hopkins Univ. Press
- Grotjahn, R. and J. O'Brien. 1976. Some inaccuracies in finite differencing hyperbolic systems. Monthly Weather Review 104: 180-194.

- Hamming, R. 1973. Numerical methods for scientists and engineers. New York: McGraw-Hill.
- Kreiss, H-O. and J. Olinger. 1972. Comparison of accurate methods for the integration of hyperbolic equations. Tellus 24: 199-215.
- Kreiss, H-O. and J. Olinger. 1973. Methods for the approximate solution of time dependent problems. Global Atmospheric Research Program Publication Series no. 10. World Meteorological Organization.
- Lax, P. 1957. Hyperbolic systems of conservation laws II. Communications on Pure and Applied Mathematics 10: 537-566.
- Le Méhauté, B. 1976. An introduction to hydrodynamics and water waves. New York: Springer-Verlag.
- Matsuno, T. 1966. False reflection of waves at the boundary due to the use of finite differences. J. Meteorological Soc. Japan 44: 145-157.
- Mesinger, F. and A. Arakawa. 1976. Numerical methods used in atmospheric models. Global Atmospheric Research Program Publication Series no. 17, vol. 1. World Meteorological Organization.
- Moretti, G. 1969. Importance of Boundary conditions in the numerical treatment of hyperbolic equations. Physics of Fluids 12 (Supplement II): 13-20.
- O'Brien, G., M. Hyman, and S. Kaplan. 1950. A study of the numerical solution of partial differential equations. J. of Mathematics and Physics 29: 223-251.
- Okland, H. 1970. On the adjustment toward balance in primitive equation weather prediction models. Monthly Weather Review 98: 271-279.
- Phillips, N. 1959. An example of nonlinear computational instability. In The atmosphere and sea in motion, 501-504. Rockefeller Institute Press, New York.
- Pielke, R. 1984. Mesoscale meteorological Modelling. Orlando, Fla.: Academic Press
- Robert, A., F. Schuman, and J. Gerrity. 1970. On partial difference equations in mathematical physics. Monthly Weather Review 98: 1-6.

- Sadourny, R. 1975. The dynamics of finite difference models of the shallow water equations. J. of the Atmospheric Sciences 32: 680-689.
- Saha, K. and P. Suryanarayana. 1971. Numerical solutions of geopotential with different forms of balance relationships in the tropics. J. Meteorological Soc. Japan 49: 510-515.
- Smith, G. 1975. Numerical solution of partial differential equations. London: Oxford Univ. Press.
- Sundtröm, A. and T. Elvius. 1979. Computational problems related to limited area modelling. In Numerical methods used in atmospheric models. Global Atmospheric Research Program Publication Series no. 17, vol. 2 379-416. World Meteorological Organization.
- Thompson, P. 1961. Numerical weather analysis and prediction. New York: Macmillan.
- Vemuri, V. and W. Karplus. 1981. Digital computer treatment of partial differential equations. Englewood Cliffs, New Jersey: Prentice-Hall.
- Wiin-Nielson, A. 1979. On phase speed errors due to various time differencing schemes. In Numerical methods used in atmospheric models. Global Atmospheric Research Program Publication Series no. 17, vol. 2 438-473. World Meteorological Organization.
- Williamson, D. 1976. Normal mode initialization procedure applied to forecasts with the global shallow water equations. Monthly Weather Review 104: 195-206.